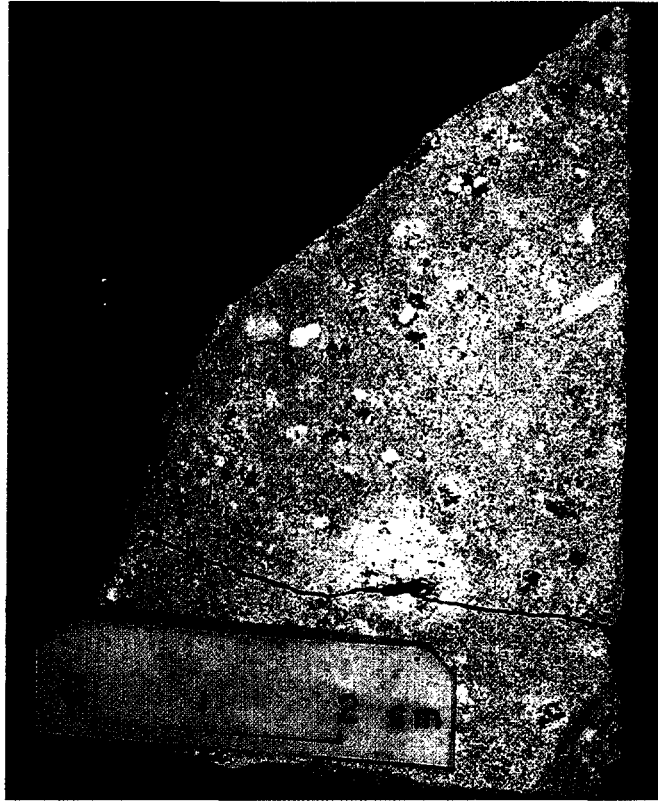
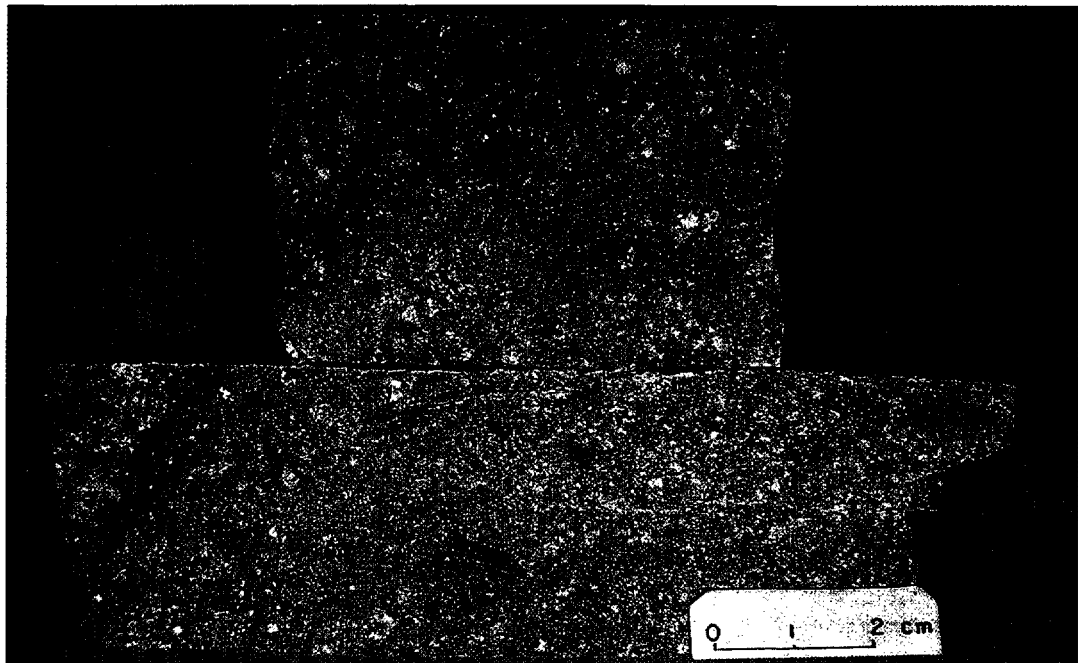


**Appendix 3:9**

**PLATES 3:9-1 – 3:9-8**



*PLATE 3:9-1. Reduced porphyritic phonolite. Note the white alkali-feldspar phenocrysts, microporosities and medium-grey, nearly rectangular pseudomorphs after nepheline.  
Sample no.: F1/69-1A.*



*PLATE 3:9-2. Reduced medium-grained porphyritic phonolite with massive structures. The dark seams in the left hand corners of the drillcores are hydrothermally altered fractures mineralised with microcrystalline pyrite.*



*PLATE 3:9-3. Reduced phonolite near redox front. Note the fracture-related formation and dissolution of pitchblende nodules (black).  
Open pit sample no. S/N-18 (8-2BI 33).*

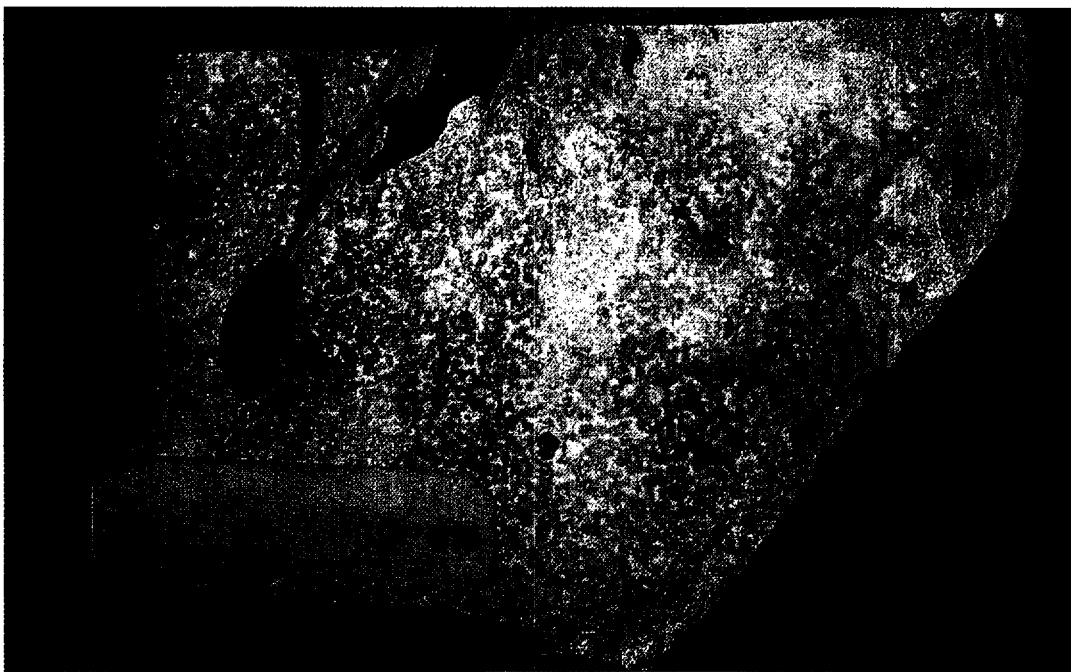


*PLATE 3:9-4. Sawn surface of sample illustrated in Plate 3:9-3. Note fine-grained texture of the reduced phonolite and the elongated fracture dependent forms of the black pitchblende nodules.*

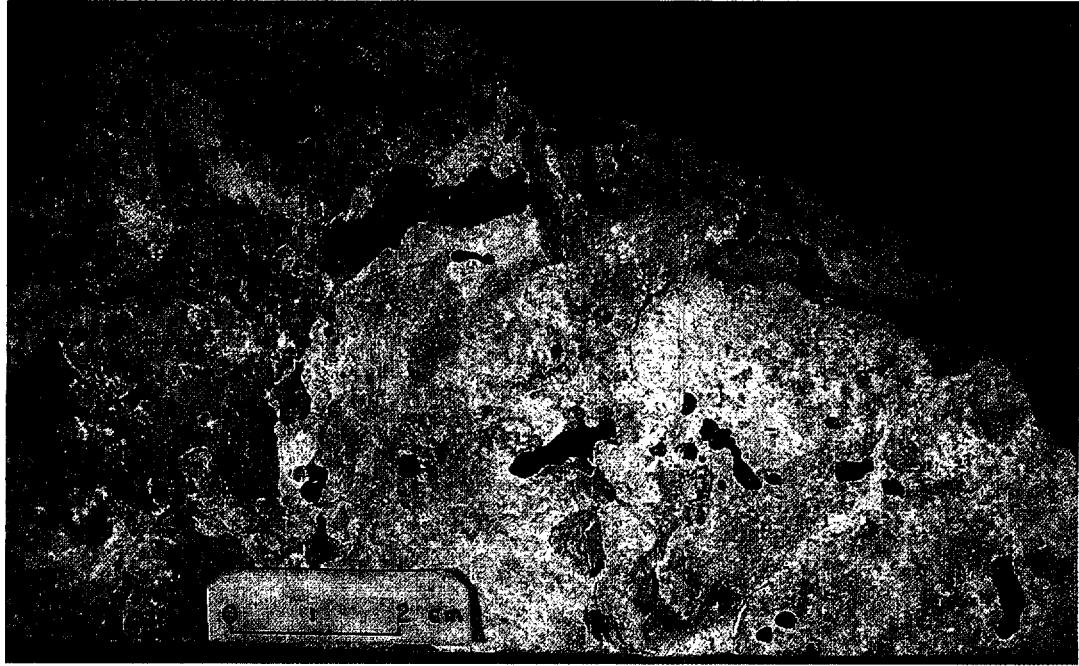


*PLATE 3:9-5. Phonolite with redox front. Note the forms of the pitchblende nodules on the natural fracture plane and the incipient dissolution of the nodules near the redox front; these nodules change colour from black to medium-grey. Open pit sample no.: S/N 21 (8-2 AH 63).*



*PLATE 3:9-6. Sawn surface of sample illustrated in Plate 3:9-5. Note the sharp redox front in the microxenolithic, fine-grained phonolite. The left-hand part consists of reduced rock, light-grey coloured, and shows microporosities and one (kidney shaped) millimetre-sized pitchblende nodule (upper left, about 1 cm from redox front). The right-hand part of the specimen is oxidised, showing the typical colouration caused by finely disseminated limonite/ HFO-minerals resulting from pyrite oxidation.*



*PLATE 3:9-7. Massive pitchblende nodule. Note external concretionary "Löss-Kindl" shape.  
Specimen no. S/N-24.*



*PLATE 3:9-8. Sawn surface of the nodule illustrated in Plate 3:9-7. The nodule consists of a white coloured core of hydrothermally altered and argillised rock (phonolite), surrounded by a black nodule-forming pitchblende zone and a fine external yellowish white clay shell. Note the "horizontal" zone which is extremely rich in secondary coarse-grained pyrites in the top portion of the pitchblende zone (yellow reflectivity). This probably represents a former water table-related phenomenon.*

## **Appendix 4**

### **Whole-rock geochemical data and geochemical profiles of boreholes F1, F3 and F4.**

**(Compiled by N. Waber, University of Bern).**

# Contents

	page
Abbreviations	325
Borehole F1; Osamu Utsumi mine, ore body E	327
Borehole F3; " " " , " " E	339
Borehole F4; " " " , " " B	347

## Abbreviations

LPh	–	leucocratic phonolite
VLPPh	–	volcanic leucocratic phonolite
PlcPh	–	pseudoleucite-bearing phonolite
PlcCpxPh	–	pseudoleucite-clinopyroxene-bearing phonolite
NeS	–	nepheline syenite xenolith
VBr	–	volcanic breccia
PhD	–	phonolite dyke
RF	–	redox front
ox.	–	oxidised
red.	–	reduced
a.	–	argillic
b.	–	brecciated
f.	–	fractured
l.	–	leached
m.	–	mineralised
vm.	–	vein mineralisation

## Analysed Samples

Ns	–	nepheline syenite xenolith
VB	–	volcanic breccia
PH	–	volcanic phonolite

## **Borehole F1**

### **Osamu Utsumi mine, ore body E**

Mine coordinates:	9-1WC11
Altitude:	1324 m above sea level
Depth of borehole:	126 m
Inclination:	Vertical borehole
Drilling equipment:	Rotary coring system with water flushing
Core diameter:	47.6 mm

## Borehole F1: Major and trace element analyses.

Sample	1-1B	1-1C	10-1A	14-1A	16-1A	20-1A	20-1B	23-1A	26-1A	31-1A	33-1A	34-1B-B	34-1B-E	39-1A	41-1A
Depth (m)	0.6	0.75	9.85	13.45	15.05	19.1	19.65	22.05	25.17	30.2	32.94	33.38	33.63	38.22	40.08
Rock type	VLP Ox/a.	VLP Ox/a, vm,	VLP Ox/a.	VLP Ox/a.	VLP Ox.	VLP Ox/a.	VLP Ox/a.	VLP Ox/a.	VLP Ox/a, b.	VLP Ox.	VLP Ox.	VLP Ox/RF.	VLP Red/RF.	VLP Red.	LPh Red/a.
SiO <sub>2</sub>	54.49	42.24	56.05	55.51	57.30	57.04	56.02	58.32	53.67	56.67	58.61	59.45	60.92	56.77	58.28
TiO <sub>2</sub>	0.49	0.41	0.40	0.47	0.22	0.52	0.52	0.38	0.49	0.45	0.50	0.18	0.13	0.36	0.17
Al <sub>2</sub> O <sub>3</sub>	24.05	31.78	23.14	23.09	22.37	23.84	22.71	21.69	23.10	24.17	21.41	21.95	20.54	24.70	22.88
Fe <sub>tot</sub>	3.65	7.33	3.50	3.57	0.70	1.18	3.30	2.03	3.56	1.46	1.49	0.81	0.73	0.92	0.88
MnO	0.00	0.00	0.01	0.00	0.00	0.00	0.00	0.00	0.00	0.00	0.00	0.00	0.00	0.00	0.01
MgO	0.02	0.13	0.01	0.04	0.05	0.04	0.02	0.06	0.05	0.03	0.04	0.00	0.00	0.03	0.02
CaO	0.00	0.00	0.00	0.00	0.00	0.00	0.00	0.00	0.00	0.00	0.00	0.00	0.00	0.00	0.00
Na <sub>2</sub> O	0.35	0.18	0.27	0.39	3.03	0.27	0.26	0.30	2.19	0.48	0.34	0.84	0.45	0.28	1.00
K <sub>2</sub> O	12.33	9.95	13.64	13.62	13.53	13.42	13.58	14.33	11.76	13.10	13.81	14.22	14.50	11.99	14.19
P <sub>2</sub> O <sub>5</sub>	0.07	0.05	0.02	0.03	0.05	0.05	0.03	0.03	0.05	0.05	0.05	0.05	0.05	0.05	0.05
H <sub>2</sub> O	3.37	5.42	2.36	2.47	2.44	3.04	2.39	1.85	3.96	2.91	2.23	2.00	2.04	4.10	2.44
CO <sub>2</sub>	n.a.	n.a.	n.a.	n.a.	n.d.	n.a.	n.a.	n.a.	n.a.	n.a.	n.a.	n.a.	n.a.	n.a.	n.a.
Total (wt.%)	98.82	97.49	99.40	99.19	99.69	99.4	98.83	98.99	98.83	99.32	98.48	99.50	99.36	99.20	99.92
F (ppm)	n.a.	903	n.a.	n.a.	n.a.	1100	n.a.	1508	n.a.	n.a.	n.a.	n.a.	n.a.	n.a.	n.a.
Ba	567	225	568	618	767	650	626	733	4585	1324	1497	1067	870	418	553
Rb	321	320	350	359	414	343	351	369	304	345	353	355	373	319	347
Sr	176	35	175	163	243	180	183	155	174	136	193	139	146	80	136
Pb	34	19	23	39	19	9	45	59	23	b.d.	11	b.d.	48	11	13
Th	62	140	18	14	24	30	26	16	36	28	217	78	145	21	65
U	69	151	23	36	23	78	108	51	88	27	41	11	391	29	79
Nb	121	74	125	143	47	104	197	216	149	114	146	45	46	68	192
La	307	289	117	97	256	211	121	1498	176	140	120	137	131	1128	556
Ce	805	192	b.d.	393	268	1606	574	1276	327	136	137	185	184	746	468
Nd	105	114	21	51	71	26	42	288	67	31	22	40	55	254	128
Y	76	206	37	39	60	36	55	103	63	53	61	70	102	92	53
Zr	912	7847	567	649	403	420	892	977	1345	783	702	560	364	333	251
V	238	1352	150	156	212	196	143	165	257	142	144	119	30	65	109
Cr	b.d.	b.d.	b.d.	b.d.	14	b.d.	b.d.	b.d.	14	b.d.	b.d.	b.d.	b.d.	b.d.	b.d.
Ni	12	b.d.	9	9	9	b.d.	b.d.	b.d.	9	b.d.	b.d.	7	8	10	7
Co	b.d.	b.d.	b.d.	b.d.	b.d.	b.d.	b.d.	b.d.	b.d.	b.d.	b.d.	b.d.	7	7	b.d.
Cu	b.d.	b.d.	b.d.	b.d.	17	b.d.	b.d.	b.d.	10	b.d.	7	b.d.	b.d.	b.d.	4
Zn	20	46	10	14	18	b.d.	b.d.	7	18	b.d.	b.d.	b.d.	b.d.	b.d.	22
Hf	n.a.	169	n.a.	n.a.	n.a.	2	n.a.	12	n.a.	n.a.	n.a.	n.a.	n.a.	n.a.	n.a.
Ga	37	n.a.	35	42	42	n.a.	35	b.d.	44	37	30	26	18	29	34
Sc	2	6	1	1	7	4	3	6	10	2	1	1	b.d.	2	b.d.
S	b.d.	b.d.	b.d.	b.d.	b.d.	b.d.	b.d.	b.d.	104	64	127	24	2548	1983	2545

XRF-data; n.a. = not analysed, b.d. = below detection.

Borehole F1: Major and trace element analyses (contd.).

Sample Depth (m)	42-1A 41.87	43-1A 42.1	45-1A 44.87	47-1A 46.1	50-1A 49.82	55-1A 54.33	59-1A 58.15	59-1B 58.35	63-1A 62.9	67-1A-A 66.17	67-1A-E 66.27	68-1A 67.08	68-1AA 67.15	68-1AB 67.25	68-1AC 67.35	
Rock type	LPh Red/RF	LPh Ox/RF	LPh Ox.	LPh Ox/f.	LPh Ox/a.	LPh Ox/a, f.	LPh Ox.	LPh Ox/a.	LPh Ox/a, f.	LPh Ox/RF	LPh Red/RF	LPh Red/a, b.	LPh Red/a, b.	LPh Red/a, b.	LPh Red/a.	
SiO <sub>2</sub>	53.82	54.37	54.52	56.75	57.21	56.36	54.76	54.20	54.85	55.21	54.92	54.10	55.22	55.50	54.13	
TiO <sub>2</sub>	0.67	0.54	0.58	0.75	0.38	0.53	0.46	0.59	0.49	0.49	0.48	0.52	0.50	0.52	0.52	
Al <sub>2</sub> O <sub>3</sub>	23.28	22.66	23.56	22.56	23.56	22.08	23.77	23.28	24.13	23.53	22.89	21.46	22.64	22.14	21.77	
Fe <sub>tot</sub>	2.78	4.56	4.05	1.97	1.46	3.30	3.71	4.33	3.72	3.21	3.52	4.07	3.81	3.76	3.72	
MnO	0.02	0.01	0.00	0.00	0.00	0.00	0.00	0.00	0.01	0.00	0.00	0.01	0.00	0.00	0.00	
MgO	0.03	0.07	0.03	0.06	0.00	0.06	0.04	0.05	0.01	0.08	0.04	0.11	0.09	0.12	0.10	
CaO	0.00	0.00	0.00	0.00	0.00	0.00	0.00	0.00	0.00	0.00	0.00	0.00	0.00	0.01	0.00	
Na <sub>2</sub> O	1.25	1.51	0.30	0.16	0.28	0.16	0.57	0.21	0.25	0.31	0.39	1.31	0.24	0.25	0.18	
K <sub>2</sub> O	12.93	12.39	13.11	13.75	12.84	13.03	12.59	11.79	12.45	13.39	13.10	12.96	13.20	13.28	13.06	
P <sub>2</sub> O <sub>5</sub>	0.07	0.09	0.07	0.09	0.05	0.08	0.09	0.10	0.06	0.06	0.05	0.05	0.05	0.05	0.05	
H <sub>2</sub> O	3.74	3.35	2.86	2.95	3.03	3.98	3.28	4.97	3.50	2.68	3.87	4.84	3.99	3.94	4.29	
CO <sub>2</sub>	n.a.	n.a.	n.a.	n.a.	n.a.	n.a.	n.a.	n.a.	n.a.	n.a.	n.a.	n.a.	n.a.	n.a.	n.a.	
Total	(wt.%)	98.59	99.55	99.08	99.04	98.81	99.58	99.27	99.52	99.47	98.96	99.26	99.43	99.74	99.57	97.82
F	(ppm)	n.a.	n.a.	n.a.	1340	n.a.	1095	n.a.	1000	n.a.	n.a.	n.a.	n.a.	1091	1220	883
Ba	540	571	510	702	578	524	598	528	587	1449	386	383	310	298	315	
Rb	343	311	313	324	336	309	295	283	311	295	286	309	299	295	277	
Sr	205	191	158	160	196	180	207	211	226	140	149	196	192	167	148	
Pb	34	21	17	35	b.d.	31	29	27	59	8	13	22	15	13	b.d.	
Th	28	105	30	75	41	27	61	58	42	36	32	17	9	12	8	
U	2305	49	190	212	91	153	263	308	198	42	131	191	61	45	25	
Nb	272	197	324	184	70	236	278	328	256	238	268	306	244	257	220	
La	259	235	250	412	183	428	298	361	281	208	197	213	233	229	208	
Ce	152	188	772	2331	204	301	277	401	150	186	242	188	178	157	111	
Nd	70	69	97	85	84	79	90	71	60	47	82	46	33	25	16	
Y	99	55	59	68	86	66	101	141	56	63	52	38	48	39	23	
Zr	945	1451	752	857	3057	1101	1794	2208	596	649	1102	826	1425	1004	588	
V	388	312	171	400	135	170	263	269	296	200	148	318	259	244	251	
Cr	13	20	12	b.d.	b.d.	b.d.	b.d.	b.d.	b.d.	b.d.	b.d.	14	b.d.	b.d.	b.d.	
Ni	11	7	7	b.d.	7	b.d.	10	b.d.	6	7	7	6	b.d.	b.d.	b.d.	
Co	7	10	b.d.	b.d.	b.d.	b.d.	b.d.	b.d.	b.d.	b.d.	b.d.	b.d.	b.d.	b.d.	b.d.	
Cu	b.d.	8	4	b.d.	4	b.d.	4	b.d.	4	4	4	b.d.	b.d.	b.d.	b.d.	
Zn	b.d.	47	25	20	b.d.	80	9	14	7	b.d.	99	21	11	11	13	
Hf	n.a.	n.a.	n.a.	13	n.a.	11	n.a.	27	n.a.	n.a.	n.a.	n.a.	15	7	2	
Ga	532	48	41	n.a.	29	n.a.	45	n.a.	43	40	33	47	n.a.	n.a.	n.a.	
Sc	6	8	b.d.	5	b.d.	6	b.d.	6	b.d.	b.d.	b.d.	6	5	4	3	
S	1170	b.d.	62	b.d.	32	b.d.	b.d.	b.d.	47	350	16028	1414	1527	7384	7115	

XRF-data; n.a. = not analysed, b.d. = below detection.

## Borehole F1: Major and trace element analyses (contd.).

Sample Depth (m)	69-1B 68.9	71-1A 70.1	71-1B 70.55	74-1A 73.7	75-1BA 74.85	75-1BB 74.95	77-1A 76.5	77-1B 76.85	78-1A 77.45	81-1A 80.72	85-1A 84.2	90-1B 89.2	91-1A 90.8	95-1A 84.65	101-1A 100.3
Rock type	LPh Red/a.	NeS Red/a, b.	NeS Red/a, b.	LPh Red/a, vm.	LPh Red.	LPh Red.	LPh Red.	LPh Red.	LPh Red.	LPh Red.	LPh Red/a, vm.	LPh Red.	PicPh Red.	LPh Red.	LPh Red.
SiO <sub>2</sub>	55.68	57.19	58.23	53.59	55.82	56.53	56.51	56.59	56.70	56.10	51.82	56.01	56.52	57.71	55.33
TiO <sub>2</sub>	0.46	0.24	0.24	0.32	0.47	0.45	0.44	0.46	0.43	0.46	0.42	0.47	0.46	0.57	0.52
Al <sub>2</sub> O <sub>3</sub>	22.29	24.11	21.54	19.41	21.60	21.77	21.90	21.71	21.51	21.69	20.59	21.73	22.12	23.23	21.95
Fe <sub>tot</sub>	3.65	0.80	1.73	4.48	3.28	3.18	2.83	2.96	3.51	3.28	6.41	3.41	2.63	0.90	3.75
MnO	0.00	0.00	0.00	0.02	0.01	0.00	0.00	0.00	0.00	0.01	1.48	0.00	0.01	0.01	0.00
MgO	0.10	0.06	0.03	0.23	0.04	0.10	0.06	0.09	0.10	0.02	0.24	0.07	0.01	0.01	0.00
CaO	0.00	0.00	0.00	0.57	0.23	0.22	0.03	0.30	0.09	0.00	0.21	0.01	0.00	0.00	0.01
Na <sub>2</sub> O	0.20	0.16	0.42	0.35	0.58	0.33	0.43	0.36	0.29	0.33	0.49	0.68	0.30	0.38	0.35
K <sub>2</sub> O	13.44	13.07	13.25	12.35	13.70	13.76	13.96	13.86	14.04	14.04	11.39	13.01	13.06	14.49	13.48
P <sub>2</sub> O <sub>5</sub>	0.05	0.05	0.05	0.02	0.03	0.03	0.04	0.04	0.05	0.04	0.05	0.03	0.05	0.06	0.03
H <sub>2</sub> O	3.79	3.68	3.14	4.44	3.32	3.03	3.10	3.09	3.10	2.96	6.13	3.77	3.59	1.73	3.55
CO <sub>2</sub>	n.a.	n.a.	n.a.	n.a.	n.a.	n.a.	n.a.	n.a.	n.a.	n.a.	n.a.	n.a.	n.a.	n.a.	n.a.
Total (wt.%)	99.66	99.36	98.63	95.78	99.08	99.40	99.30	99.46	99.82	98.93	99.23	99.19	98.75	99.09	98.97
F (ppm)	953	1003	n.a.	n.a.	n.a.	2660	n.a.	2888	1527	n.a.	n.a.	n.a.	n.a.	n.a.	n.a.
Ba	345	457	417	533	375	415	445	477	451	477	973	1668	631	710	607
Rb	296	299	316	273	301	283	302	299	300	315	264	286	302	342	292
Sr	132	109	97	183	216	307	122	167	171	112	174	96	121	170	109
Pb	b.d.	b.d.	b.d.	27	b.d.	b.d.	b.d.	b.d.	b.d.	b.d.	b.d.	b.d.	b.d.	b.d.	b.d.
Th	14	13	31	6	15	b.d.	21	b.d.	5	21	41	14	22	26	30
U	86	206	89	17	20	5	17	3	30	30	37	25	14	13	31
Nb	249	395	445	240	211	234	235	207	222	243	247	200	241	241	248
La	260	291	337	6843	272	281	226	248	170	133	232	205	241	327	264
Ce	182	221	479	6272	335	208	278	205	141	203	362	308	351	398	339
Nd	31	43	145	1854	85	31	69	29	12	49	76	52	78	89	71
Y	43	22	50	461	34	29	38	30	19	23	39	32	35	54	48
Zr	806	198	2222	1109	706	655	544	767	851	667	645	1218	894	453	970
V	231	134	72	116	142	161	113	153	262	111	82	102	96	299	208
Cr	b.d.	b.d.	b.d.	46	b.d.	b.d.	b.d.	b.d.	b.d.	b.d.	b.d.	b.d.	b.d.	b.d.	b.d.
Ni	b.d.	b.d.	10	47	5	b.d.	b.d.	b.d.	b.d.	5	6	5	6	5	7
Co	b.d.	b.d.	b.d.	b.d.	b.d.	b.d.	b.d.	b.d.	b.d.	b.d.	b.d.	b.d.	b.d.	b.d.	b.d.
Cu	b.d.	b.d.	4	6	4	b.d.	4	b.d.	b.d.	4	4	4	4	4	4
Zn	16	b.d.	9	714	753	843	299	413	311	93	520	123	432	25	213
Hf	6	b.d.	n.a.	n.a.	n.a.	4	n.a.	4	5	n.a.	n.a.	n.a.	n.a.	n.a.	n.a.
Ga	n.a.	n.a.	39	45	38	n.a.	32	n.a.	n.a.	34	31	28	26	40	36
Sc	4	4	b.d.	b.d.	b.d.	4	b.d.	4	4	b.d.	b.d.	b.d.	b.d.	b.d.	b.d.
S	5821	2164	6785	18153	14074	1024	11477	9447	8004	13139	9126	9120	12576	890	17483

XRF-data; n.a. = not analysed, b.d. = below detection.

Borehole F1: Major and trace element analyses (contd.).

Sample Depth (m)	104-1A 103.9	105-1A 104.82	106-1A 105.43	107-1A 106.78	109-1A 108.92	109-1B 108.98	111-1A 110.13	112-1A 111.12	112-1AB 111.2	113-1A 112.13	113-1B 112.42	117-1A 116.96	118-1A 117.75	119-1A 118.2	121-1A 120.17
Rock type	LPh Red/vm.	VBr Red/a,vm.	LPh Red/f.	LPh Red/f.	LPh Red/a, f, l.	LPh Red.	LPh Red.	LPh Red/vm.	LPh Red.	LPh Red.	LPh Red.	LPh Red/a.	LPh Red.	LPh Red.	LPh Red.
SiO <sub>2</sub>	56.71	48.40	56.20	56.96	51.20	56.88	56.09	55.97	56.36	59.03	59.51	55.73	56.86	56.15	61.54
TiO <sub>2</sub>	0.55	0.37	0.48	0.52	0.72	0.51	0.48	0.56	0.41	0.08	0.39	0.55	0.32	0.49	0.08
Al <sub>2</sub> O <sub>3</sub>	21.73	20.48	21.66	21.92	25.54	22.25	22.18	18.51	21.71	22.18	21.63	22.44	21.76	22.66	19.12
Fe <sub>tot</sub>	2.38	1.56	3.20	2.56	3.84	2.28	3.12	5.64	3.09	0.73	0.99	3.34	2.75	2.44	0.84
MnO	0.01	0.00	0.00	0.01	0.03	0.00	0.00	0.00	0.00	0.01	0.00	0.00	0.02	0.02	0.01
MgO	0.04	0.00	0.02	0.04	0.07	0.06	0.03	0.02	0.08	0.02	0.05	0.07	0.04	0.02	0.00
CaO	0.00	0.09	0.00	0.00	0.46	0.00	0.00	0.00	0.01	0.50	0.28	0.13	0.02	0.06	0.24
Na <sub>2</sub> O	0.13	0.49	0.86	0.07	0.36	0.23	0.43	0.54	0.36	0.05	0.21	0.39	0.28	0.44	0.60
K <sub>2</sub> O	13.40	10.40	13.86	13.61	8.23	13.51	13.96	13.85	13.60	14.13	14.42	12.64	13.24	12.86	15.02
P <sub>2</sub> O <sub>5</sub>	0.11	0.68	0.10	0.06	0.09	0.09	0.05	0.04	0.04	0.07	0.06	0.06	0.09	0.07	0.05
H <sub>2</sub> O	3.34	5.33	3.13	3.24	7.50	3.47	2.99	3.70	3.25	2.17	2.21	4.11	3.58	3.70	1.25
CO <sub>2</sub>	n.a.	n.a.	n.a.	n.a.	n.a.	n.a.	n.a.	n.a.	n.a.	n.a.	n.a.	n.a.	n.a.	n.a.	n.a.
Total (wt.%)	9840	87.80	99.51	98.99	98.04	99.28	99.33	98.83	98.91	98.97	99.75	99.46	98.96	98.91	98.75
F (ppm)	n.a.	n.a.	n.a.	n.a.	n.a.	1102	n.a.	n.a.	1331	n.a.	2343	1098	n.a.	n.a.	n.a.
Ba	1095	937	779	719	446	891	589	376	634	882	761	660	786	783	715
Rb	316	151	292	331	197	286	304	290	305	345	331	284	305	286	379
Sr	480	689	453	255	112	421	237	289	180	240	188	155	100	128	130
Pb	7	1202	9	b.d.	b.d.	b.d.	48	11	b.d.	b.d.	b.d.	b.d.	b.d.	b.d.	b.d.
Th	127	3651	91	29	12	83	59	45	35	52	22	13	26	51	40
U	18	210	51	25	94	10	24	24	b.d.	17	b.d.	79	12	42	10
Nb	202	105	225	229	336	205	286	507	224	17	91	303	76	338	83
La	168	14204	276	155	259	308	259	322	504	193	417	259	167	227	233
Ce	258	22807	435	240	446	243	371	572	535	341	374	230	293	321	310
Nd	22	5578	97	41	65	41	88	187	127	60	68	47	41	69	65
Y	89	970	127	67	77	68	59	110	91	88	59	72	51	46	43
Zr	2323	405	1559	1754	2084	898	855	2785	2790	1735	740	2068	733	431	258
V	592	247	258	311	90	408	176	185	247	257	218	231	155	97	36
Cr	b.d.	102	b.d.	b.d.	b.d.	b.d.	b.d.	b.d.	b.d.	b.d.	b.d.	b.d.	b.d.	b.d.	b.d.
Ni	b.d.	93	12	b.d.	b.d.	b.d.	6	15	b.d.	b.d.	b.d.	b.d.	b.d.	b.d.	b.d.
Co	b.d.	9	b.d.	b.d.	b.d.	b.d.	b.d.	b.d.	b.d.	b.d.	b.d.	b.d.	b.d.	b.d.	b.d.
Cu	b.d.	21	4	b.d.	b.d.	b.d.	4	4	b.d.	b.d.	b.d.	b.d.	b.d.	4	4
Zn	139	4424	145	107	119	151	83	188	81	81	144	494	42	109	19
Hf	n.a.	n.a.	n.a.	n.a.	n.a.	8	n.a.	n.a.	38	n.a.	6	23	n.a.	n.a.	n.a.
Ga	56	34	41	42	37	n.a.	36	41	n.a.	40	n.a.	n.a.	43	31	29
Sc	7	8	b.d.	7	4	4	b.d.	b.d.	4	7	4	4	6	b.d.	b.d.
S	10081	7548	14482	10079	15148	842	11823	29553	4191	2459	3831	3743	11741	11914	2366

XRF-data; n.a. = not analysed, b.d. = below detection.

## Borehole F1: Major and trace element analyses (contd.).

Sample	126-1A	126-1BA	126-1BB	
Depth (m)	125.35	125.6	125.7	
Rock type	LPh Red.	LPh Red.	LPh Red.	
SiO <sub>2</sub>	56.09	56.56	55.72	
TiO <sub>2</sub>	0.45	0.53	0.69	
Al <sub>2</sub> O <sub>3</sub>	22.10	22.03	21.41	
Fe <sub>tot</sub>	1.83	2.36	2.83	
MnO	0.13	0.11	0.44	
MgO	0.02	0.06	0.07	
CaO	1.09	0.28	0.43	
Na <sub>2</sub> O	0.32	0.31	0.48	
K <sub>2</sub> O	13.25	13.62	13.22	
P <sub>2</sub> O <sub>5</sub>	0.05	0.06	0.06	
H <sub>2</sub> O	3.50	3.46	3.93	
CO <sub>2</sub>	n.a.	n.a.	n.a.	
Total	(wt.%)	98.83	99.38	99.28
F	(ppm)	n.a.	2100	2733
Ba		750	863	824
Rb		301	296	291
Sr		206	132	131
Pb		b.d.	b.d.	b.d.
Th		14	10	5
U		7	b.d.	b.d.
Nb		97	100	131
La		301	352	457
Ce		355	302	430
Nd		82	49	71
Y		55	33	44
Zr		248	403	532
V		232	471	393
Cr		b.d.	b.d.	b.d.
Ni		b.d.	b.d.	b.d.
Co		b.d.	b.d.	b.d.
Cu		4	b.d.	b.d.
Zn		132	77	139
Hf		n.a.	b.d.	1
Ga		37	n.a.	n.a.
Sc		b.d.	5	6
S		5273	9303	7972

XRF-data; n.a. = not analysed, b.d. = below detection.

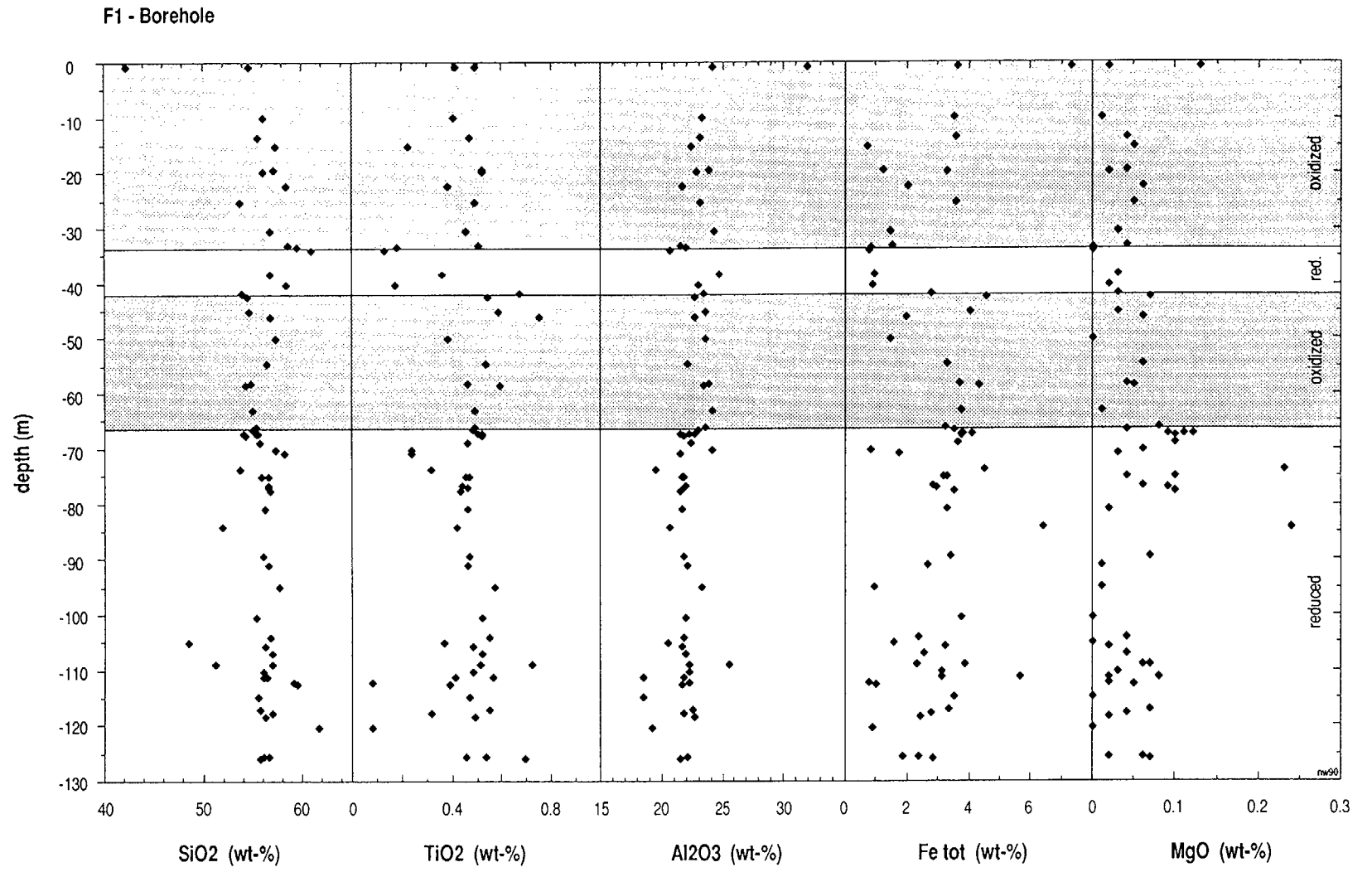
Borehole F1: As and Se-analyses.

Sample	Depth (m)	Rock	Type	As (ppm)	Se (ppb)
F1-16-1A	15.05	VLPb	Ox.	5	n.a.
F1-26-1A	25.17	VLPb	Ox.	21	139
F1-33-1A	32.94	VLPb	Ox.	5	n.a.
F1-34-1B-E	33.63	VLPb	Red.	5	n.a.
F1-39-1A	38.22	LPh	Red.	b.d.	n.a.
F1-42-1A	41.87	LPh	Red.	b.d.	14
F1-43-1A	42.10	LPh	Ox.	13	62
F1-45-1A	44.87	LPh	Ox.	17	n.a.
F1-59-1A	58.35	LPh	Ox.	50	n.a.
F1-66-1A	65.92	LPh	Ox.	4	n.a.
F1-67-1A-E	66.27	LPh	Red.	7	n.a.
F1-68-1A	67.08	LPh	Red.	10	n.a.
F1-74-1A	73.70	LPh	Red.	b.d.	0.74
F1-91-1A	90.80	PlcPh	Red.	7	n.a.
F1-101-1A	100.32	LPh	Red.	n.a.	1.4
F1-105-1A	104.82	VBr	Red.	b.d.	n.a.
F1-119-1A	108.92	LPh	Red.	7	n.a.
F1-122-1A	121.75	LPh	Red.	n.a.	1.4
F1-126-1A	125.35	LPh	Red.	17	n.a.

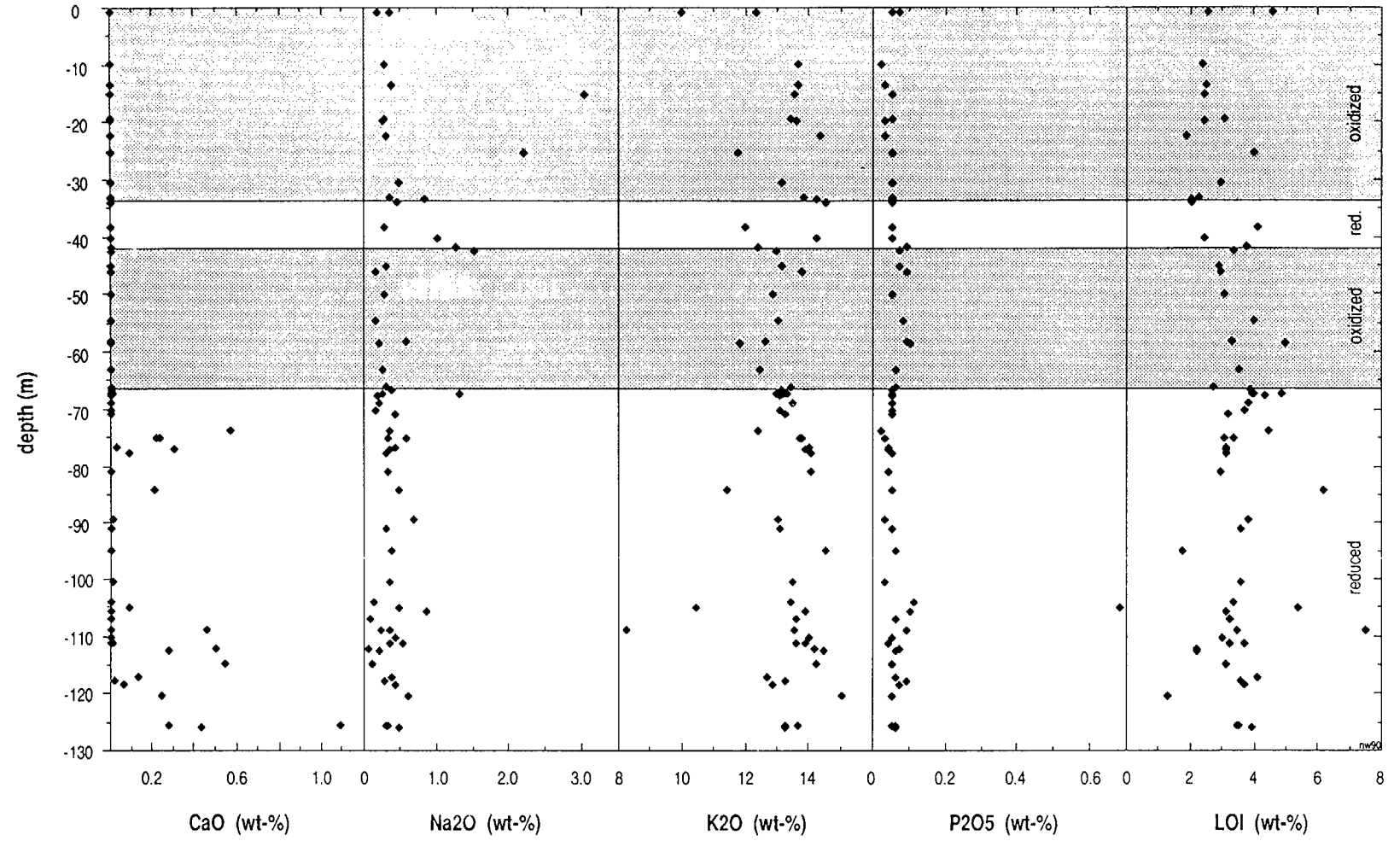
As: manual XRF-data (detection limit 1 ppm).

Se: neutron activation data.

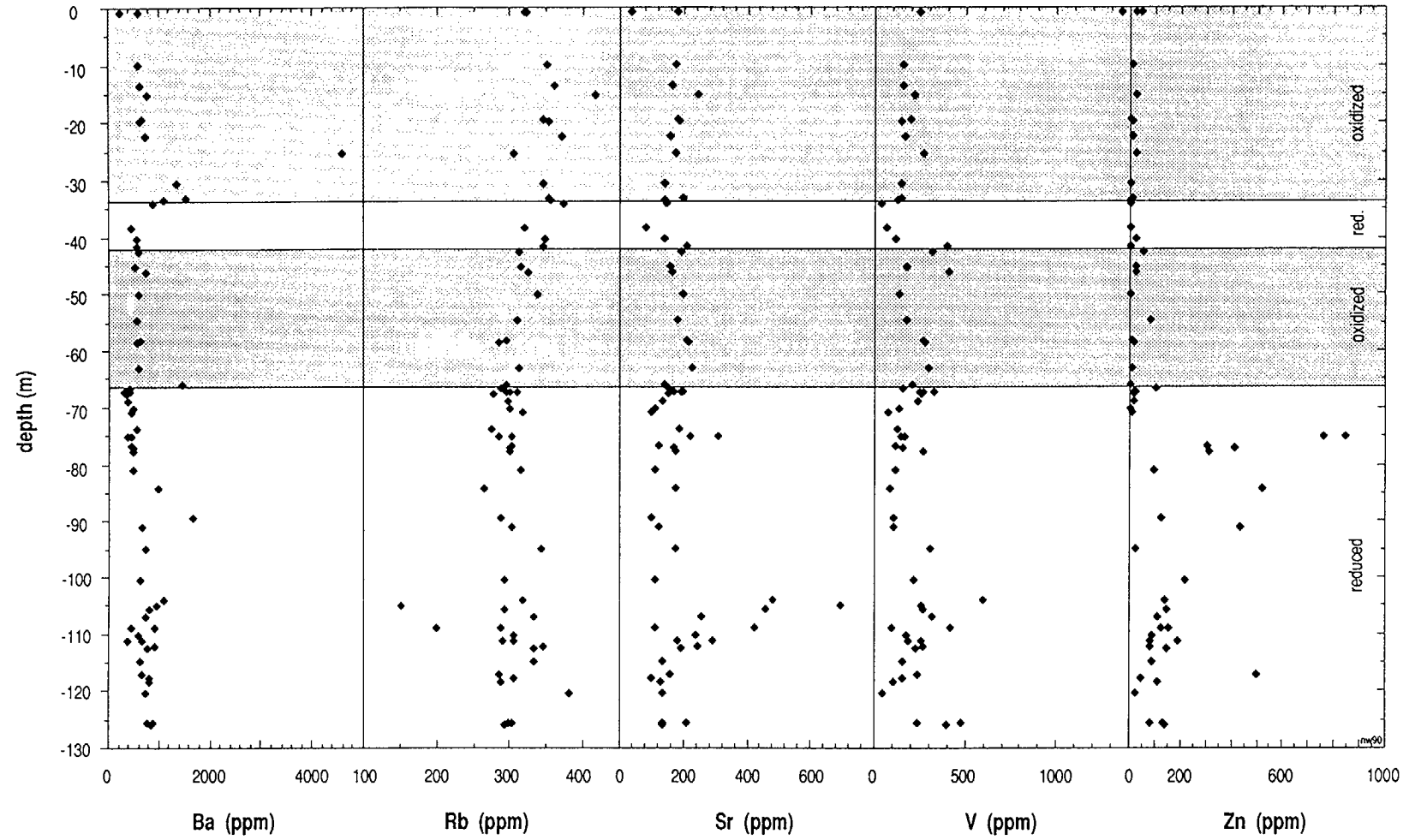
n.a. = not analysed; b.d. = below detection.



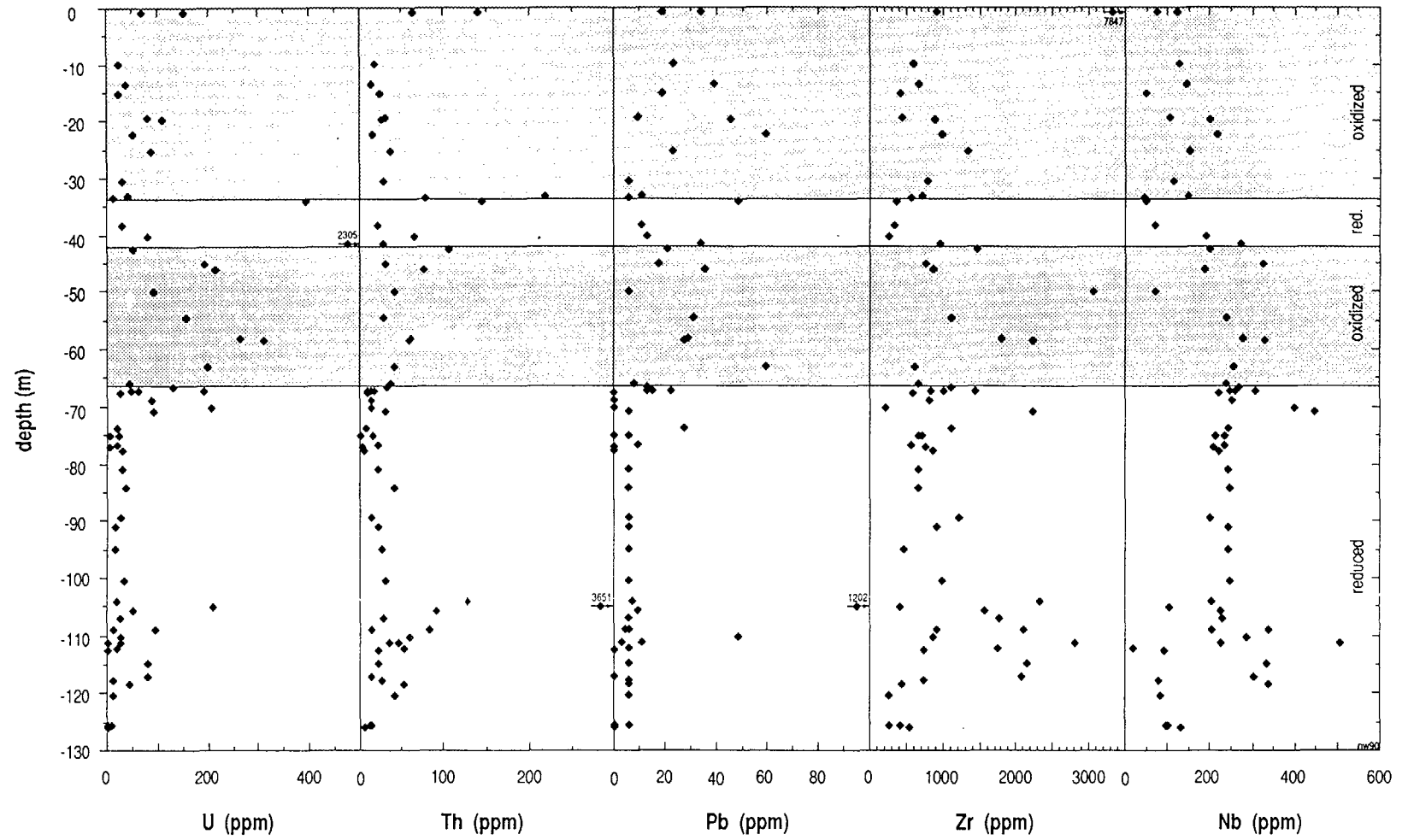
F1 - Borehole



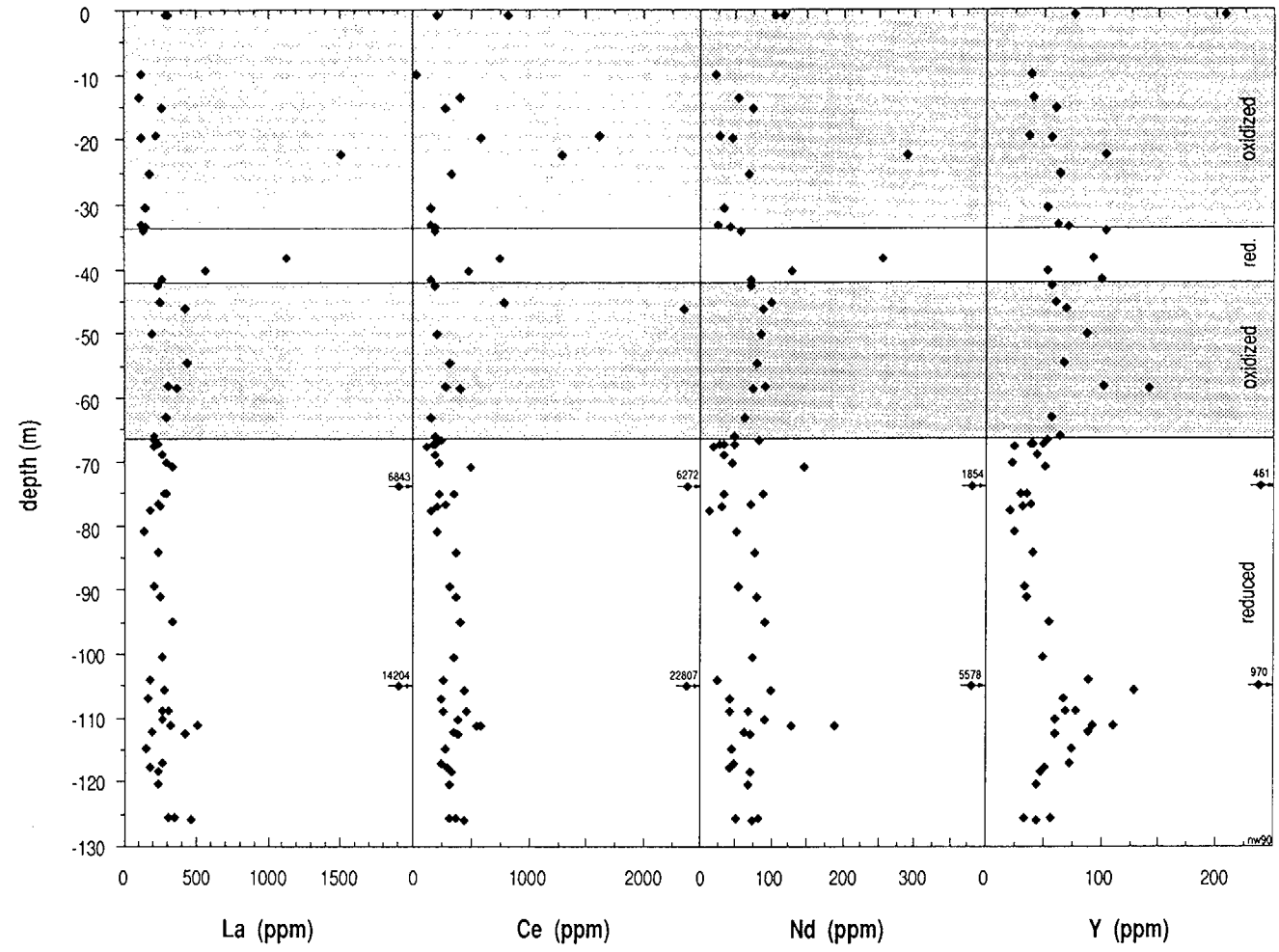
F1 - Borehole



F1 - Borehole



F1 - Borehole



### **Borehole F3**

#### **Osamu Utsumi mine, ore body E**

Mine coordinates:	9-1NH47
Altitude:	1320 m above sea level
Depth of borehole:	80 m
Inclination:	55° to the horizontal plane
Drilling equipment:	Rotary coring system with water flushing
Core diameter:	0.0 – 27.45 m : 63.5 mm 27.65 – 80.0 m : 47.6 mm

## Borehole F3: Major and trace element analyses.

Sample Depth (m)	2-1A 1.25	10-1A 9.45	20-1B 19.75	21-1B 20.80	23-1B 22.38	28-1A 27.23	36-1A 35.18	43-1A 41.98	46-1B 45.84	48-1A 47.27	49-1A 48.60	53-1A 52.51	59-1A 58.49	64-1A 63.85	69-1A 68.50	
Rock type	VLPh Red/a, b.	VLPh Red.	PlcCpxPh Red.	PlcCpxPh Red.	PlcCpxPh Red.	PlcCpxPh Red.	PlcCpxPh Red.	PlcCpxPh Red.	PlcCpxPh Red/a, b.	PlcCpxPh Red.	PlcCpxPh Red.	PlcCpxPh Red/b, vm.	PlcCpxPh Red/b, vm.	PlcCpxPh Red/b, vm.	PlcCpxPh Red.	
SiO <sub>2</sub>	53.75	56.00	54.74	54.74	55.14	55.58	57.29	54.95	56.64	56.76	55.58	55.32	53.59	55.62	56.32	
TiO <sub>2</sub>	0.47	0.61	0.45	0.41	0.39	0.36	0.43	0.41	0.44	0.40	0.39	0.38	0.43	0.40	0.40	
Al <sub>2</sub> O <sub>3</sub>	21.65	21.48	22.01	21.84	21.56	21.33	23.23	22.76	23.19	22.83	22.01	21.44	21.97	22.16	21.62	
Fe <sub>tot</sub>	4.22	3.02	3.39	3.56	3.25	2.67	1.21	2.77	1.34	1.05	3.22	2.97	3.22	2.24	2.41	
MnO	0.00	0.00	0.00	0.00	0.00	0.00	0.00	0.00	0.00	0.00	0.00	0.00	0.00	0.00	0.00	
MgO	0.11	0.16	0.20	0.17	0.11	0.22	0.17	0.12	0.16	0.11	0.20	0.15	0.14	0.11	0.11	
CaO	0.07	0.10	0.07	0.07	0.04	0.07	0.08	0.06	0.07	0.04	0.07	0.05	0.10	0.05	0.05	
Na <sub>2</sub> O	0.83	1.62	0.90	1.22	0.95	0.88	1.05	0.80	0.99	0.77	1.62	0.89	1.22	1.05	1.13	
K <sub>2</sub> O	11.55	13.16	13.50	13.21	13.16	13.40	13.56	12.74	13.72	13.43	13.41	13.49	11.87	13.38	13.59	
P <sub>2</sub> O <sub>5</sub>	0.14	0.14	0.09	0.09	0.08	0.30	0.07	0.10	0.06	0.06	0.08	0.21	0.36	0.11	0.08	
H <sub>2</sub> O	5.05	3.47	3.03	3.16	3.18	2.96	2.23	3.42	1.86	2.23	2.61	2.83	4.22	2.58	2.51	
CO <sub>2</sub>	0.33	0.33	0.19	0.44	0.38	0.27	0.10	0.32	0.16	0.12	0.24	0.26	0.26	0.23	0.24	
Total	(wt.%)	98.17	100.09	98.57	98.91	98.24	98.04	99.42	98.45	98.63	97.80	99.43	97.99	97.38	97.93	98.46
F	(ppm)	1706	1495	1735	1671	1631	1597	1354	1302	1478	1146	1369	1578	1830	1271	1312
Ba	444	357	741	661	704	1941	692	965	640	1215	773	1346	2072	847	779	
Rb	235	280	303	277	264	278	308	268	322	301	286	285	249	282	315	
Sr	307	531	435	508	436	704	617	456	675	559	481	795	842	622	619	
Pb	134	62	96	136	19	69	39	20	16	30	401	38	385	41	11	
Th	90	44	23	41	45	47	61	158	41	76	40	18	113	38	50	
U	81	50	111	58	36	120	17	b.d.	b.d.	b.d.	25	169	116	26	30	
Nb	326	296	246	201	198	207	238	223	237	212	190	228	248	201	228	
La	1551	617	556	572	622	511	273	292	199	273	275	305	858	399	220	
Ce	1626	546	590	576	643	539	265	240	189	269	299	303	907	382	158	
Nd	366	119	126	139	137	115	43	52	30	60	53	65	162	70	b.d.	
Y	125	85	132	148	117	183	83	95	102	93	67	84	119	78	60	
Zr	1090	643	1788	1691	988	2914	883	679	1009	1124	1266	2782	1949	772	929	
V	120	175	179	143	132	181	351	773	147	233	203	225	172	315	283	
Cr	10	b.d.	b.d.	b.d.	b.d.	b.d.	b.d.	b.d.	b.d.	b.d.	b.d.	b.d.	b.d.	b.d.	b.d.	
Ni	b.d.	b.d.	b.d.	b.d.	b.d.	b.d.	b.d.	b.d.	b.d.	b.d.	b.d.	b.d.	b.d.	b.d.	b.d.	
Co	4	4	5	4	b.d.	b.d.	5	4	7	b.d.	4	4	b.d.	b.d.	b.d.	
Cu	b.d.	b.d.	b.d.	b.d.	b.d.	b.d.	b.d.	b.d.	b.d.	b.d.	b.d.	b.d.	b.d.	b.d.	b.d.	
Zn	371	185	172	285	299	279	108	298	97	156	338	307	472	342	239	
Hf	13	5	24	21	7	38	11	4	12	14	13	34	26	6	8	
Sc	5	5	8	7	7	5	5	5	5	5	6	5	8	6	5	
S	12480	8498	13969	9502	8621	7186	1011	7968	504	1406	7367	8747	11011	5193	5937	

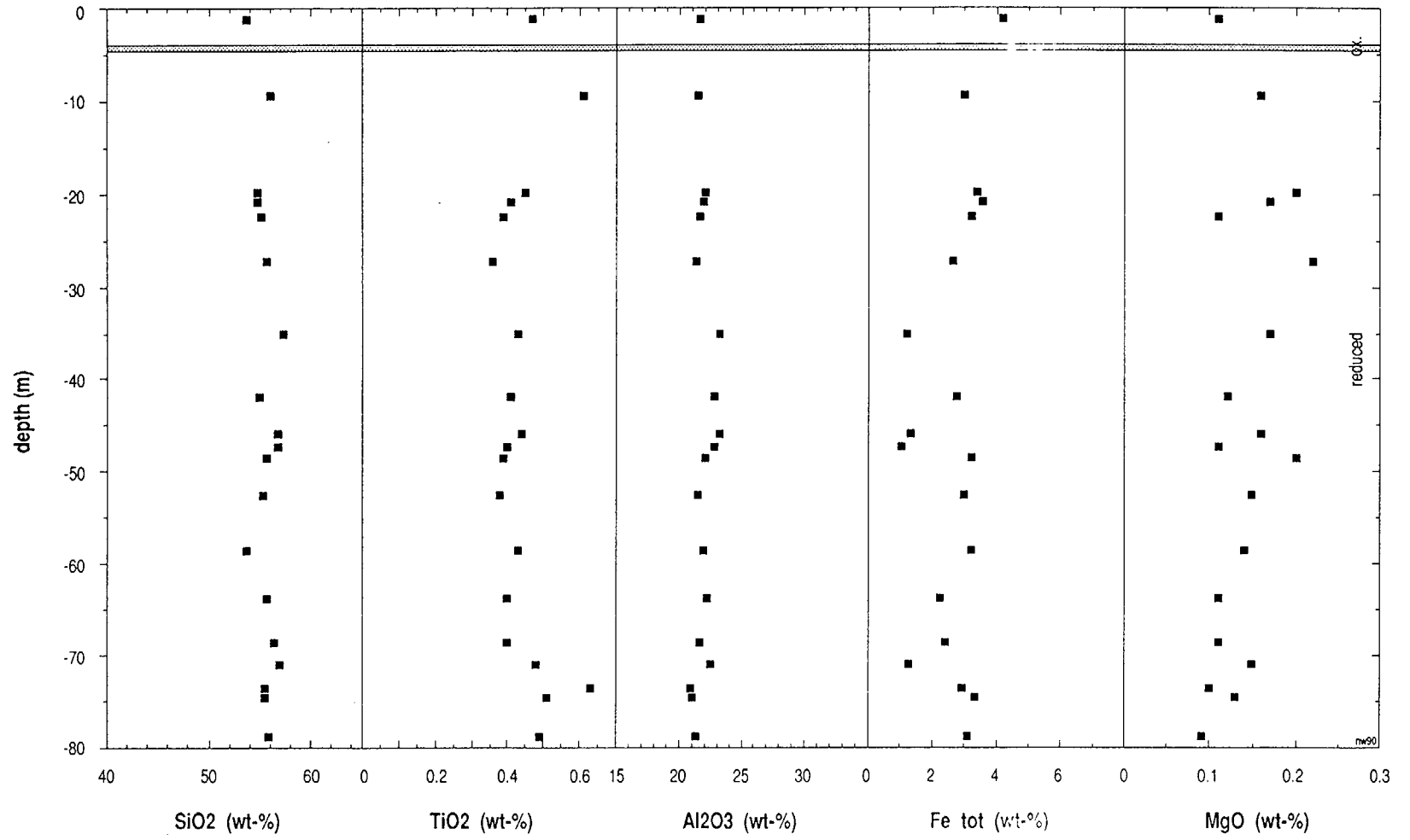
XRF-data; n.a. = not analysed, b.d. = below detection.

Borehole F3: Major and trace element analyses (contd.).

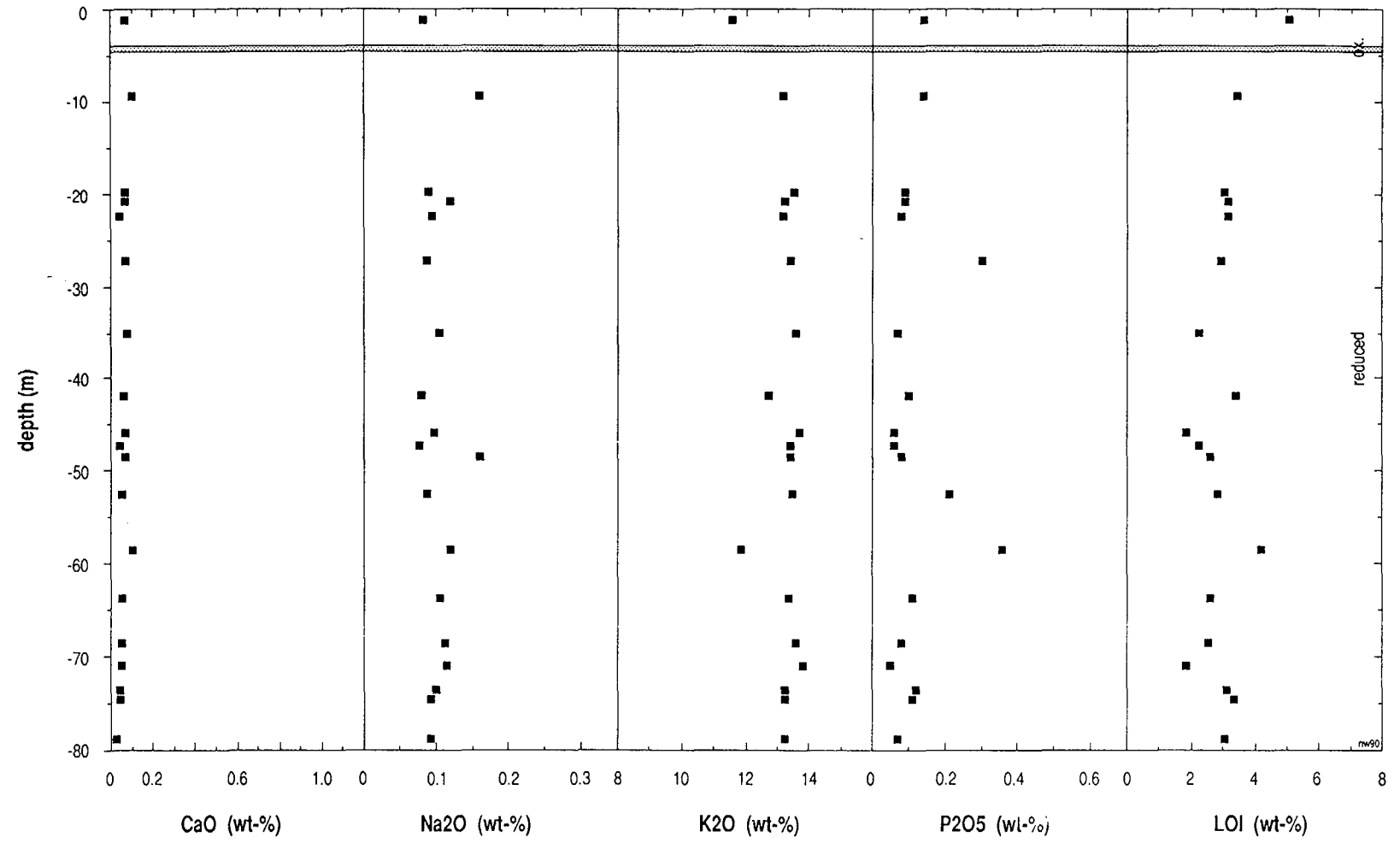
Sample	72-1A	74-1B	75-1A	79-1A	
Depth (m)	71.07	73.62	74.66	78.75	
Rock type	PlcPh Red/f.	PlcPh Red.	PlcPh Red.	PlcPh Red.	
SiO <sub>2</sub>	56.83	55.47	55.41	55.87	
TiO <sub>2</sub>	0.48	0.63	0.51	0.49	
Al <sub>2</sub> O <sub>3</sub>	22.46	20.84	21.10	21.35	
Fe <sub>tot</sub>	1.26	2.91	3.31	3.09	
MnO	0.00	0.00	0.00	0.00	
MgO	0.15	0.10	0.13	0.09	
CaO	0.05	0.04	0.04	0.03	
Na <sub>2</sub> O	1.15	1.01	0.93	0.92	
K <sub>2</sub> O	13.84	13.23	13.22	13.24	
P <sub>2</sub> O <sub>5</sub>	0.05	0.12	0.11	0.07	
H <sub>2</sub> O	1.83	3.09	3.34	3.05	
CO <sub>2</sub>	0.09	0.24	0.27	0.23	
<b>Total</b>	<b>(wt.%)</b>	<b>98.19</b>	<b>97.68</b>	<b>98.37</b>	<b>98.43</b>
F	(ppm)	1487	1280	1332	1229
Ba		354	752	630	627
Rb		327	302	299	280
Sr		559	222	307	214
Pb		15	60	28	40
Th		55	103	41	66
U		43	77	64	17
Nb		247	250	266	249
La		276	549	354	220
Ce		271	561	324	190
Nd		51	114	59	37
Y		71	101	87	49
Zr		1449	2011	1650	1159
V		205	180	212	211
Cr		b.d.	b.d.	b.d.	b.d.
Ni		b.d.	b.d.	b.d.	b.d.
Co		5	b.d.	b.d.	b.d.
Cu		b.d.	b.d.	b.d.	b.d.
Zn		274	189	320	223
Hf		21	27	22	11
Sc		6	6	6	5
S		863	7988	8904	7889

XRF-data; n.a. = not analysed, b.d. = below detection.

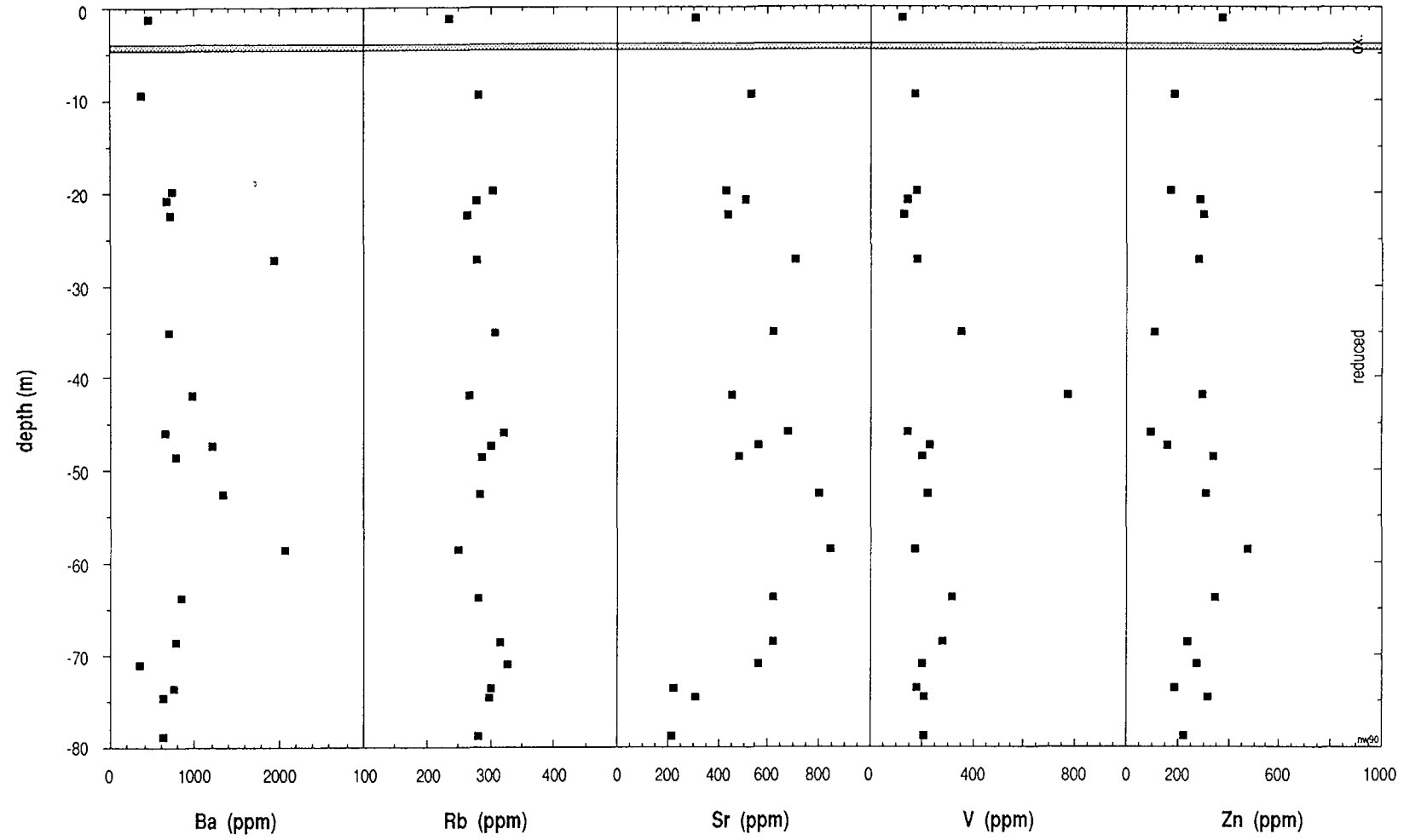
F3 - Borehole



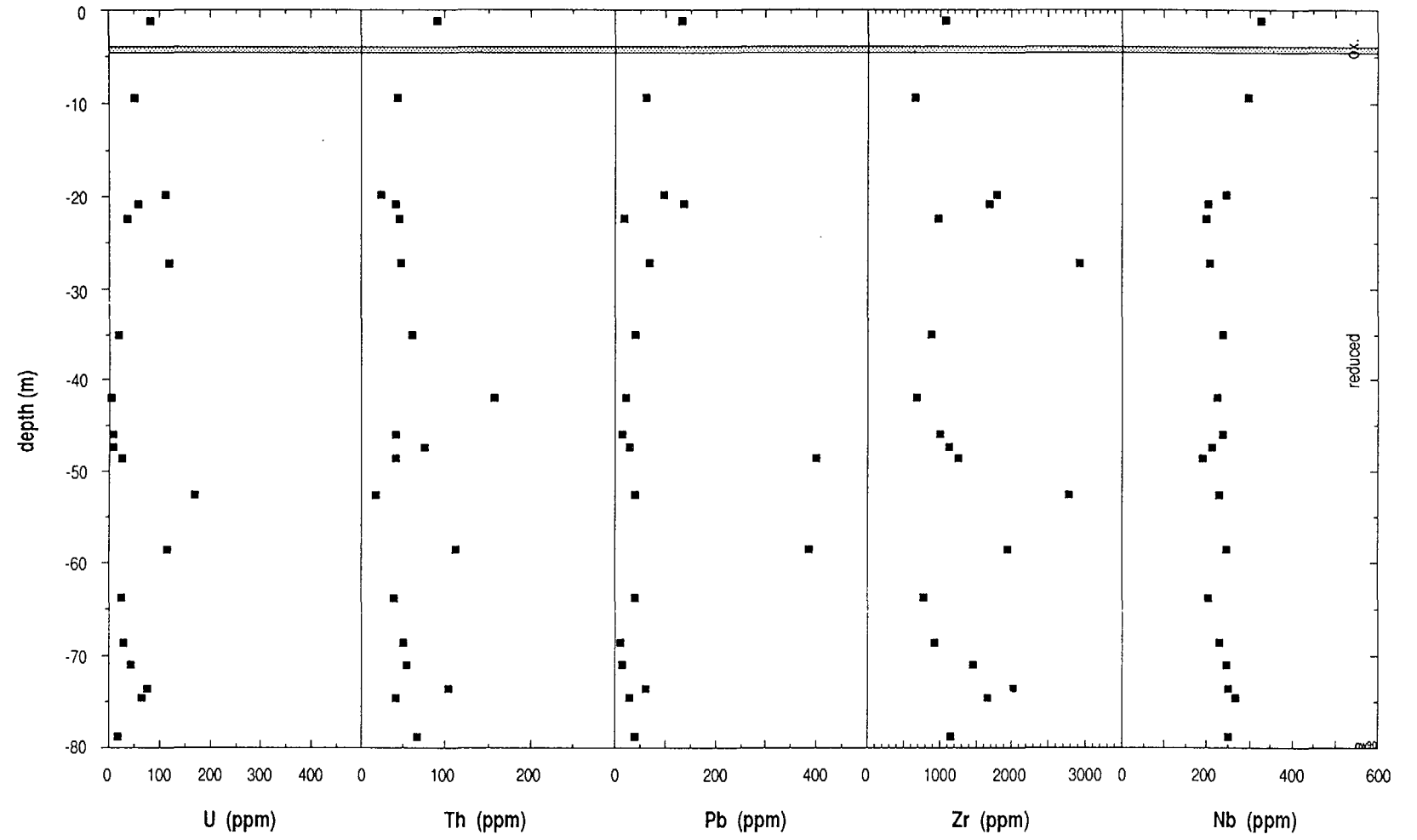
F3 - Borehole



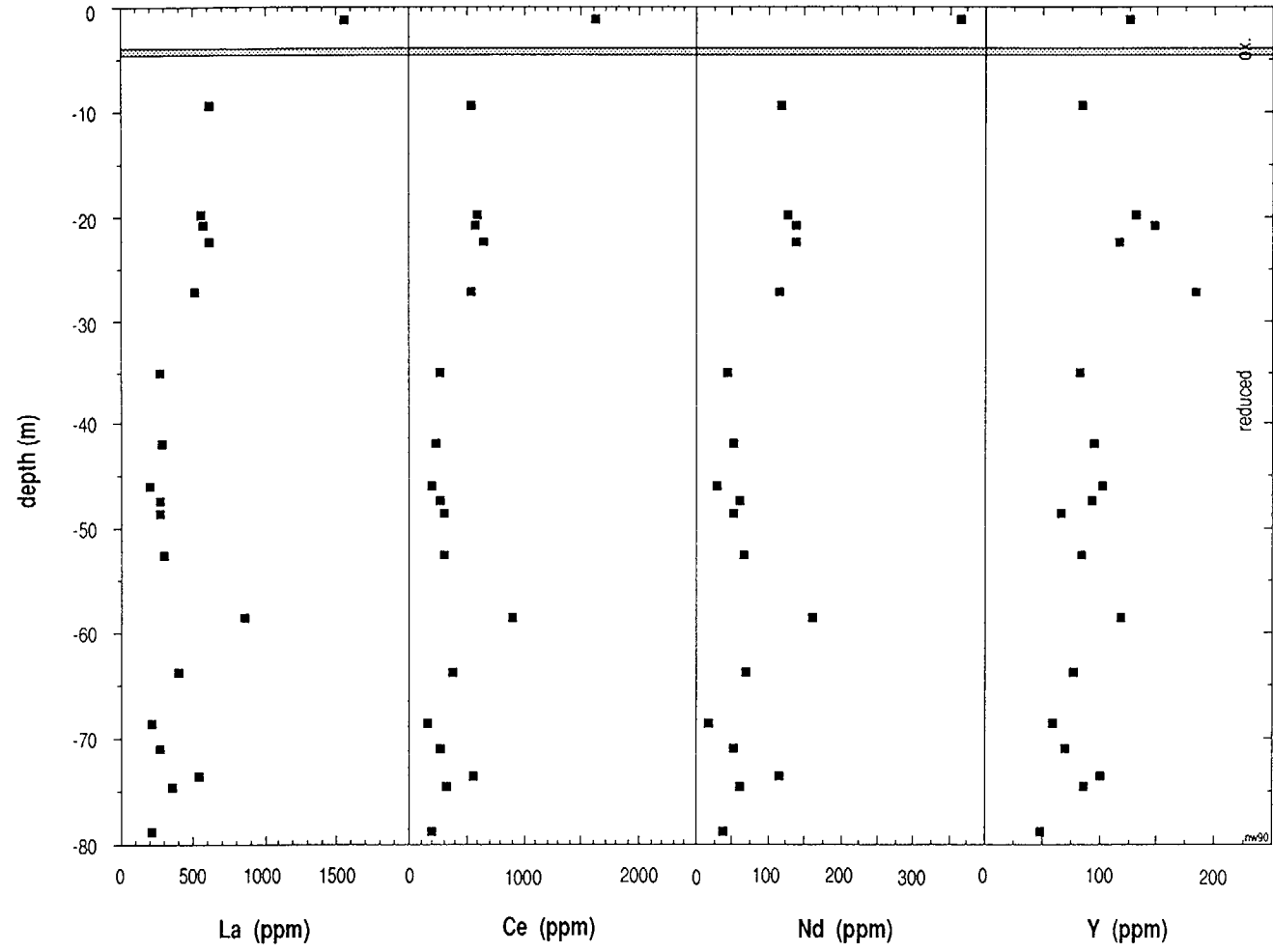
F3 - Borehole



F3 - Borehole



F3 - Borehole



## **Borehole F4**

### **Osamu Utsumi mine, ore body B**

Mine coordinates:	8-1UK11
Altitude:	1332 m above sea level
Depth of borehole:	414.76 m
Inclination:	55° to the horizontal plane
Drilling equipment:	Rotary coring system with water flushing
Core diameter:	0.0 – 100.22 m : 63.5 mm 100.22 – 414.76 m : 47.6 mm

## Borehole F4: Major and trace element analyses.

Sample	19-1A	22-1A	39-1A	91-1B	107-1A	123-1A	129-1A	210-A	210-AB	210-A2	210-A3	212-A1	212-A2	243-A1	243-A2
Depth (m)	18.61	21.1	38.75	90.05	106.44	122.71	128.48	209.59	209.59	209.59	209.59	212.7	212.7	243.3	243.3
Rock type	LPh Ox/a.	NeS Ox/a.	PlcPh Ox/a.	NeS Red/b.	NeS Red/a, b.	NeS Red/vm.	LPh Red/b, vm.	LPh Red/b, vm.	LPh Red/b, vm.	VBr Red/m.	LPh Red/b, vm.	VBr Red/m.	VBr Red/m.	VBr Red/m.	VBr Red/m.
SiO <sub>2</sub>	53.04	53.45	54.33	52.60	54.16	55.18	52.48	54.44	53.66	52.4	52.61	55.06	54.47	55.08	49.23
TiO <sub>2</sub>	0.65	0.70	0.99	0.56	0.50	0.44	0.41	0.45	0.52	0.48	0.33	0.38	0.52	0.51	0.35
Al <sub>2</sub> O <sub>3</sub>	25.22	24.88	23.75	22.49	23.07	20.11	18.64	20.85	20.63	21.91	20.63	22.08	21.18	21.82	17.83
Fe <sub>tot</sub>	2.79	2.41	2.57	3.16	2.99	3.57	3.89	5.09	4.61	3.32	5.99	3.74	3.26	2.72	7.39
MnO	0.00	0.17	0.02	0.00	0.16	0.40	0.91	0.01	0.01	0.01	0.01	0.01	0.02	0.02	0.03
MgO	0.16	0.12	0.12	0.17	0.19	0.10	0.15	0.16	0.17	0.19	0.13	0.17	0.19	0.19	0.12
CaO	0.04	0.02	0.02	1.63	1.32	1.19	2.49	0.11	0.13	0.22	0.77	0.51	0.39	0.14	0.3
Na <sub>2</sub> O	1.04	0.83	0.74	0.80	1.90	0.55	0.53	0.01	0.01	0.01	0.01	0.01	0.01	0.01	0.01
K <sub>2</sub> O	11.64	11.96	12.48	12.77	9.46	13.27	12.24	13.12	12.55	12.12	12.48	12.96	12.55	12.9	11.24
P <sub>2</sub> O <sub>5</sub>	0.17	0.13	0.14	0.09	0.11	0.05	0.18	0.27	0.31	0.55	0.27	0.26	0.58	0.35	0.56
H <sub>2</sub> O	3.79	3.54	2.92	3.90	4.07	2.53	3.68	4.77	5.1	5.05	6.3	4.59	4.39	3.98	7
CO <sub>2</sub>	0.12	0.15	0.19	0.19	0.44	0.69	1.42	n.a.	n.a.	n.a.	n.a.	n.a.	n.a.	n.a.	n.a.
Total	(wt.%)	98.66	98.36	98.27	98.36	98.37	98.08	97.02	99.28	97.7	96.26	99.53	99.77	97.56	94.06
F	(ppm)	1820	1699	1544	8101	5946	6989	11579	n.a.	n.a.	n.a.	n.a.	n.a.	n.a.	n.a.
Ba	679	815	1312	787	677	780	444	655	446	291	780	651	437	437	311
Rb	268	282	280	315	239	289	248	300	278	274	283	291	310	303	285
Sr	123	144	100	335	387	176	577	454	415	726	561	449	707	1482	1372
Pb	39	313	43	5	51	11	59	87	68	363	59	63	186	62	170
Th	51	94	62	28	17	17	62	72	19	121	94	97	244	54	84
U	107	118	101	43	864	78	184	1480	1509	2225	1714	899	4212	1771	5057
Nb	264	264	299	215	276	148	232	241	262	293	183	178	458	379	498
La	1836	1230	634	479	395	186	1641	715	876	1328	674	726	1422	280	514
Ce	1459	1658	659	538	396	189	2253	829	1030	1568	743	835	1785	376	631
Nd	448	266	142	108	70	35	441	212	285	439	185	208	488	104	170
Y	83	147	120	35	32	62	105	159	247	246	125	120	238	91	139
Zr	616	1072	1167	645	383	2082	4529	4498	10574	9715	2132	2779	7449	15242	19997
V	268	404	418	345	336	192	146	260	250	400	228	337	331	231	129
Cr	b.d.	b.d.	b.d.	b.d.	b.d.	b.d.	12	9	14	18	13	11	16	8	21
Ni	b.d.	b.d.	b.d.	b.d.	b.d.	b.d.	b.d.	98	235	595	303	50	158	34	117
Co	6	8	6	4	5	5	9	38	32	570	33	15	27	29	23
Cu	b.d.	b.d.	b.d.	b.d.	b.d.	b.d.	b.d.	b.d.	b.d.	b.d.	b.d.	b.d.	b.d.	b.d.	b.d.
Zn	76	74	72	37	79	256	68	1965	1850	2716	2261	1264	2699	555	2755
Ga	n.a.	n.a.	n.a.	n.a.	n.a.	n.a.	n.a.	36	34	45	33	42	43	43	34
Hf	5	10	9	b.d.	b.d.	25	57	73	150	138	38	48	115	203	245
Sc	4	6	6	3	b.d.	4	3	n.a.	n.a.	n.a.	n.a.	n.a.	n.a.	n.a.	n.a.
S	196	56	b.d.	18134	5498	13441	22781	20611	21911	21658	27858	15870	15381	17203	34162

XRF-data; n.a. = not analysed, b.d. = below detection.

Borehole F4: Major and trace element analyses (contd.).

Sample	243-A3	243-A4A	243-A4B	243-A5	243-A6	252-A1	252-A2	252-A3	252-A4	252-A5	252-A6	252-A7	265-1A-B	383-A	386-A	
Depth (m)	243.3	243.3	243.3	243.5	243.5	252.7	252.7	252.7	252.8	252.8	252.8	252.8	264.35	382.55	385.52	
Rock type	VBr Red/m.	VBr Red/m.	VBr Red/m.	NeS Red/m.	NeS Red/m.	NeS Red/vm.	NeS Red/vm.	NeS Red/vm.	VBr Red/m.	VBr Red/m.	VBr Red/m.	VBr Red/m.	NeS Red/m.	VBr Red/m.	VBr Red/m.	
SiO <sub>2</sub>	52.31	54.94	56.99	59.3	60.02	53.77	54.21	55.11	52.53	54.37	54.02	51.36	50.45	44.9	48.62	
TiO <sub>2</sub>	0.48	0.47	0.34	0.2	0.14	0.81	0.76	0.81	0.56	0.53	0.75	0.55	0.49	0.35	2.86	
Al <sub>2</sub> O <sub>3</sub>	21.03	20.32	19.14	19.12	19.75	23.8	23.39	23.08	20.55	16.62	16.91	15.42	22.98	13.86	14.78	
Fe <sub>tot</sub>	3.52	2.46	2.19	1.75	1.57	3.19	3.05	2.42	2.35	5.22	4.02	3.94	4.32	17.24	13.63	
MnO	0.02	0.03	0.03	0.03	0.02	0.01	0.01	0.01	0.02	0.02	0.03	0.04	0.07	0.02	0.01	
MgO	0.17	0.12	0.1	0.1	0.12	0.17	0.16	0.12	0.1	0.1	0.1	0.1	0.34	0.1	0.1	
CaO	0.28	0.22	0.22	0.22	0.26	0.63	1.13	0.4	0.2	0.08	0.11	0.12	0.60	0.23	0.26	
Na <sub>2</sub> O	0.01	0.01	0.01	0.01	0.01	0.01	0.01	0.01	0.01	0.01	0.01	0.01	0.62	0.01	0.01	
K <sub>2</sub> O	12.17	12.48	13.09	13.93	14.36	12.18	12.3	12.12	10.54	11.93	11.06	9.74	11.30	11.39	12	
P <sub>2</sub> O <sub>5</sub>	0.6	0.49	0.56	0.36	0.25	0.24	0.21	0.43	1.06	0.29	0.39	0.43	0.32	0.16	0.09	
H <sub>2</sub> O	5.13	4.13	3.82	3.02	2.48	4.96	5.05	4.7	5.36	4.74	3.49	4.71	4.51	9.46	7.69	
CO <sub>2</sub>	n.a.	n.a.	n.a.	n.a.	n.a.	n.a.	n.a.	n.a.	n.a.	n.a.	n.a.	n.a.	n.a.	n.a.	n.a.	
Total	(wt.%)	95.72	95.67	96.49	98.04	98.98	99.77	100.28	99.21	93.28	93.91	90.89	86.42	96.22	97.72	100.05
F	(ppm)	n.a.	n.a.	n.a.	n.a.	n.a.	n.a.	n.a.	n.a.	n.a.	n.a.	n.a.	n.a.	3665	n.a.	n.a.
Ba	446	374	504	314	302	478	511	595	369	252	91	0	1135	1001	1194	
Rb	333	332	328	311	312	257	261	259	208	233	224	191	277	239	262	
Sr	1623	1406	1595	1286	1013	1140	1088	2001	3750	730	880	741	355	330	201	
Pb	109	86	84	59	52	70	61	113	306	676	434	254	43	37	54	
Th	114	98	115	68	45	41	38	134	390	131	170	157	214	374	236	
U	5588	4749	4708	2181	1266	135	89	238	858	716	977	1183	281	7	23	
Nb	484	483	453	345	303	216	193	308	526	554	778	852	258	112	1116	
La	484	376	412	245	168	154	134	343	989	183	262	256	1396	295	186	
Ce	565	478	509	314	295	223	194	427	1097	323	438	490	1809	367	244	
Nd	165	133	144	82	80	48	42	100	284	100	139	171	312	110	53	
Y	150	135	148	117	94	67	56	118	363	234	325	384	320	146	111	
Zr	17486	19297	19168	14268	13671	4429	3152	8649	24260	24853	32800	41857	4621	226	1781	
V	222	152	75	55	87	151	132	220	169	85	120	92	279	99	462	
Cr	14	14	15	11	10	6	6	8	16	14	15	16	b.d.	16	18	
Ni	73	56	72	40	28	9	9	18	49	38	48	50	b.d.	18	17	
Co	17	12	15	13	18	7	6	4	19	49	32	28	5	b.d.	9	
Cu	15	14	16	b.d.	b.d.	b.d.	b.d.	b.d.	24	b.d.	16	17	b.d.	b.d.	b.d.	
Zn	627	998	751	479	378	391	475	175	64	1941	767	90	506	653	242	
Ga	42	34	24	30	40	43	40	41	31	23	21	18		25	25	
Hf	232	260	254	189	182	70	54	128	385	337	478	653	63	5	27	
Sc	n.a.	n.a.	n.a.	n.a.	n.a.	n.a.	n.a.	n.a.	n.a.	n.a.	n.a.	n.a.	5	n.a.	n.a.	
S	14509	11787	12211	47983	46638	34625	41316	11145	11516	27360	20385	18307	21098	76425	54466	

XRF-data; n.a. = not analysed, b.d. = below detection.

## Borehole F4: Major and trace element analyses (contd.).

Sample	394-A	413-1A-A	413-1A-B	413-1A-C	413-1A-D	413-1A-E	
Depth (m)	394.51	411.85	412.15	412.45	412.75	412.98	
Rock type	NeS Red/m.	NeS Red/f.	NeS Red/f.	NeS Red/f.	NeS Red/f.	NeS Red/f.	
SiO <sub>2</sub>	58.13	54.86	54.64	55.62	57.26	52.42	
TiO <sub>2</sub>	0.59	0.71	0.87	0.65	0.38	1.16	
Al <sub>2</sub> O <sub>3</sub>	19.56	18.67	19.00	18.94	17.44	17.88	
Fe <sub>tot</sub>	3.73	4.35	4.21	4.11	4.22	6.78	
MnO	0.01	1.12	0.99	0.42	0.11	1.25	
MgO	0.11	0.15	0.14	0.17	0.09	0.11	
CaO	0.49	0.27	0.21	0.42	0.49	0.15	
Na <sub>2</sub> O	0.01	0.68	0.67	0.57	0.63	0.50	
K <sub>2</sub> O	14.52	13.33	13.27	13.38	14.14	12.92	
P <sub>2</sub> O <sub>5</sub>	0.11	0.03	0.05	0.05	0.05	0.03	
H <sub>2</sub> O	3.17	2.04	2.21	2.92	2.62	2.79	
CO <sub>2</sub>	n.a.	1.85	1.53	0.95	0.40	1.95	
Total	(wt.%)	100.43	98.06	97.79	98.20	97.83	97.94
F	(ppm)	n.a.	2394	2174	2929	3320	2158
Ba		445	670	685	619	596	554
Rb		381	411	414	406	450	393
Sr		515	205	172	218	219	179
Pb		22	11	12	8	13	18
Th		81	38	38	34	44	52
U		110	56	48	38	64	65
Nb		350	454	357	346	520	597
La		175	301	325	324	349	379
Ce		238	294	357	333	401	387
Nd		65	55	73	58	72	82
Y		50	39	36	27	32	33
Zr		1094	2432	1876	1223	1629	1515
V		157	98	90	81	45	111
Cr		6	b.d.	b.d.	b.d.	b.d.	b.d.
Ni		12	b.d.	b.d.	b.d.	b.d.	b.d.
Co		8	9	8	8	5	10
Cu		b.d.	b.d.	b.d.	b.d.	b.d.	b.d.
Zn		1820	201	295	568	475	309
Ga		36	n.a.	n.a.	n.a.	n.a.	n.a.
Hf		20	31	22	10	19	19
Sc		n.a.	5	5	5	4	5
S		15258	9285	9523	12975	13843	15080

XRF-data; n.a. = not analysed, b.d. = below detection.

Borehole F4: F4-353 Xenolith, major and trace elements.

Sample Depth (m)	Ns 1-11 353.40	Ns 1-10 353.41	Ns 1-9 353.42	Ns 1-8 353.43	Ns 1-7 353.44	Ns 1-6 353.45	Ns 1-5 353.46	Ns 1-4 353.47	Ns 1-3 353.48	Ns 1-2 353.49	Ns 1-1 353.50	PH 353.52	
Rock type	NeS Red.	NeS Red.	NeS Red.	NeS Red.	NeS Red.	NeS Red.	NeS Red.	NeS Red.	NeS Red.	NeS Red.	NeS Red.	PhD Red.	
SiO <sub>2</sub>	55.00	54.00	53.90	52.50	50.60	49.70	50.60	50.90	51.00	50.90	52.20	53.70	
Al <sub>2</sub> O <sub>3</sub>	18.70	19.30	20.40	20.40	20.20	20.10	19.90	20.80	20.30	20.40	21.20	19.60	
TiO <sub>2</sub>	1.27	1.50	1.33	1.33	1.51	1.40	1.26	1.05	1.11	1.17	0.86	0.66	
Fe <sub>2</sub> O <sub>3</sub>	4.60	4.45	3.89	4.82	6.30	6.38	6.28	5.39	5.61	5.58	4.76	5.07	
MnO	0.98	0.96	0.82	0.87	1.38	1.52	1.70	1.39	1.51	1.40	1.13	0.73	
MgO	0.18	0.20	0.22	0.25	0.29	0.28	0.28	0.29	0.28	0.29	0.25	0.21	
CaO	0.03	0.04	0.04	0.06	0.11	0.11	0.13	0.11	0.12	0.12	0.14	0.17	
Na <sub>2</sub> O	0.17	0.08	0.10	0.07	0.11	0.12	0.08	0.11	0.10	0.11	0.14	0.12	
K <sub>2</sub> O	14.10	13.80	13.90	13.10	12.80	12.60	12.90	12.80	13.10	12.90	13.50	13.70	
P <sub>2</sub> O <sub>5</sub>	0.04	0.04	0.04	0.05	0.06	0.07	0.08	0.06	0.06	0.08	0.06	0.05	
LOI	3.77	3.85	3.77	4.77	5.39	5.70	5.31	5.08	5.16	4.77	4.31	4.16	
CO <sub>2</sub>	n.a.	n.a.	n.a.	n.a.	n.a.	n.a.	n.a.	n.a.	n.a.	n.a.	n.a.	n.a.	
Total	(wt.%)	98.84	98.22	98.41	98.22	98.75	97.98	98.52	97.98	98.35	97.72	98.55	98.17
F	(ppm)	n.a.	n.a.	n.a.	n.a.	n.a.	n.a.	n.a.	n.a.	n.a.	n.a.	n.a.	n.a.
Ba	1370	1360	1490	140	1520	1490	1630	1470	1480	1360	1200	671	
Rb	307	305	303	298	278	284	294	279	292	279	293	328	
Sr	306	274	280	338	422	443	606	1040	740	1210	957	584	
Pb	n.a.	n.a.	n.a.	n.a.	n.a.	n.a.	n.a.	n.a.	n.a.	n.a.	n.a.	n.a.	
Th	32	32	30	32	33	33	34	30	30	36	30	27	
U	24.3	27.4	20.3	18.6	19.8	16.5	16	13.6	13.4	15.2	13.5	24	
Nb	285	322	272	299	392	341	306	264	277	288	232	272	
La	201	195	162	182	226	278	382	275	273	349	265	211	
Ce	255	260	208	262	346	409	579	410	408	535	395	311	
Nd	64	66	52	65	87	104	147	108	105	140	101	65	
Y	n.a.	n.a.	n.a.	n.a.	n.a.	n.a.	n.a.	n.a.	n.a.	n.a.	n.a.	n.a.	
Zr	644	915	889	931	941	726	627	568	564	737	665	1050	
V	100	120	140	160	140	140	120	130	130	110	140	140	
Cr	2.3	1.9	1.9	1.4	0.9	2.9	2.7	0.9	4.1	8	1.1	3	
Ni	4	1	b.d.	2	3	3	2	3	2	4	3	3	
Co	b.d.	b.d.	0.8	b.d.	0.7	b.d.	1.3	0.8	0.6	1.8	0.8	b.d.	
Cu	5	5.5	3	5	5.5	4	3.5	5.5	3.5	5	5	5	
Zn	240	130	130	200	300	320	340	210	260	200	210	280	
Hf	11	17	16	17	15	13	11	11	10	13	12	17	
Sc	0.53	0.66	0.6	0.73	1	0.92	1	0.82	0.83	1.03	0.84	1	
S	n.a.	n.a.	n.a.	n.a.	n.a.	n.a.	n.a.	n.a.	n.a.	n.a.	n.a.	n.a.	

ICP-data; n.a. = not analysed, b.d. = below detection.

## Borehole F4: F4-353 Xenolith, major and trace elements (contd.).

Sample Depth (m)	VB 2-1 353.53	VB 2-2 353.54	VB 2-3 353.55	VB 2-4 353.56	VB 2-5 353.57	VB 2-6 353.58	
Rock type	VBr Red.	VBr Red.	VBr Red.	VBr Red.	VBr Red.	VBr Red.	
SiO <sub>2</sub>	55.80	55.80	56.20	55.60	58.00	59.00	
Al <sub>2</sub> O <sub>3</sub>	19.80	19.60	18.70	16.00	15.40	15.80	
TiO <sub>2</sub>	0.36	0.33	0.42	0.49	0.47	0.49	
Fe <sub>2</sub> O <sub>3</sub>	4.10	5.14	4.98	8.05	5.21	4.54	
MnO	0.36	0.51	0.39	0.29	0.26	0.32	
MgO	0.16	0.16	0.15	0.18	0.26	0.24	
CaO	0.04	0.01	0.02	0.03	0.04	0.05	
Na <sub>2</sub> O	0.15	0.17	0.17	0.33	0.63	0.54	
K <sub>2</sub> O	14.10	13.80	13.90	13.70	13.50	13.80	
P <sub>2</sub> O <sub>5</sub>	0.05	0.04	0.05	0.05	0.05	0.05	
LOI	3.85	4.00	3.70	4.54	3.31	3.08	
CO <sub>2</sub>	n.a.	n.a.	n.a.	n.a.	n.a.	n.a.	
Total	(wt.%)	98.77	99.56	98.68	99.26	97.13	97.91
F	(ppm)	n.a.	n.a.	n.a.	n.a.	n.a.	n.a.
Ba		596	570	511	414	431	414
Rb		335	322	361	355	389	396
Sr		238	194	170	179	183	173
Pb		n.a.	n.a.	n.a.	n.a.	n.a.	n.a.
Th		34	34	33	54	140	130
U		25.1	20.6	15.7	23.2	44.8	42
Nb		220	195	136	234	339	280
La		233	218	253	255	254	277
Ce		310	287	312	328	357	366
Nd		73	76	77	75	93	84
Y		n.a.	n.a.	n.a.	n.a.	n.a.	n.a.
Zr		1170	1750	1060	7800	23700	18500
V		80	90	82	36	26	28
Cr		0.6	1.9	0.8	2	2.8	1.2
Ni		4	3	3	6	2	3
Co		0.6	1	1.3	2.2	1.3	0.9
Cu		4.5	3.5	3	4.5	3.5	3
Zn		110	100	160	160	140	130
Hf		21	30	17	120	430	330
Sc		0.65	0.68	0.62	0.52	0.75	0.74
S		n.a.	n.a.	n.a.	n.a.	n.a.	n.a.

ICP-data; n.a. = not analysed, b.d. = below detection.

Borehole F4: F4-353 Xenolith, As, Mo and Cd analyses.

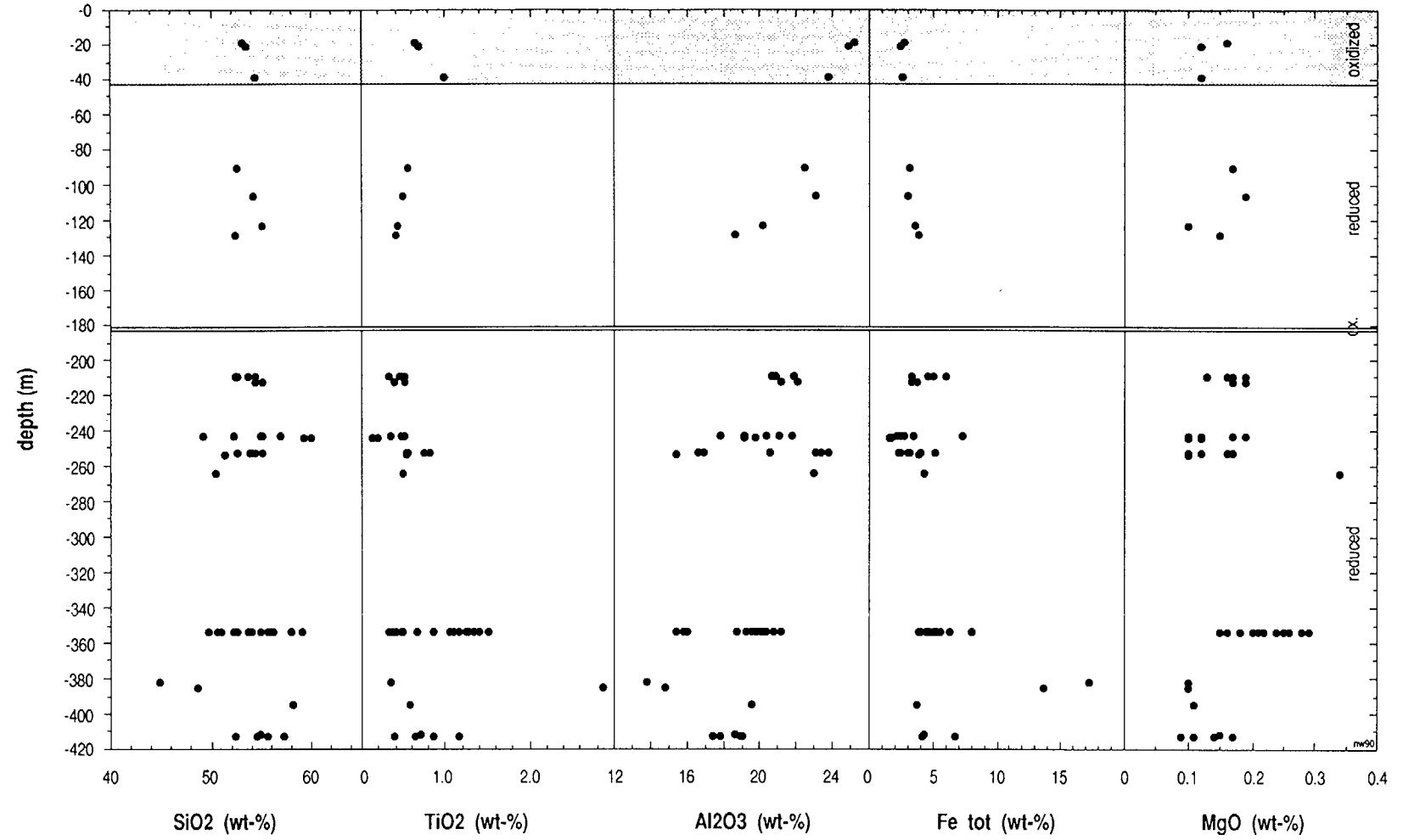
Sample	Depth (m)	Rock type	As	Mo	Cd
Ns 1-11	353.40	NeS	29	50	<1
Ns 1-10	353.41	NeS	30	52	<1
Ns 1-9	353.42	NeS	20	44	<1
Ns 1-8	353.43	NeS	26	35	2
Ns 1-7	353.44	NeS	23	24	<1
Ns 1-6	353.45	NeS	16	17	2
Ns 1-5	353.46	NeS	15	14	1
Ns 1-4	353.47	NeS	13	15	1
Ns 1-3	353.48	NeS	13	20	1
Ns 1-2	353.49	NeS	14	11	2
Ns 1-1	353.50	NeS	13	13	<1
PhD	353.52	PhD	32	23	<1
VB 2-1	353.53	VBr	37	67	<1
VB 2-2	353.54	VBr	41	61	<1
VB 2-3	353.55	VBr	54	72	1
VB 2-4	353.56	VBr	85	84	<1
VB 2-5	353.57	VBr	56	61	2
VB 2-6	353.58	VBr	60	53	2

## Borehole F4: F4-413 Xenolith, trace elements.

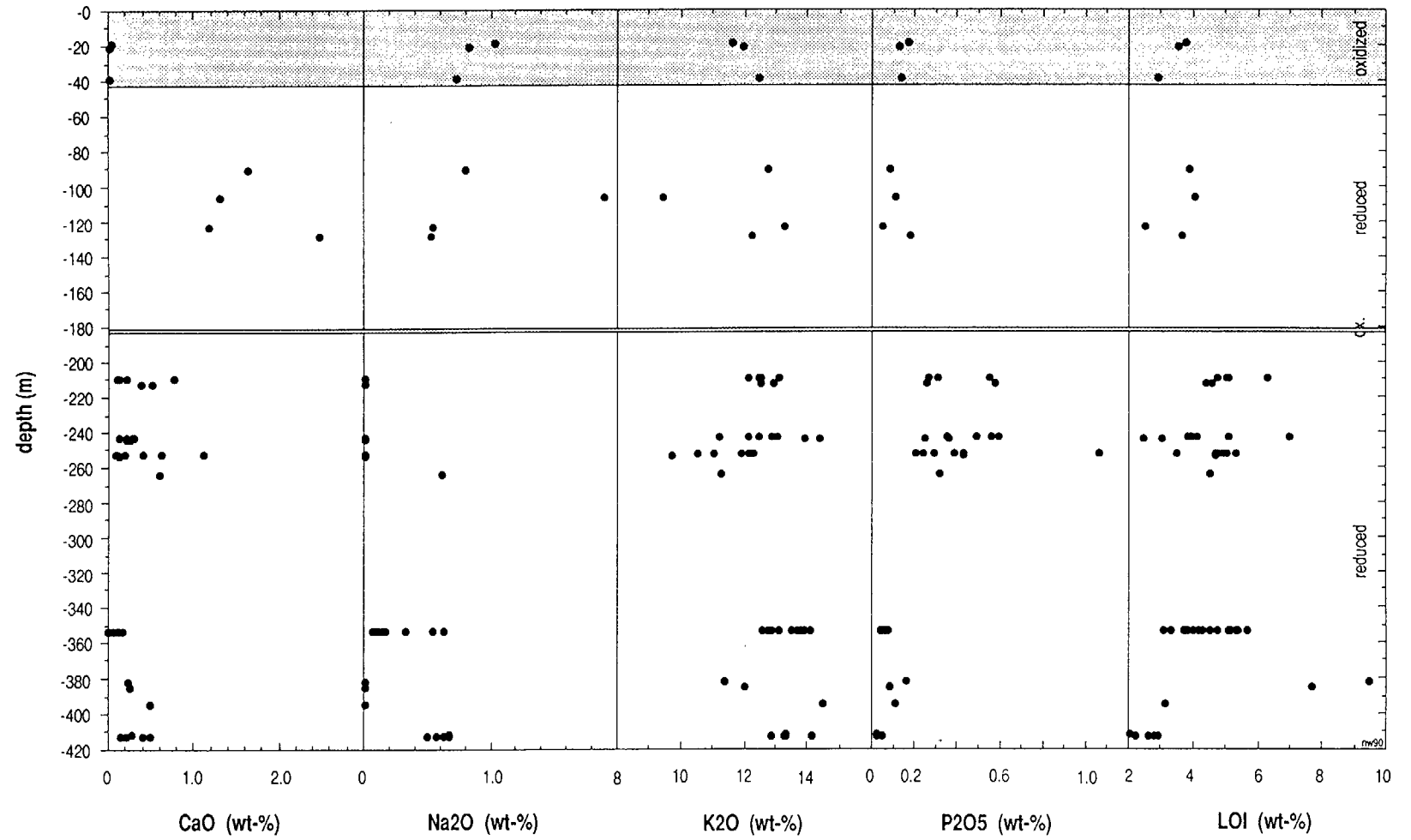
Sample	413-1A-A	413-1A-B	413-1A-C	413-1A-D	413-1A-E	413-1A-F	413-1A-G	413-1A-H	413-1A-I	413-1A-K	413-1A-L	413-1A-M	413-1A-N	413-1A-O	413-1A-P
Depth (m)	411.72	411.79	411.86	411.98	412.10	412.22	412.34	412.46	412.58	412.70	412.82	412.94	413.00	413.04	413.11
Rock type	NeS														
	Red.														
Ba (ppm)	887	844	1492	n.a.	1848	n.a.	n.a.	2662	752	1105	564	764	664	142	433
Rb	333	328	347	n.a.	315	n.a.	n.a.	326	356	329	318	404	292	308	282
Sr	225	208	225	n.a.	210	n.a.	n.a.	210	256	304	274	288	178	234	139
Pb	38	35	26	n.a.	26	n.a.	n.a.	35	33	142	38	41	79	40	45
Th	23	23	22	n.a.	23	n.a.	n.a.	23	29	24	27	31	29	25	18
U	33	39	32	n.a.	33	n.a.	n.a.	47	57	32	28	64	54	42	50
Nb	224	211	191	n.a.	271	n.a.	n.a.	238	226	149	125	371	410	118	386
La	148	159	150	163	140	195	172	102	157	151	155	189	104	122	22
Ce	273	630	242	352	236	324	251	180	256	250	258	325	241	226	136
Nd	66	74	60	51	62	73	61	45	67	64	67	83	56	60	16
Y	21	21	18	n.a.	16	n.a.	n.a.	15	32	16	17	14	11	16	5
Zr	312	408	263	n.a.	194	n.a.	n.a.	142	346	99	157	123	171	174	295
V	44	65	52	n.a.	69	n.a.	n.a.	82	48	59	39	29	81	93	79
Cr	b.d.	1	1	n.a.	b.d.	n.a.	n.a.	2	1	1	3	1	5	10	9
Ni	3	3	2	n.a.	1	n.a.	n.a.	4	3	2	4	1	10	55	2
Co	4	11	11	n.a.	11	n.a.	n.a.	7	5	5	7	13	10	8	6
Cu	8	7	6	n.a.	7	n.a.	n.a.	28	12	9	108	13	28	167	17
Zn	406	255	244	n.a.	270	n.a.	n.a.	618	795	972	702	997	730	757	508
Hf	6	8	4	n.a.	4	n.a.	n.a.	3	6	3	3	3	4	4	7
Ga	38	48	57	n.a.	53	n.a.	n.a.	83	45	54	34	43	42	41	42
Sc	4	10	4	n.a.	3	n.a.	n.a.	7	2	5	1	1	3	1	5
S	n.a.														
As	12	23	39	n.a.	18	n.a.	n.a.	88	26	18	4	37	42	31	16
Mo	30	47	35	n.a.	33	n.a.	n.a.	27	40	30	28	20	27	25	25
Cd	4	2	1	n.a.	1	n.a.	n.a.	1	6	3	1	3	12	3	5

ICP-data; n.a. = not analysed, b.d. = below detection.

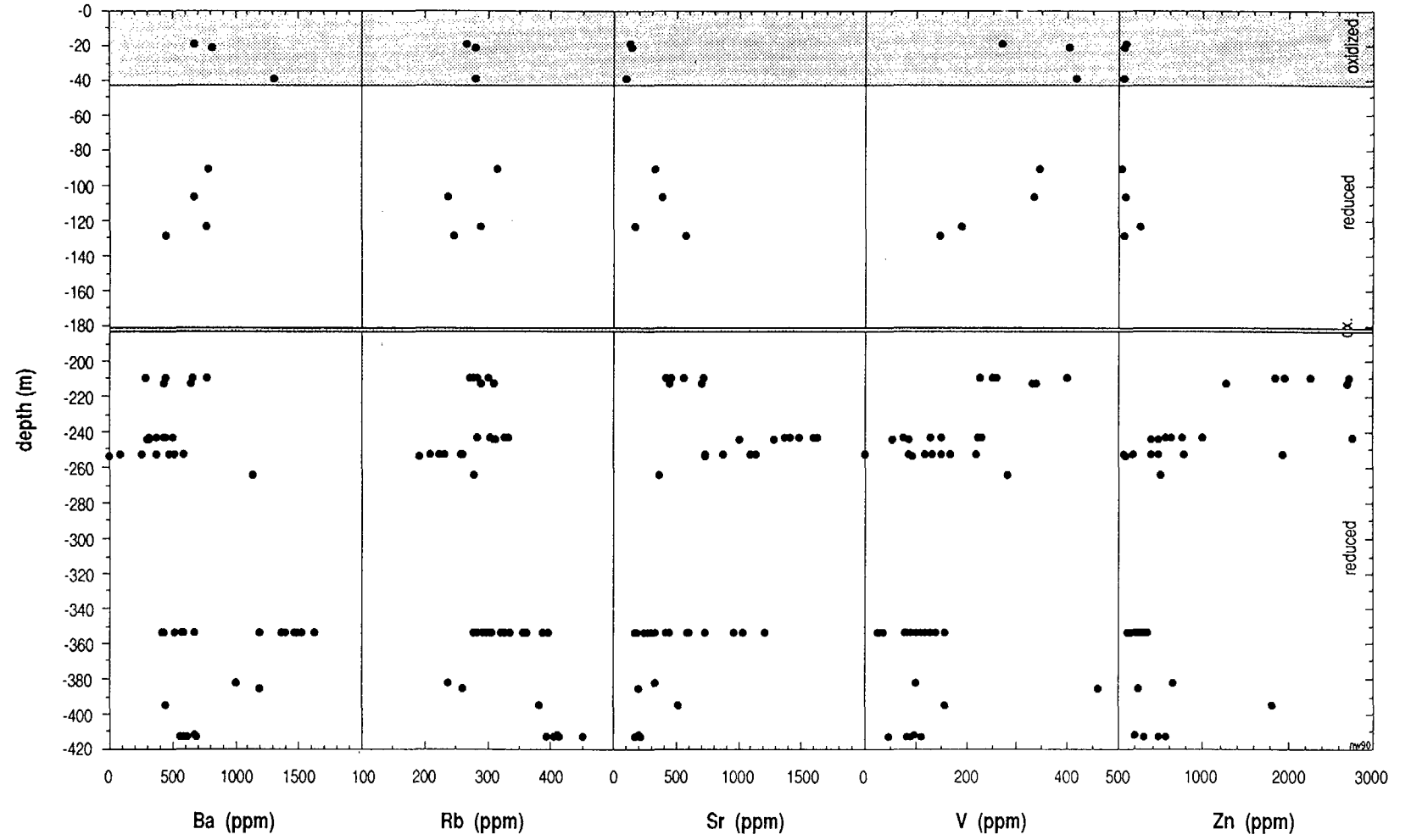
F4 - Borehole



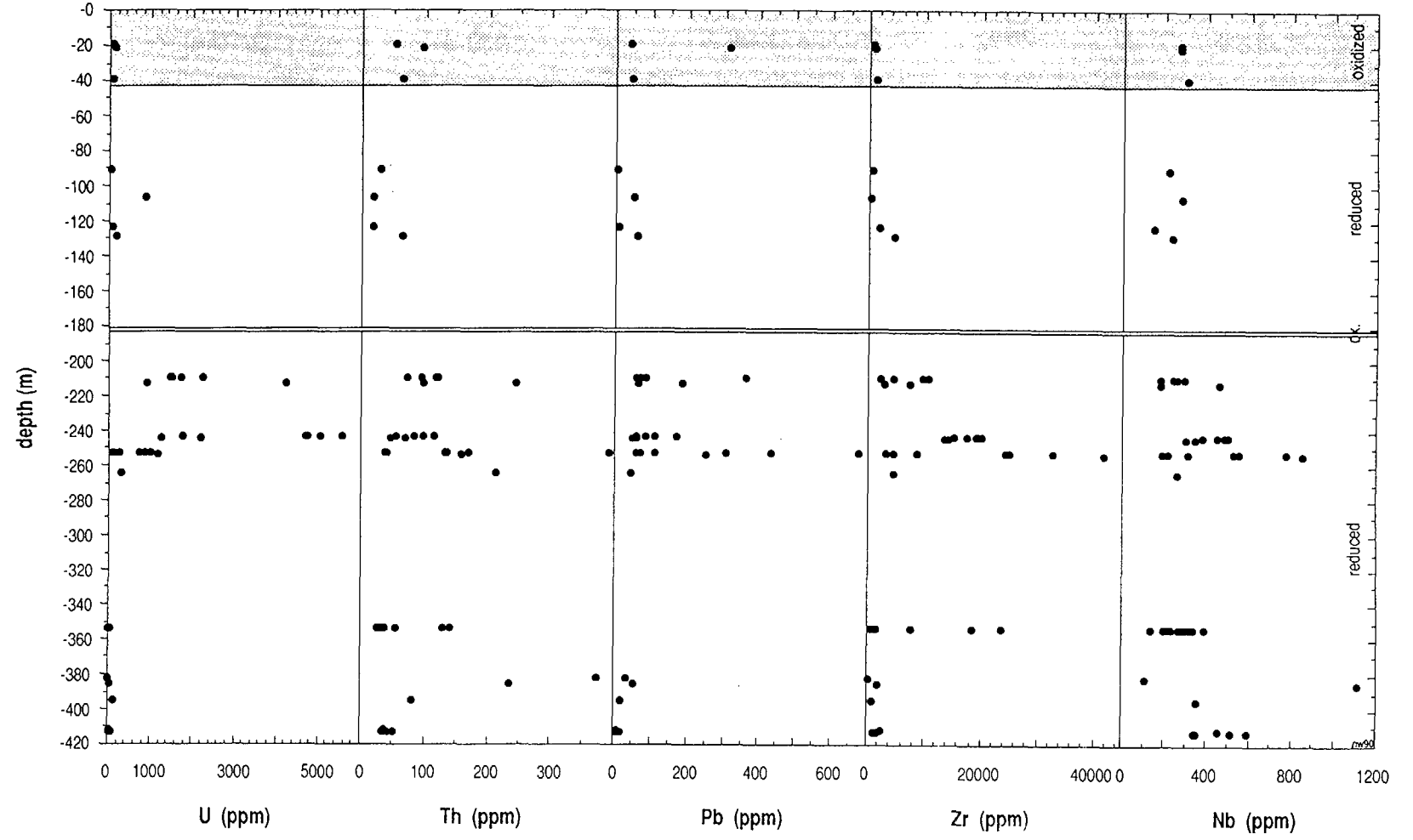
F4 - Borehole



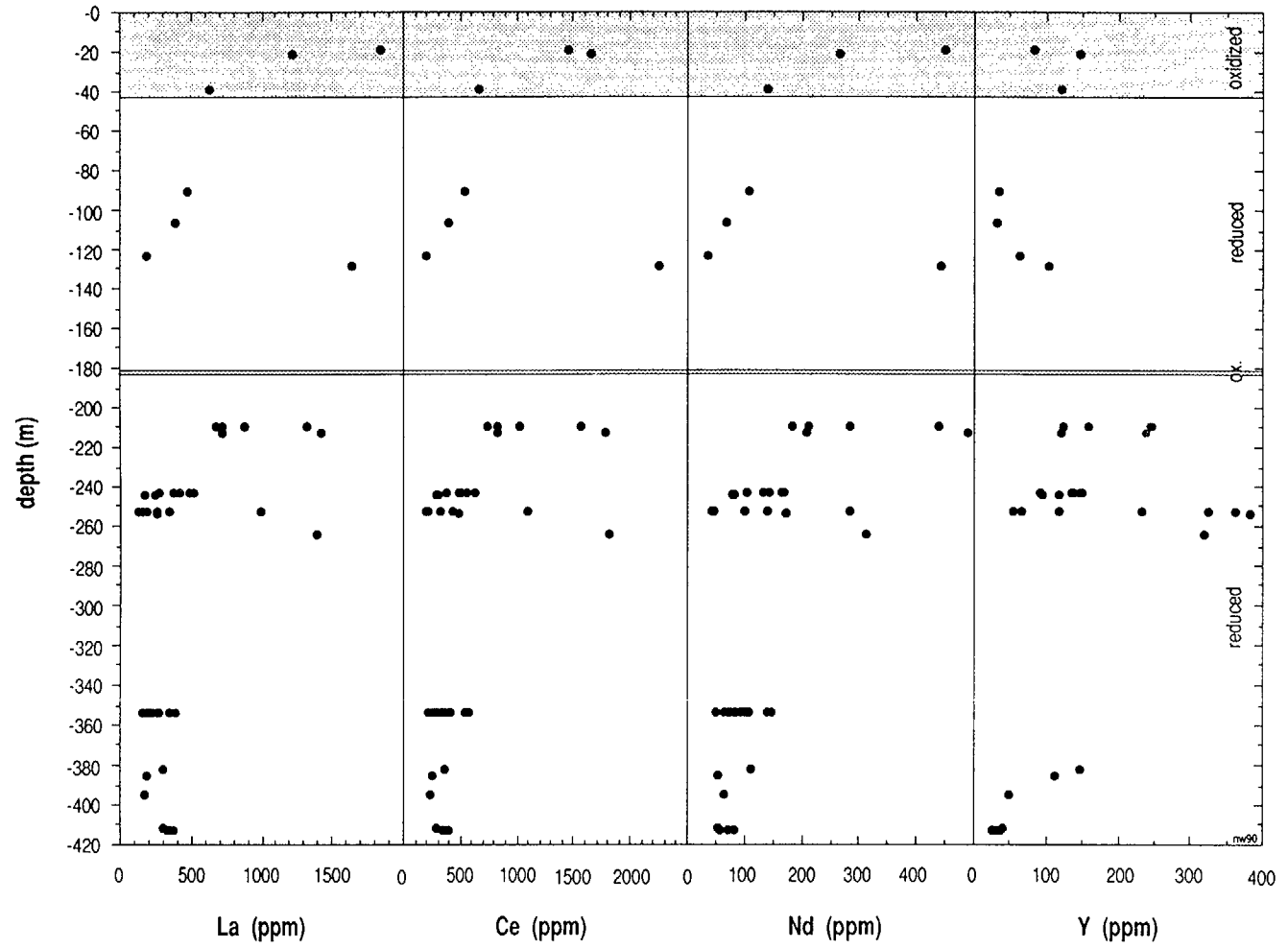
F4 - Borehole



F4 - Borehole



F4 - Borehole



## **Appendix 5**

### **Mineralogy of borehole F4.**

**(Compiled by H.D. Schorscher, University of São Paulo).**

# Contents

Mineralogy of borehole F4	365
APPENDICES:	
Appendix 5:1: PLATES 5:1-1 – 5:1-12	387
Appendix 5:2: Model for the evolution of the rock sequence observed at the Osamu Utsumi mine	401

TABLE 5-I

Samples selected from drillcore F4 for mineralogical and petrographic studies.

Sample number	Depth in m	Summarised rock description	Radiation total cps above bg
4-1A	3.30 – 3.44	Oxid. breccia with mainly phonolite and minor nepheline syenite fragments. Fe-ox./hydroxides are irregularly distributed among rock fragments, being relatively more concentrated along grain boundaries and fractures.	10
14-1A	13.24 – 13.51	Oxid. breccia with mainly phonolite and minor nepheline syenite fragments. Fe-ox./hydroxide distribution as above.	10
19-1A	18.47 – 19.26	Oxid. breccia with phonolite, pseudoleucite phonolite and nepheline syenite fragments. Fe-ox./hydroxide distribution as above.	
22-1A	20.82 – 21.33	Oxid. porphyritic hypabyssal nepheline syenite. Fe-ox./hydroxide distribution as above.	
24-1A	22.85 – 23.33	Oxid. hypabyssal nepheline syenite; fractured. Fe-ox./hydroxide distribution as above.	10
29-1A	28.03 – 28.17	Oxid. brecciated porphyritic phonolite with pseudoleucite. Fe-ox./hydroxide distribution as above.	
34-1A	33.05 – 33.35	Oxid. porphyritic, xenolithic, phonolite with fine-grained, flow-oriented groundmass; fractured. Fe-ox./hydroxide distribution as above.	5
39-1A	38.40 – 39.04	Oxid. subvolcanic porphyritic phonolite with pseudoleucite. Fe-ox./hydroxide distribution as above.	
54-1A	52.95 – 53.03	Reduced porphyritic, xenolithic phonolite with pseudoleucite (nepheline syenite xenolith).	5
57-1A	56.46 – 56.61	Reduced breccia with predominant phonolite and minor nepheline syenite fragments set in a pyrite- and fluorite-rich matrix. Fragments show variable degrees of pyritisation.	35
60-1A	59.77 – 60.00	Reduced porphyritic phonolite with fine-grained flow-oriented groundmass; strong sericitisation.	5
68-1A	67.27 – 67.37	Reduced porphyritic, xenolithic phonolite (phonolite and nepheline syenite xenoliths).	5
76-1A	75.20 – 75.45	Reduced breccia with phonolite and nepheline syenite fragments and massive violet fluorite mineralisation in breccia matrix and veins. Fragments show variable pyritisation.	65
80-1A	79.50 – 79.82	Reduced breccia (microbreccia); matrix predominates over fragments. These show variable pyritisation.	85

TABLE 5-I (contd.).

Sample number	Depth in m	Summarised rock description	Radiation total cps above bg
86-1A	85.77 – 86.10	Reduced breccia (phonolite and nepheline syenite fragments) with blue Mo-mineral (ilsemannite) in some fragments. Fragments show variable pyritisation.	45
91-1B	90.60 – 91.26	Reduced nepheline syenite, fractured and brecciated, together with reduced breccia with nepheline syenite and phonolite fragments of variable pyritisation.	
93-1A	92.92 – 93.04	Reduced breccia (microbreccia) with predominantly phonolite fragments of variable pyritisation.	20
105-1A	104.55 – 104.72	Reduced hypabyssal nepheline syenite; fractured.	15
107-1A	106.00 – 106.88	Reduced breccia with nepheline syenite and phonolite fragments of variable pyritisation.	
111-1A	110.15 – 110.36	Reduced breccia with phonolite fragments of variable pyritisation. Breccia matrix shows fracturing with pyrite and/or opaque ore-rich fillings.	25
123-1A	122.47 – 122.94	Reduced breccia (fragments of various phonolites) zone in reduced porphyritic to non-porphyritic, fractured phonolite.	
129-1A	128.21 – 128.75	Reduced, porphyritic (fine-grained groundmass) and fractured phonolite.	
135-1A	134.40 – 134.59	Reduced breccia (fragments mainly of phonolites) with fracture fillings and breccia matrix of massive violet Ca F <sub>2</sub> .	65
139-1A	138.24 – 138.56	Reduced, porphyritic (fine-grained groundmass) and fractured phonolite.	15
146-1A	144.95 – 145.07	Fractures in phonolite; fracture fillings of clays, pyrite and muscovite.	
148-1A	146.97 – 147.27	Reduced breccia (phonolite fragments), locally with pyrite and violet Ca F <sub>2</sub> -rich matrix and fractures. One level suffered partial oxidation earlier than the main brecciation and Ca F <sub>2</sub> mineralisation.	45
155-1A	154.06 – 154.32	Reduced breccia with predominant phonolite and minor nepheline syenite fragments. Breccia matrix is partially of massive violet Ca F <sub>2</sub> .	25
164-1A	163.30 – 163.39	Reduced breccia (fragments of phonolites) of polygenetic origin: the originally magmatic breccia (fragments in a matrix of very fine-grained phonolite) suffered late- to postmagmatic fracturing with pyrite and kaolinite mineralisation.	15
175-1A	174.21 – 174.36	Reduced breccia (microbreccia) with phonolite and nepheline syenite fragments. Breccia is of magmatic origin (matrix of very fine-grained phonolite) and suffered late- to postmagmatic fracturing and mineralisation (pyrite, fluorite, zircon, semi-opaque rare metal minerals, clay minerals).	25

TABLE 5-I (contd.)

Sample number	Depth in m	Summarised rock description	Radiation total cps above bg
178-1A	176.90 – 177.12	Reduced phonolite breccia with mineralised matrix. Zonally arranged mineralisation (from phonolite fragments to matrix): hydrothermalised phonolite (freshest rock with K-feldspar and minor sericite, kaolinite and pyrite); zone of argillic alteration of phonolite (major sericite, kaolinite, increasing pyrite contents and minor zircon and semi-opaque rare metal minerals); first discontinuous matrix zone of mainly clay minerals (sericite, kaolinite, minor pyrite, zircon and semi-opaque, rare minerals); second continuous matrix zone of maximum U-mineralisation (major zircon, semi-opaque, rare minerals, opaque ore minerals: pyrite and tentatively identified U-oxides); voids and pores of this zone are filled with kaolinite and colourless Ca F <sub>2</sub> , both replaced by young sericite.	
181-1A	180.66 – 180.76	Reduced phonolite breccia with mineralised matrix (mainly opaque ore minerals, pyrite).	20
192-1A	191.18 – 191.35	Reduced very fine-grained porphyritic phonolite breccia with opaque ore (mainly pyrite) and coarse sericite/muscovite mineralised matrix and coarse sericite/muscovite-filled fractures. The phonolite fragments are marginally affected by argillic alteration (sericitisation, kaolinisation) outside the mineralised zones.	
201-1B	200.83 – 200.96	Biotite-lamprophyre dyke with evidence of fracturing, autohydrothermal alteration and affected by intertempic decomposition.	0 (=bg)
216-1A	215.19 – 215.43	Reduced porphyritic phonolite with coarse ( $\phi > 1\text{-}2\text{ cm}$ ) pseudoleucites in fine-grained groundmass. Incipient oxidation is evidenced by limonitic alterations of minerals and along grain boundaries.	20
223-1A	222.46 – 22.61	Reduced fine-grained phonolite with ore mineral-filled micro fractures.	15
229-1A	228.02 – 228.29	Reduced breccia with ore mineral-rich microfractures and violet fluorite in voids and in the breccia matrix.	20
230-1A	229.15 – 229.36	Reduced porphyritic phonolite locally brecciated.	
238-1A	237.00 – 237.16	Reduced fine-grained porphyritic phonolite with microfractures and microbreccia portions.	10
245-1A	243.96 – 244.12	Reduced phonolite breccia with anomalous radioactivity and rich in ore minerals. Limonite – spots of incipient oxidation around radioactive minerals.	80
246-1A	245.82 – 246.00	Reduced typical (coarse-grained, isotropic) nepheline syenite. Selective complete sericite and kaolinite substitution of nepheline along with stronger pyritisation (if compared with K-feldspars) occurred.	
248-1A	247.40 – 247.60	Reduced hypabyssal porphyritic nepheline syenite.	0 (=bg)

TABLE 5-I (contd.).

Sample number	Depth in m	Summarised rock description	Radiation total cps above bg
250		Reduced subvolcanic porphyritic phonolite with fractures/fillings of fluorite and pyrite. Fluorite is rich in carbonate and fluid inclusions ( $\phi > 25 \mu$ ).	
260-1B	259.69 – 259.84	Reduced breccia, mainly phonolite with minor nepheline syenite fragments, locally with ore mineral-rich matrix. Fragments show variable pyritisation.	0 (=bg)
262-1A	261.22 – 261.37	Reduced phonolite with fracturing and breccia zone.	25
263-1A	262.63 – 262.76	Reduced porphyritic phonolite with fractures and breccia zone.	
265-1A	263.97 – 264.70	Reduced hypabyssal nepheline syenite with pegmatoid vein.	
271-1A	270.36 – 270.58	Reduced phonolite breccia (pseudoleucite phonolite and subvolcanic phonolite fragments) with violet fluorite in breccia matrix.	45
276-1A 276-1B	274.87 – 275.10	Biotite-lamprophyre dyke with xenoliths of hydrothermalised phonolites and nepheline syenites. Lamprophyres suffered auto-hydrothermal alterations (distinct from the xenoliths).	
280-1A	279.87 – 279.96	Reduced hypabyssal nepheline syenite, with fractures. Micropores of nepheline syenites are fluorite-bearing, being concentrically replaced by sericite.	5
287-1A	286.49 – 286.73	Reduced breccia (nepheline syenite and phonolite fragments) with ore mineral-rich matrix.	10
289-1A	288.13 – 288.28	Reduced phonolite breccia with carbonates; fluorite mineralised matrix and fractures.	
290-1A	289.38 – 289.50	Reduced phonolite breccia with mineralised matrix (violet fluorite, ore minerals – mainly pyrite).	0 (=bg)
296-1A	295.14 – 295.20	Reduced phonolite and phonolite breccia with mineralised pores and matrix (fluorite, ore minerals – mainly pyrite), including pseudoleucite phonolite and phonolite with preserved chessboard-albite phenocrysts.	0 (=bg)
301-1A	300.10 – 300.39	Reduced breccia with phonolite and nepheline syenite fragments. Fragments show different grades and patterns of pre-breccia pyritisation. Matrix and fractures are mineralised with mainly clays, carbonates, fluorite and ore minerals – mainly pyrite.	5
314-1A	313.06 – 313.20	Reduced phonolite breccia with mineralised matrix and fractures (carbonates, clays, violet fluorite). In polished thin sections 314/1 and 314/2 the matrix predominates and only a few rock microfragments occur.	
315-1A	314.39 – 314.53	Reduced phonolite breccia with mineralised matrix (pyrite-rich).	0 (=bg)
320-1A	319.46 – 319.57	Reduced porphyritic phonolite (no carbonate or mineralisation).	0 (=bg)

TABLE 5-I (contd.).

Sample number	Depth in m	Summarised rock description	Radiation total cps above bg
328-1A	327.47 – 327.65	Reduced porphyritic and xenolithic phonolite with minor fractures.	5
330-1A	329.41 – 329.55	Biotite-lamprophyre dyke; border zone affected by oxidic alteration from deep circulating weathering solutions along the hanging contact of the dykes.	
331-1A	329.92 – 330.32	Biotite-lamprophyre dyke; centre of the dyke is best preserved, rich in relatively coarse-grained accessory apatites.	
375-1B	374.26 – 374.53	Reduced porphyritic phonolite and breccia with ore mineral (mainly pyrite)-rich breccia matrix.	10
381-1A	380.57 – 380.81	Reduced xenolithic phonolite (nepheline syenite xenolith).	0 (=bg)
382-1A	381.72 – 381.88	Reduced porphyritic and xenolithic phonolite with fluorite in rock pores.	5
384-1A	383.42 – 383.54	Reduced porphyritic (pseudoleucites) and xenolithic (phonolites) fractured phonolite.	0 (=bg)
387-1A	386.05 – 386.20	Reduced subvolcanic phonolite and breccia with ore mineral (mainly pyritic)-rich matrix and blue secondary molybdenum mineral staining (ilsemannite?).	0 (=bg)
388-1A	387.52 – 387.72	Reduced porphyritic and xenolithic phonolite (nepheline syenite and phonolite xenoliths) and reduced nepheline syenite with hydrothermalised pegmatoid (zoned structure: colourless fluorite surrounded/enclosed by kaolinite, both being surrounded and replaced by sericite).	
391-1B	390.65 – 390.76	Reduced nepheline syenite breccia with ore mineral (mainly pyrite)-rich matrix. Fragment boundaries show stylolite-type sutured structures caused by pressure dissolution.	15
395-1A	394.70 – 394.85	Reduced nepheline syenite with minor fracturing and brecciation. Hydrothermal fracture-related zircon formation and zonal (centre to border) pseudomorphism of nepheline by: fluorite, kaolinite and sericite (replacing kaol. and Ca F <sub>2</sub> ).	20
404-1B	403.42 – 403.63	Reduced nepheline syenite and phonolite breccia with ore mineral (pyrite)-rich matrix.	10
406-1A	405.61 – 405.82	Reduced, hypabyssal nepheline syenite with ore (pyrite)- and zircon-rich fractures.	10
407-1A	405.93 – 406.23	Reduced porphyritic phonolite (subvolcanic) with interstitial hydrothermal zircon.	

TABLE 5-I (contd.).

Sample number	Depth in m	Summarised rock description	Radiation cps above bg
409-1B	408.51 – 408.66	Reduced phonolite with hypabyssal nepheline syenite xenolith. Contact zone is enriched in opaque ores (pyrite) and zircon.	0 (=bg)
414-1A	413.56 – 413.78	Reduced xenolithic phonolite slightly fractured with xenoliths of hypabyssal nepheline syenites. Contacts with xenoliths and fractures are enriched in opaque ores (pyrite).	0 (=bg)

cps = counts per second

bg = background

TABLE 5-II

Breccia-related main hydrothermal mineral assemblages (based on macroscopic studies and radioactivity measurements).

Assemblage minerals	Type of assemblage	Radioactivity (refer to PLATES in Appendix 5:1)
1: pyrite	Monomineralic, microcrystalline masses to coarse (millimetric) idiomorphic crystals filling open spaces between breccia fragments.	None = bg
2: clay minerals + pyrite	Cryptocrystalline clay masses containing disseminated microcrystalline pyrites. This assemblage is intergradational with assemblage 4 through molybdenum contents.	None = bg (Plates 5:1-1 and 5:1-9)
3: fluorite + carbonate + pyrite ± clay minerals	Microcrystalline components of the matrix and coarser masses cementing breccia fragments. Carbonates occur always as inclusions in fluorite.	Minor positive anomalies (Plate 5:1-7)
4: pyrite + clay minerals + molybdenum minerals (unidentified)	Microcrystalline pyrite-clay assemblages with blue, secondary Mo-mineral staining.	Minor to medium positive anomalies (Plate 5:1-8)
5: pyrite + uranium mineral (unidentified) + sulphide minerals (unidentified)	Microcrystalline masses filling open spaces between breccia fragments.	Maximum observed positive anomalies (Plate 5:1-10)





TABLE 5-III (contd.).

Sample no.	Thin section no.	Rock mineralogy											Mineralogy of rock-pores and interstices											Mineralogy of fractures-F, breccia matrix-Mx, fractures in breccia matrix-FMx											cps								
		1	2	3	4	5	6	7	8	9	10	11	12	13	15	16	17	18	19	20	21	22	23	24	25	26	27	28	30	31	32	33	34	35		36	37	38	39	40	41	42	43
57-1A	06/16	M	m	m	m	tr	M	tr	tr	tr	m	m:1, s	-	Ph	-	tr	v	v	-	tr	tr	v	tr	v	v	-	-	F	tr	tr	v	tr	-	M	-	tr	-	-	m	-	-	35	
												2,4,5		NeS	tr	M	v	m	-	-	-	tr	-	-	-	-	-	F	-	-	tr	M	tr	tr	-	tr	-	-	tr	-	-		
																											Mx	tr	tr	tr	tr	-	M	tr	m	m:1, s	-	m	m	s	-	2,4,5	
60-1A	07/17	M	M	m	m	tr	m	tr	-	-	tr	-	-	Ph	-	v	M	tr	-	tr	-	v	-	-	-	-	-	F	-	-	m	v	-	v	-	tr	-	-	tr	-	-	5	
68-1A	08/15	M	M	M	m	tr	m	tr	tr	-	tr	-	-	Ph	-	v	v	m	tr	-	-	m	tr	-	-	-	-	F	tr	tr	m	tr	-	M	-	m	-	-	tr	-	-	5	
														NeS	-	M	m	tr	-	-	-	tr	-	-	-	-	-	F	tr	tr	tr	m	-	M	-	m	-	-	tr	-	-		
76-1A	09/12	M	m	M	m	tr	m	m	tr	m	m	m	s	-	Ph	-	m	v	m	-	tr	tr	v	m	-	v	-	-	F	tr	m	m	m	-	v	-	m	-	v	m	-	-	65
																												Mx	tr	v	v	m	-	v	tr	v	v:1, s	-	v	m	s	-	2,4,5
														NeS	-	v	v	m	tr	tr	m	v	m	m:4	v	-	-	F	tr	m	tr	tr	-	M	-	m	-	m	tr	-	-		
	09/13	M	v	M	m	tr	m	m	tr	m	m	m	s	-	Ph	-	m	v	m	-	tr	tr	v	m	-	v	-	-	F	tr	tr	m	v	-	m	-	m	-	v	m	-	-	
																											Mx	tr	m	v	v	-	v	tr	m	m:1, s	-	v	m	s	-	2,4,5	
																											FMx	tr	m	m	tr	-	m	s	m	-	M	tr	-	-			
80-1A	10/01	M	m	M	m	tr	v	m	tr	tr	m	tr	s	-	Ph	-	m	v	m	-	tr	tr	v	m	tr	-	-	-	F	tr	tr	v	m	-	m	-	m	m	tr	m	-	-	85
																											Mx	tr	m	v	v	-	v	tr	m	m:2,4	m	m	s	-			





TABLE 5-III (contd.).

Sample no.	Thin section no.	Rock mineralogy											Mineralogy of rock-pores and interstices											Mineralogy of fractures-F, breccia matrix-Mx, fractures in breccia matrix-FMx											cps										
		1	2	3	4	5	6	7	8	9	10	11	12	13	15	16	17	18	19	20	21	22	23	24	25	26	27	28	30	31	32	33	34	35		36	37	38	39	40	41	42	43	44	
123-1A	123-1A-A	M	M	v	m	tr	m	tr	-	m	tr	tr	-	-	Ph	-	tr	tr	-	-	-	-	tr	-	M:4	tr	-	-	F	tr	tr	tr	tr	-	tr	-	m	v:1,4	tr	-	-	-			
	123-1A-C	M	m	m	tr	tr	m	tr	-	tr	tr	tr:4	-	-	Ph	-	m	m	m	-	tr	tr	M	tr	-	-	-	-	M	tr	tr	m	M	-	M	-	m	-	-	m	tr	-	-		
	123-1A-D	M	m	m	tr	tr	m	tr	-	tr	tr	tr:4	-	-	Ph	-	tr	tr	tr	-	tr	tr	M	M	m:4	M	-	-	F	tr	-	tr	M	-	tr	-	tr	m:4	m	tr	-	-			
129-1A	129-1A-B	M	m	m	tr	tr	m	tr	-	tr	tr	tr:4	-	-	Ph	-	M	M	tr	-	tr	tr	M	m	m:4	tr	-	-	F	tr	-	M	M	-	tr	-	-	tr:4	tr	tr	-	-			
	129-1A-C	M	M	m	tr	tr	m	tr	-	tr	m	tr:4	-	-	Ph	-	tr	M	m	-	tr	tr	tr	M	m:4	tr	-	-	-	-	-	-	-	-	-	-	-	-	-	-	-	-	-		
	129-1A-E	M	m	M	tr	tr	m	tr	-	m	m	tr:1,4	-	-	Ph	-	-	-	-	-	tr	-	tr	tr	M:1,4	M	-	-	F	tr	tr	M	m	-	m	-	v	-	-	m	tr	-	-		
135-1A	15/23A	M	v	v	m	tr	v	tr	-	m	m	m:1,4,5	s	-	Ph	-	m	m	tr	-	tr	tr	M	-	-	-	-	-	-	-	-	-	-	-	-	-	-	-	-	-	-	-	-	65	
	15/23B	M	v	v	m	tr	m	tr	-	m	m	m:1,4,5	s	-	Ph	-	m	M	-	-	tr	tr	m	m	-	m	-	-	F	tr	-	m	M	-	tr	-	m	v:1,4	m	tr	-	-			
139-1A	16/21	M	v	v	tr	tr	m	tr	-	m	m	tr:4	-	-	Ph	-	M	M	tr	-	tr	tr	m	v	m:4	M	-	-	F	tr	tr	tr	tr	-	M	-	tr	-	tr	tr	-	-	15		
146-1A	UK-146 M	M	tr	M	tr	tr	m	tr	-	-	tr	-	-	-	-	-	-	-	-	-	-	-	-	-	-	-	-	F	tr	tr	v	m	M	v	-	m	-	-	tr	-	-	-	-		
	UK-146 Z																												F	tr	tr	v	m	M	v	-	m	-	-	tr	-	-	-	-	

TABLE 5-III (contd.).

Sample no.	Thin section no.	Rock mineralogy											Mineralogy of rock-pores and interstices											Mineralogy of fractures-F, breccia matrix-Mx, fractures in breccia matrix-FMx											cps								
		1	2	3	4	5	6	7	8	9	10	11	12	13	15	16	17	18	19	20	21	22	23	24	25	26	27	28	30	31	32	33	34	35		36	37	38	39	40	41	42	43
148-1A	17/16A	M	M	M	m	m	m	tr	-	tr	v	m:1,4	s	-	Ph	-	m	m	tr	-	v	v	m	M	tr:4	tr	s	-	F	tr	m	tr	tr	-	m	-	v	v:1,4	tr	m	s	-	45
															Ph	-	tr	m	tr	-	-	tr	m	M	M:1	tr	-	-	Mx	tr	tr	M	m	-	M	-	m	-	-	m	s	-	
																													Mx	tr	tr	M	M	-	m	-	m	m:1,4	tr	m	s	-	
	17/16B	M	m	m	tr	tr	m	tr	tr	tr	tr	v:1,4	s	-	Ph	-	tr	m	tr	-	tr	tr	v	m	M:1,4	-	s	-	Mx	m	tr	v	m	-	v	m	v	v:1,3,4	tr	m	s	-	
																												FMx	-	tr	-	-	-	tr	-	-	M:1,3,4	-	-	s	-		
	17/16C	M	M	m	tr	tr	m	tr	tr	tr	tr	m:1,4	s	-	Ph	-	-	m	tr	-	tr	tr	M	m	m:1,4	m	-	-	Mx	m	tr	v	M	-	v	m	v	m:1,4	tr	m	s	-	
															Ph	-	tr	m	tr	-	tr	tr	m	tr	M:1,4	tr	-	-	FMx	tr	tr	m	v	-	tr	-	m	v:1	tr	tr	-	-	
	17/16D	M	M	v	tr	tr	m	tr	tr	tr	m	m:1,4	s	-															Mx	m	tr	v	M	-	v	m	v	m:1,4	tr	m	s	-	
155-1A	18/17A	M	M	v	m	tr	v	tr	tr	m	m	tr:4	s	-															Mx	m	tr	M	M	-	v	tr	M	m:1,4	v	m	s	-	25
																													FMx	-	-	-	M	-	tr	-	-	-	-	-	-	-	
	18/17B	M	v	v	m	tr	m	tr	tr	m	m	tr:1,4	s	-	Ph	-	m	M	tr	-	tr	tr	M	m	-	-	-	Mx	m	tr	M	M	-	M	m	M	m:4,1	m	m	s	-		
															Ph	-	m	M	tr	-	tr	tr	m	M	M:1,4,5	tr	-	-	FMx	tr	tr	tr	m	-	M	-	m	M:4,1	tr	tr	-	-	
	18/17C	M	v	v	m	tr	m	tr	tr	m	m	tr:1,4	s	-	Ph	-	m	m	tr	-	tr	tr	m	M	M:1,4	tr	-	-	Mx	m	tr	v	v	-	v	m	M	v:1,3,4	v	m	s	-	
	18/17D	M	M	v	m	tr	v	tr	tr	m	v	m:1,3,4	s	-															Mx	tr	tr	v	M	-	m	tr	v	m:4	m	tr	s	-	
																													Mx	m	tr	v	tr	-	m	tr	v	M:1,3,4	v	m	s	-	
164-1A	19/22A	M	tr	m	tr	tr	m	tr	tr	-	tr	-	-	-	Ph	-	tr	m	tr	-	tr	tr	M	-	-	-	-	-	Mx	tr	tr	M	tr	-	M	-	tr	-	-	tr	-	-	15
																													F	tr	tr	v	tr	-	M	-	tr	-	-	-	-	-	
	19/22B	M	m	v	tr	tr	m	tr	tr	-	tr	-	-	-															Mx	tr	tr	v	m	-	v	tr	v	-	-	tr	-	-	

TABLE 5-III (contd.).

Sample no.	Thin section no.	Rock mineralogy											Mineralogy of rock-pores and interstices											Mineralogy of fractures-F, breccia matrix-Mx, fractures in breccia matrix-FMx											cps																
		1	2	3	4	5	6	7	8	9	10	11	12	13	15	16	17	18	19	20	21	22	23	24	25	26	27	28	30	31	32	33	34	35		36	37	38	39	40	41	42	43	44							
175-1A	20/13A	M	v	v	m	tr	m	tr	tr	-	m	tr:4	s	-	NeS	-	v	v	tr	-	tr	tr	v	tr	v:4	tr	-	-	Mx	tr	m	v	v	-	m	tr	v	v:4	tr	m	s	-	-	-	-	-	-	-	25		
	20/13B	M	v	v	m	tr	m	tr	tr	-	m	tr:4	s	-															Mx	tr	tr	v	v	-	v	m	v	m:4	tr	m	s	-	-	-	-	-	-	-	-		
178-1A	178-1A-A	M	m	m	tr	tr	m	tr	m	tr	m	m:4	s	-	Ph	-	M	m	-	tr	-	-	M	tr	v:4	tr	-	-	F	-	-	tr	M	-	tr	-	-	-	-	-	-	-	-	-	-	-	-	-	-		
	178-1A-B	M	v	v	m	m	m	tr	m	tr	m	m:4	s	-														Mx	m	tr	v	v	-	m	M	M	m:4	tr	tr	s	-	-	-	-	-	-	-	-	-		
	178-1A-C	M	m	m	tr	tr	m	tr	v	tr	v	m:4	-	-	Ph	-	tr	tr	tr	-	tr	tr	M	-	v:4	-	-	-	Mx	v	m	v	v	-	m	M	M	m:4	tr	m	s	-	-	-	-	-	-	-	-	-	
181-1A	21/14	M	v	v	tr	tr	m	tr	tr	-	m	-	-	-	Ph	-	M	tr	-	tr	-	-	m	tr	-	-	-	-	Mx	m	tr	v	v	-	v	m	m	-	-	m	-	-	-	-	-	-	-	-	-	20	
192-1A	22/10	M	v	v	tr	tr	m	tr	tr	-	m	-	-	-	Ph	m	M	tr	-	-	tr	tr	M	m	-	-	-	-	FMx	-	-	tr	M	m	tr	-	-	-	-	-	-	-	-	-	-	-	-	-	5		
																													Mx	tr	tr	m	M	m	M	tr	m	-	-	tr	-	-	-	-	-	-	-	-	-	-	-
201-B	23/12	See table: Mineralogy of biotite-lamprophyres											See table: Mineralogy of biotite-lamprophyres											See table: Mineralogy of biotite-lamprophyres											bg																
216-1A	24/9A	M	M	m	tr	tr	m	tr	tr	-	tr	-	-	-	Ph	-	m	tr	tr	-	m	tr	M	m	-	-	-	-	F	tr	-	v	M	-	m	-	tr	-	-	-	-	-	-	-	-	-	-	-	-	20	
	24/9B	M	M	m	tr	tr	m	tr	tr	-	tr	-	-	-	Ph	-	tr	tr	tr	-	m	tr	M	m	-	-	-	-	F	M	tr	v	v	-	M	-	v	-	-	tr	-	-	-	-	-	-	-	-	-	-	-
223-1A	25/15	M	v	m	tr	tr	m	tr	tr	tr	tr	m:1,4	-	-	Ph	-	M	tr	-	tr	tr	tr	m	tr	m:1,4	tr	-	-	F	tr	tr	tr	M	-	M	-	tr	m:1,4	tr	tr	-	-	-	-	-	-	-	-	-	15	
229-1A	26/6A	M	M	m	tr	tr	m	tr	tr	tr	m	tr:1,4	-	-	Ph	-	M	tr	tr	-	tr	tr	M	m	tr:1,4	-	-	-	F	m	tr	tr	m	-	M	-	m	tr:1,4	tr	tr	-	-	-	-	-	-	-	-	-	20	
	26/6B	M	M	m	tr	tr	m	tr	tr	tr	m	m:1,4,5	-	-	Br	-	tr	tr	tr	-	-	tr	tr	m	M:1,5	tr	-	-	Mx	tr	tr	m	tr	-	v	tr	m	m:1,4	tr	m	-	-	-	-	-	-	-	-	-	-	
																												FMx	-	tr	tr	m	-	M	-	m	M:1,4	tr	tr	-	-	-	-	-	-	-	-	-	-	-	-







TABLE 5-III (contd.).

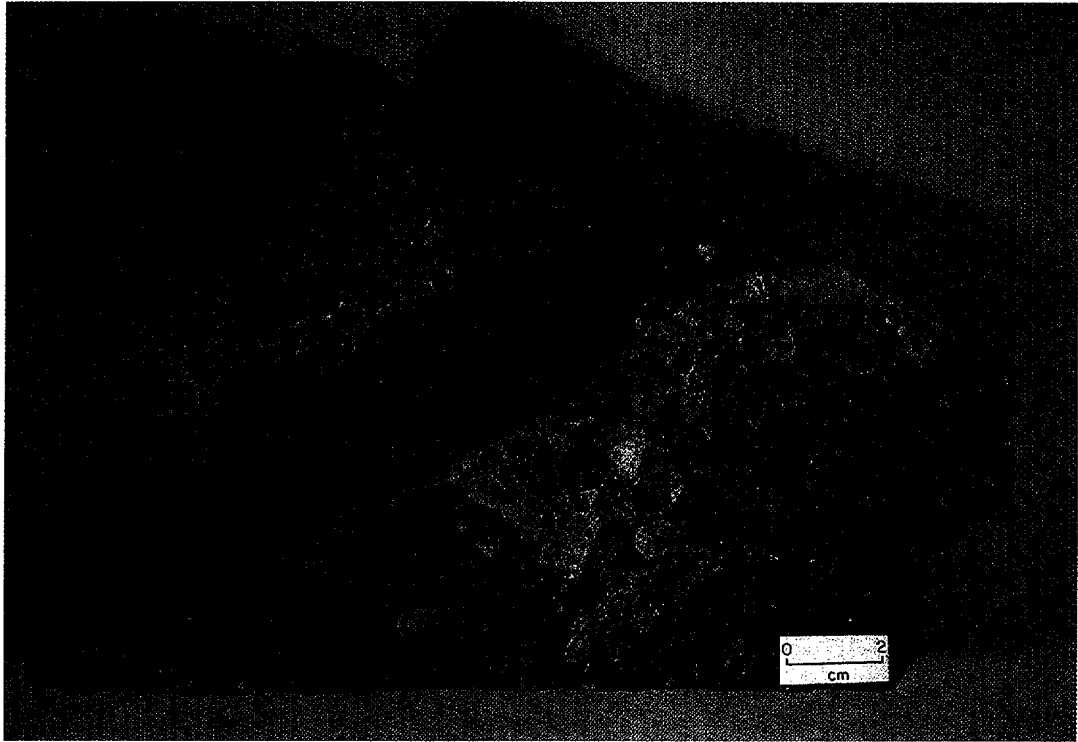
Sample no.	Thin section no.	Rock mineralogy											Mineralogy of rock-pores and interstices											Mineralogy of fractures-F, breccia matrix-Mx, fractures in breccia matrix-FMx											cps								
		1	2	3	4	5	6	7	8	9	10	11	12	13	15	16	17	18	19	20	21	22	23	24	25	26	27	28	30	31	32	33	34	35		36	37	38	39	40	41	42	43
300-1A (contd.)	36/25	M	m	m	tr	tr	tr	tr	v	m	m:1, 2,4,5	-	-																Mx	tr	tr	m	tr	-	m	tr	m	m:1 2,4,5	M	m	-	-	
	26/26	M	m	m	m	tr	m	tr	tr	m	m	-	-																Mx	tr	tr	m	tr	-	m	tr	m	-	M	M	-	-	
314-1A	314/1	m	tr	M	m	M:1-5	-	-															Mx	tr	tr	tr	-	-	tr	tr	m	M:1-5	M	tr	-	-							
	314/2	m	tr	m	tr	tr	tr	tr	tr	M	M	M:1-5	-	-															Mx	tr	tr	-	-	-	tr	-	M	M:1-5	M	tr	-	-	
	314-A/1	M	tr	m	tr	tr	m	tr	tr	v	m	m:1-5	-	-															Mx	tr	tr	m	tr	-	m	-	M	M:1-5	M	m	-	-	
	314-A/2	M	tr	m	tr	tr	tr	tr	tr	m	m	m:1-5	-	-	Ph	-	-	m	-	-	tr	-	-	tr	M:1,4	m	-	-	Mx	tr	tr	m	tr	-	tr	-	M	M:1-5	M	tr	-	-	
315-1A	37/9	M	m	M	m	tr	v	tr	tr	tr	m	m:1, 2,4,5	-	-															Mx	m	tr	v	tr	-	v	-	m	m:1, 2,4,5	tr	m	-	-	bg
320-1A	38/22	M	M	m	tr	tr	m	tr	tr	-	tr	-	-	Ph	-	M	M	m	tr	tr	tr	tr	tr	tr	-	-	-	-	F	tr	tr	m	M	-	tr	-	tr	-	-	-	-	-	bg
328-1A	39/28	M	M	m	tr	tr	m	tr		m	m	-	-	Ph															F	tr	tr	M	m	-	m	-	m	-	m	m	-	-	5
330-1A		See table: Mineralogy of biotite-lamprophyres											See table: Mineralogy of biotite-lamprophyres											See table: Mineralogy of biotite-lamprophyres																			
331-1A		See table: Mineralogy of biotite-lamprophyres											See table: Mineralogy of biotite-lamprophyres											See table: Mineralogy of biotite-lamprophyres																			
375-1B	40/44	M	M	m	tr	tr	m	tr	tr	tr	-	tr:4,5	-	-	Ph														F	tr	tr	M	v	-	M	-	tr	-	-	tr	-	-	10
	40/45	M	M	m	tr	tr	m	tr	tr	tr	m	tr:4,5	-	-	Ph	-	-	-	-	-	-	-	-	-	-	M:4,5	tr	-	-	Mx	tr	tr	m	M	tr	v	m	m	-	-	tr	-	-



TABLE 5-III (contd.).

Sample no.	Thin section no.	Rock mineralogy											Mineralogy of rock-pores and interstices											Mineralogy of fractures-F, breccia matrix-Mx, fractures in breccia matrix-FMx											cps									
		1	2	3	4	5	6	7	8	9	10	11	12	13	15	16	17	18	19	20	21	22	23	24	25	26	27	28	30	31	32	33	34	35		36	37	38	39	40	41	42	43	44
406-1A	49/41	M	M	m	tr	tr	m	tr	tr	-	-	-	-	NeS															F	m	tr	m	tr	-	M	tr	m	-	-	tr	-	-	10	
	49/42	M	m	m	tr	tr	m	tr	tr	-	tr	-	-	NeS															F	tr	tr	-	-	-	M	m	tr	-	-	-	-	-	-	
	49/43	M	m	m	tr	tr	m	tr	tr	-	tr	-	-	NeS	-	M	tr	m	-	tr	tr	m	tr	-	-	-	-	-	-	-	-	-	-	-	-	-	-	-	-	-	-	-	-	
407-1A	407/1A	M	M	m	tr	tr	m	tr	tr	-	tr	-	-	Ph	-	v	-	-	M	-	-	-	-	-	-	-	-	-	-	-	-	-	-	-	-	-	-	-	-	-	-	-	-	
409/1B	50/29	M	v	m	tr	tr	m	tr	tr	-	tr	-	-	Ph	-	M	m	-	tr	-	-	m	tr	-	-	-	-	-	-	-	-	-	-	-	-	-	-	-	-	-	-	-	-	bg
														NeS	-	-	tr	-	v	-	tr	M	-	-	-	-	-	-	-	-	-	-	-	-	-	-	-	-	-	-	-	-	-	-
414-1A	51/46	M	M	m	tr	tr	m	tr	tr	-	tr	-	-	Ph	-	M	m	-	M	-	tr	M	-	-	-	-	-	F	m	tr	v	m	-	v	tr	tr	-	-	tr	-	-	-	bg	
	51/47	M	v	m	tr	tr	v	tr	m	-	tr	-	-	Ph	-	tr	M	tr	-	tr	tr	M	M	-	-	-	-	-	-	-	-	-	-	-	-	-	-	-	-	-	-	-	-	
	51/48	M	m	m	tr	tr	m	tr	tr	-	tr	-	-	NeS	-	-	m	-	M	-	tr	M	tr	-	-	-	-	F	tr	tr	tr	-	-	M	m	tr	-	-	tr	-	-	-	-	
	51/49	M	v	v	tr	tr	m	tr	tr	-	tr	-	-	-	-	-	-	-	-	-	-	-	-	-	-	-	-	F	-	tr	-	-	-	M	tr	tr	-	-	-	-	-	-	-	

**Appendix 5:1**  
**PLATES 5:1-1 – 5:1-12.**



*PLATE 5:1-1. Clast- and clast-matrix-supported hydrothermalised breccia with redox front. Note the well-developed breccia structures in the reduced (grey-coloured) portions of the sample and their obliteration in the oxidised, Fe-oxide/hydroxide (HFO)-stained (yellow-brown coloured) parts. Compare with PLATE 5:1-2. Specimen: B-breccia ore body (mine exposure).*

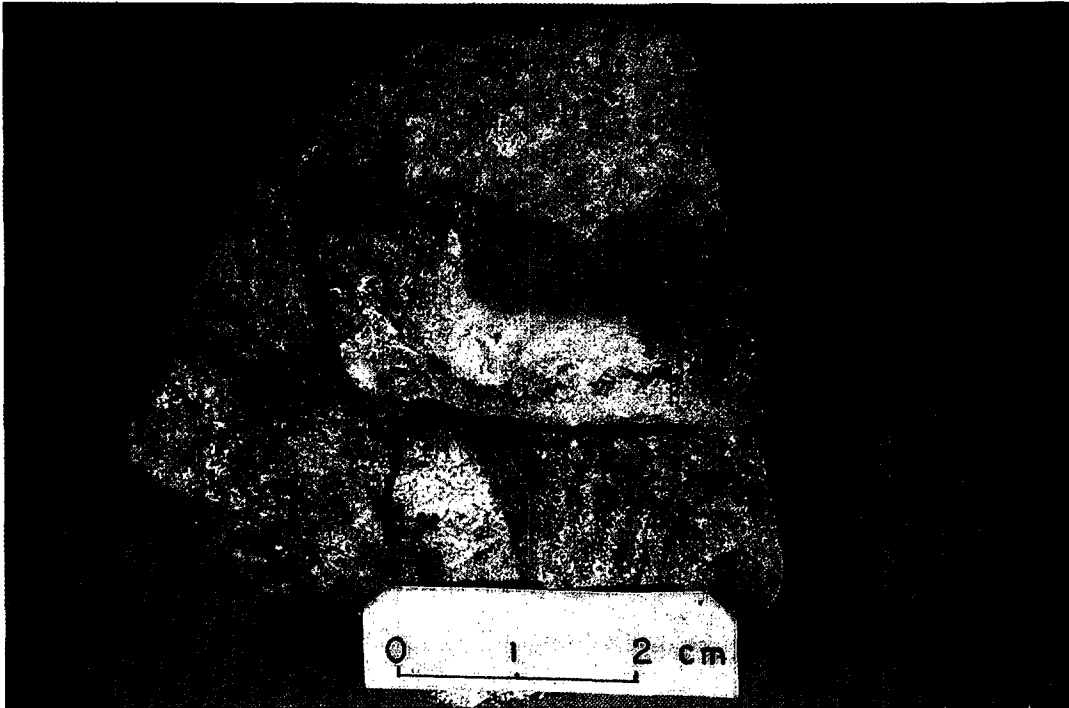


*PLATE 5:1-2. Oxidised, porphyritic and slightly fractured subvolcanic phonolite with breccia-like features due to the irregular distribution of HFO-staining. Compare with PLATE 5:1-1.  
Specimen: borehole F1 (9-1WC11); sample 47.*



*PLATE 5:1-3. Very coarse breccia of the matrix to clast-matrix-supported type, reduced in the outcrop parts with well-preserved structures (greyish-blue colouration). Oxidation masks the breccia structures (brown-coloured outcrop parts) and changes the reduced greyish-blue colours of the pyrite and Mo-mineralisations to brown, due to pervasive HFO precipitation/pigmentation.  
Specimen: B-breccia ore body (mine exposure).*

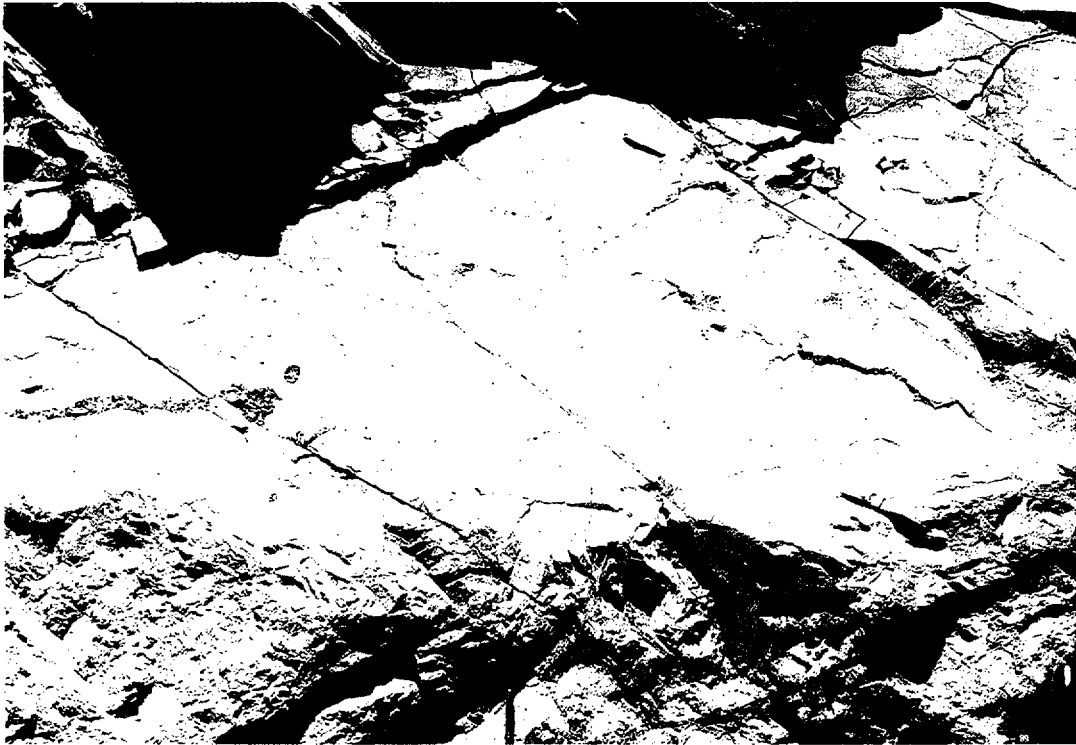


*PLATE 5:1-4. Detail of the very coarse breccia (from PLATE 5:1-3). Note the up to 1 m sized angular clasts set in a matrix coarser than the breccia shown in PLATE 5:1-1.*



*PLATE 5:1-5. Sample of hydrothermalised, reduced, heterolithic clast-supported breccia, with violet fluorite in the matrix. About 3/4 nat. size. Specimen: borehole F4 (8-1UK11); sample 202.*

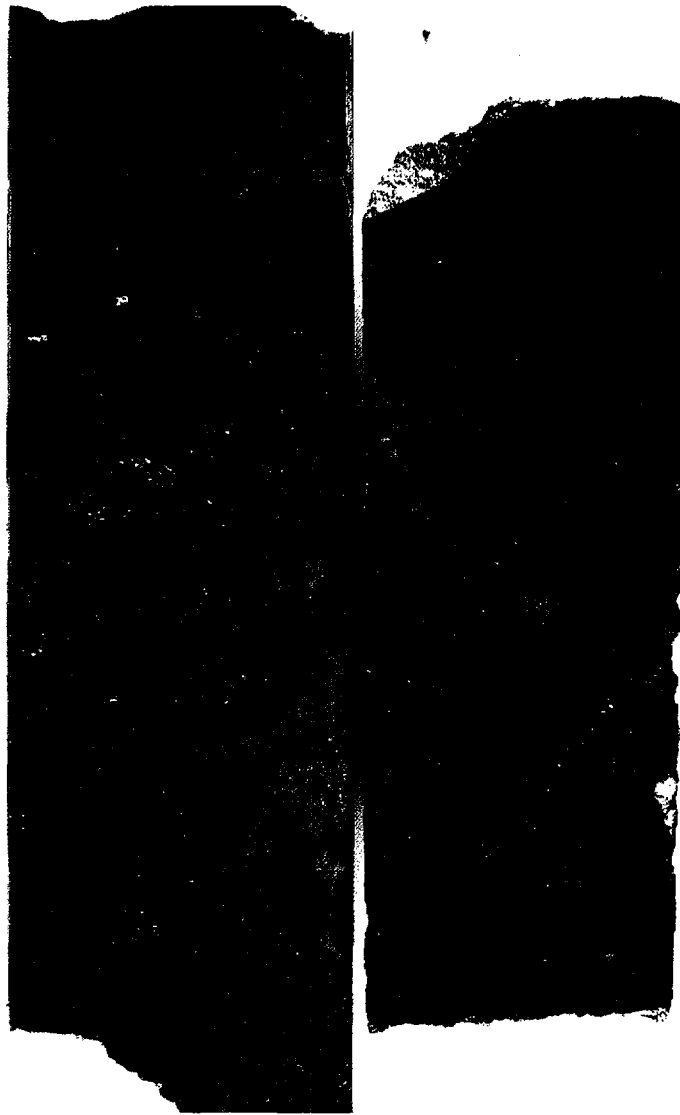


*PLATE 5:1-6. Sample of hydrothermally altered, reduced, heterolithic clast-supported breccia containing a fragment of violet fluorite (circled in the polished thin section). About nat. size.*

*Specimen: borehole F4 (8-1UK11); sample 303-1A.*



*PLATE 5:1-7. Reduced microbreccia with angular fragments and set in a hydrothermal dark violet (almost black) fluorite matrix (mineralisation). The sample is also high in radioactivity; see Table 5-1. About 3x nat. size.*



*PLATE 5:1-8. Reduced clast-matrix-supported breccia with open macropores/caverns, higher radioactivity (Table 5-I) and blue Mo-staining. Note the variable colours and grades of the pre-breccia mineralised fragments. About nat. size. Specimen: borehole F4 (8-1UK11); sample 210-1A.*

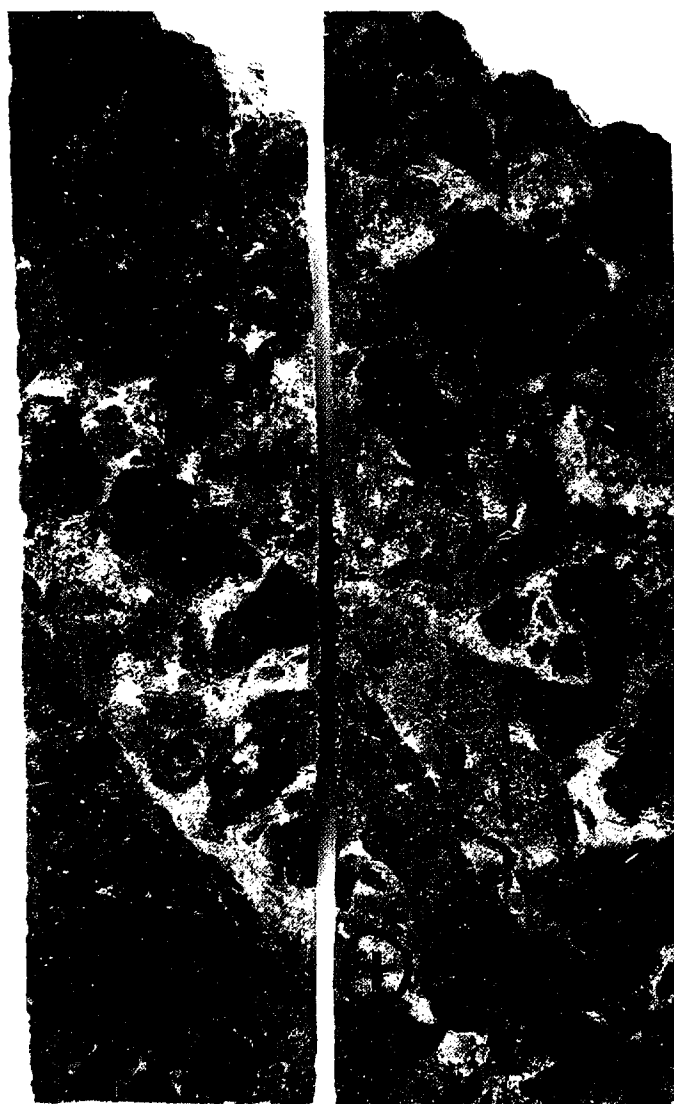


*PLATE 5:1-9. Reduced clast-matrix-supported breccia with matrix rich in white (kaolinite) clays and poor in pyrite; minor micropores and fragments show variable colours and grades of pre-breccia pyritisation and of blue Mo-staining. About nat. size. Specimen: borehole F4 (8-1UK11); sample 252-1A.*

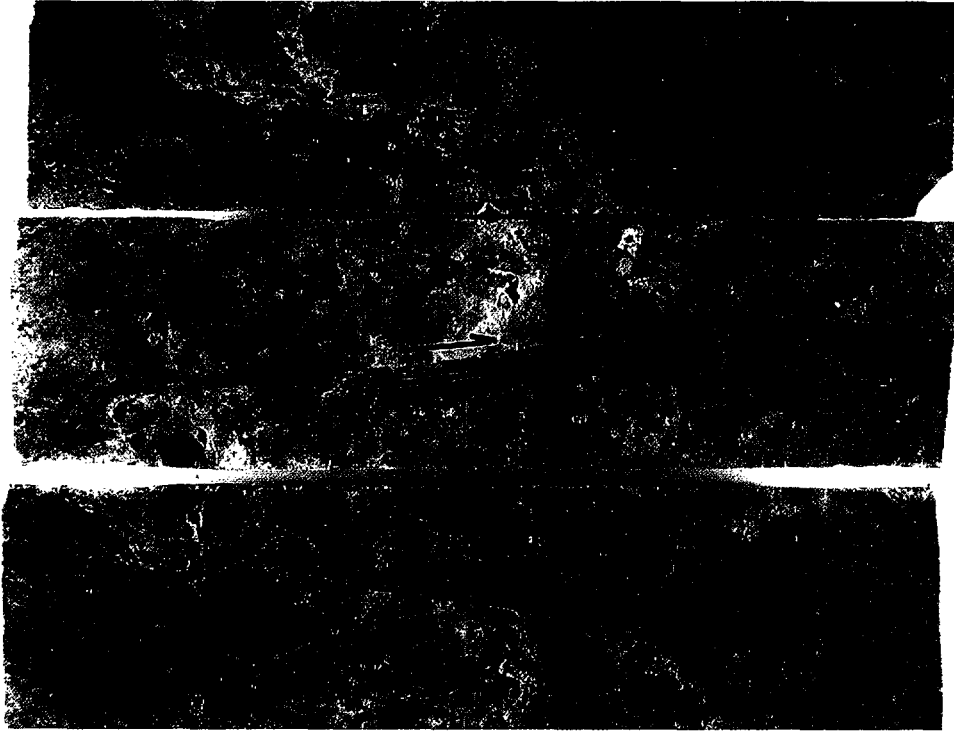


*PLATE 5:1-10. Reduced clast-supported breccia with high grade hydrothermal U-mineralisation marked by circles (90 and 100 cps above background). The breccia and U-mineralisation were transected and disrupted by post-mineralisation and post-breccia fracturing. U-mineralisation is associated with sulphides (black colouration in circle represents 100 cps, grey with whitish sulphate alterations 90 cps). Polished thin sections; about 3/4 nat. size.*

*Specimen: borehole F4 (8-1UK11); sample 243-1A.*

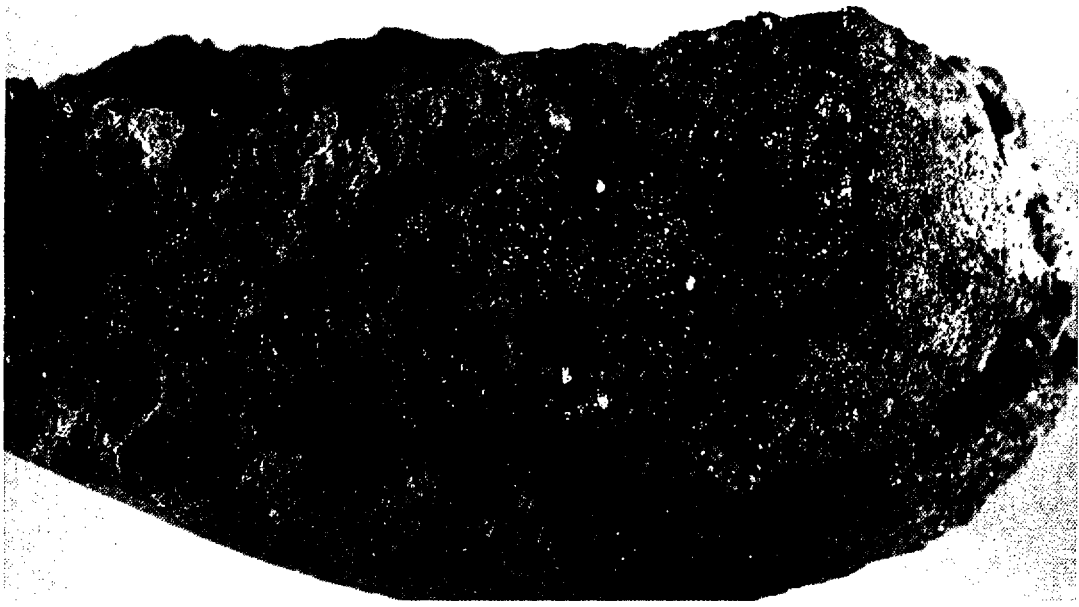


*PLATE 5:1-11. Reduced breccia with post-breccia fractures mineralised with secondary hydrothermal sulphides (mainly pyrite and coated pyrite, the coatings originally identified as possible galena, but not confirmed). About 3x nat. size. Specimen: borehole F4 (8-1UK11); sample 394-1A.*



*PLATE 5:1-12. Reduced breccia with post-breccia fractures mineralised with secondary hydrothermal sulphides, mainly pyrite and coated pyrite. Circle indicates location of polished section. Sawed surface; about 2x nat. size. Specimen: borehole F4 (8-1UK11); sample 383-1A.*

## **Appendix 5:2**

**Model for the evolution of the rock sequence observed at  
the Osamu Utsumi mine.**

## Appendix 5:2

### Model for the evolution of the rock sequence observed at the Osamu Utsumi mine.

**Stage 1** (Fig. 5:2-1) involves the main alkaline phonolite and nepheline syenite magmatism (1.1), progressing to the postmagmatic (pegmatitic-) pneumatolytic (1.2) and hydrothermal (1.3) sub-stages.

*The magmatic mineral association of sub-stage 1.1* may be considered essentially the same as in the regional rocks (Table 5-III: Ph, NeS; minerals of columns: 1, 2, 3, 4, 5, 6), as supported by the presence of pseudomorphs and relicts in the hydrothermalised host rocks and fragments of the breccias in the mine (Table 5-III: Ph-A, NeS-A; equivalent minerals).

*Mineral associations of sub-stage 1.2* were most probably similar to those observed in the regional rocks (Table 5-III; Ph, NeS; minerals of columns: 7, 8, 9), with or without additional agpaitic rare metals silicates instead of giannettite, but were not preserved in the studied rocks of the mine.

*Mineral associations of sub-stage 1.3* must also be inferred from the regional rocks (Table 5-III: Ph, NeS; minerals of columns: 9, 10). However, it is important to note that this sub-stage included the partial dissolution of rare metal silicates, as evidenced by giannettite in some of the regional rocks, and that it generally caused only incipient, incomplete alteration.

**Stage 2** includes the breccia-forming and mineralising tectono-magmatic and hydrothermal processes. A pre-breccia, pre- to early syntectonic hydrothermal sub-stage (2.1) can be distinguished, as well as the main breccia formation and Zr-U-mineralising tectono-magmatic and hydrothermal sub-stages (2.2; 2.3; 2.4; 2.5) and a post-breccia (late- to post-tectonic) hydrothermal sub-stage (2.6).

**Sub-stage 2.1** developed during increasing hydrothermal activity and an intensification of tectonic fracturing. This resulted in formation of the “potassic rock” by processes that were continuous throughout the sub-stage, for instance the general pyritisation of the rocks, and other discontinuous processes which succeeded each other in temperature and time. The latter included the sometimes total dissolution of the pneumatolytic rare metal silicates, followed at higher temperatures by the precipitation

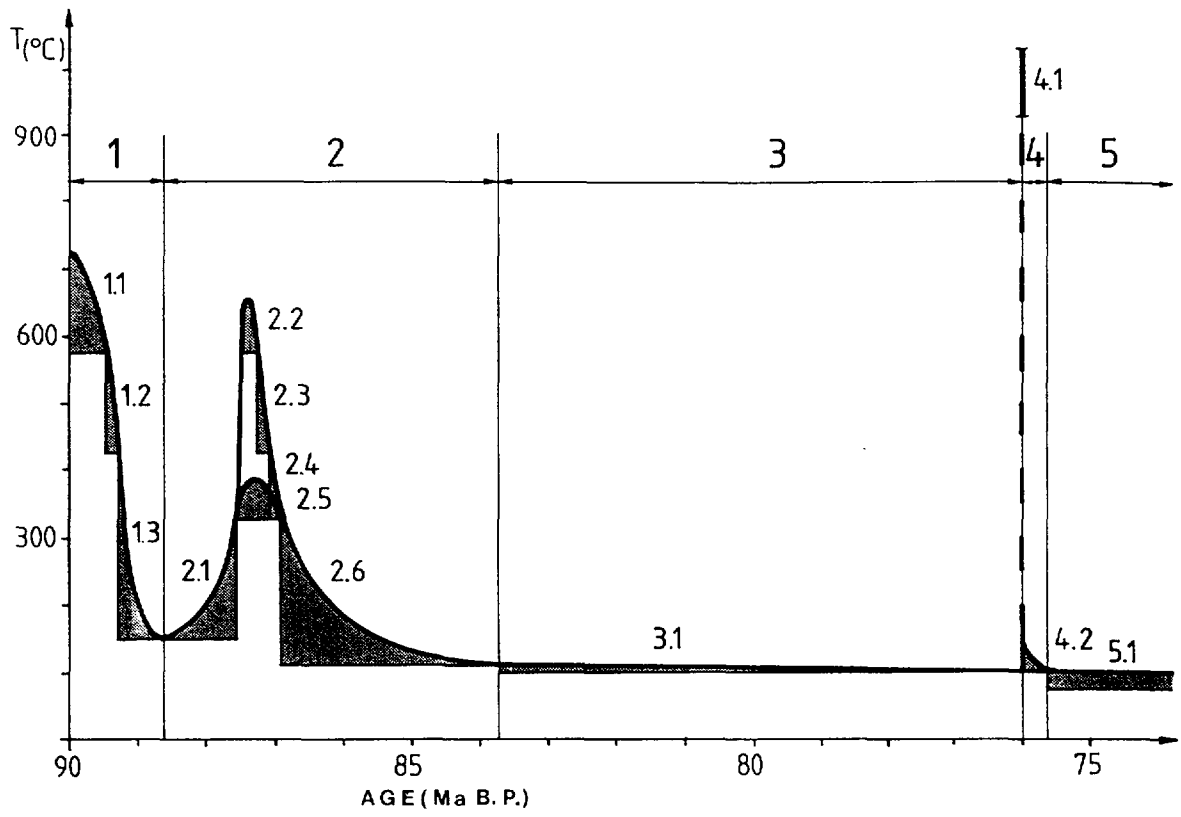


Figure 5:2-1. Model for the evolution of the rock sequence observed at the Osamu Utsumi mine.

of hydrothermal zircons and, independently, the advanced kaolinisation of the rocks. This in turn was followed by illitisation/sericitisation and the structural readjustment and alkali exchange reactions of the primary high-temperature K-Na feldspars.

**Sub-stages 2.2 – 2.5** of the main breccia-forming magmato-tectonic and hydrothermal activities included, during sub-stage 2.2, the explosive (magmato-phreatic) eruption of minor amounts of highly fluidised pseudoleucite (plc.)-phonolite magma (2.2) that produced rare high-temperature breccias, in cases grading to xenolithic plc.-phonolites. The magmatic mineral associations of these rocks (2.2) were, as far as can be deduced from pseudomorphs and relicts, similar to those of the country rocks in the mine (Table 5-III; Ph-A, NeS-A). However, textures are distinct, generally exhibiting an extremely fine to cryptocrystalline flow-oriented matrix with only rare and not very coarse plc.-phenocrysts.

**Sub-stages 2.3 and 2.4** of postmagmatic pneumatolytic and hydrothermal alteration of high-temperature breccias and phonolites could not be documented in the studied rocks; their possible existence was inferred.

**Sub-stage 2.5** represents the hydrothermal alteration of the main breccia and Zr-U-mineralising processes. These acted syntectonically and almost exclusively in the matrix of the breccias. Mineral associations vary considerably (Table 5-III: mineralogy of breccia matrix), indicating the heterogeneous composition of the hydrothermal/mineralising fluids. However, in the samples of higher radioactivity, pyrite and other unidentified opaque ore minerals, highly metamictic zircons and other unidentified semi-opaque minerals, hydrothermal clay minerals and, not infrequently, Mo-minerals, violet fluorite and associated yellowish-brown coloured carbonates are always found.

**Sub-stage 2.6** includes mainly pyrite, hydrothermal clay minerals, violet fluorite and associated yellowish-brown carbonate, which occur in post-breccia fractures. They may be partly, or totally identical to the mineral assemblages that occur as the latest fillings of voids (porosities and interstices) in the breccia matrices and rock fragments, and were therefore attributed to the final part of sub-stage 2.5.

**Stage 3, sub-stage 3.1** is in fact a continuation of sub-stage 2.6. It was assumed to represent a possible post-breccia and pre-biotite lamprophyre period of minor fracturing and weak hydrothermalism that developed under steady-state slow cooling conditions on a regional scale. The main indications are post-breccia fractures with pyrite and coated pyrites, sometimes associated with clay minerals (mainly kaolinite). In addition, true post-breccia fractures filled with colourless carbonate could also be observed.

**Stage 4** includes renewed tectonic activity, fracturing, and the intrusion and hydrothermal alteration of the biotite lamprophyres. These rocks, which originated from very deep-seated, upper mantle-derived mafic-ultramafic magmas, cut through the breccias and hydrothermally altered country rocks of the mine. They had no influence on either the regional thermal/cooling history or on a local scale, as indicated by the presence microxenoliths of hydrothermally altered country rocks of the mine (Ph and NeS) found in the lamprophyres. The highly fluidised mafic-ultramafic magmas had high eruption temperatures as indicated for sub-stage 4.1. The magmatic mineral associations of the rocks and the mineralogy of the xenoliths are described in Table 5-III. Postmagmatic hydrothermal processes considered as sub-stage 4.2 affected mainly the lamprophyres, resulting in zeolitisation and carbonatisation. These hydrothermal processes may also have a minor influence adjacent to the dykes, e.g. along fractures containing hydrothermally altered Ph, NeS and breccia wall rocks.

**Stage 5** refers to the period from post-lamprophyre to the present thermal/cooling history of the Poços de Caldas alkaline complex. It includes the onset of supergene (weathering and erosion) processes and, at least locally, the continuation (including surface manifestation) of hydrothermal processes up to the present time as documented, for instance, by active thermal springs. Additionally, the study of the regional heat flux in the surrounding parts of the Precambrian Shield gave mean values of about 40(mw/m<sup>2</sup>sec.), as compared to about 60 as mean and 80-82 as maximum values within the internal parts of the complex (Castro de Araújo, 1977). This would further support the possibility that generalised hydrothermal conditions still exist in the sub-surface of the complex. The hydrothermal processes of **sub-stage 5.1** could not be defined in this study. Furthermore, values for the regional/local cooling rates and the approximate onset time of supergene (weathering) processes are not known.

## **Bibliography**

- Castro de Araújo, R.L., 1977. Pesquisa de fluxo térmico na chaminé alcalina de Poços de Caldas. *Dissertação (inéd.)*, Inst. Astron. Geofís. (IAG), USP, São Paulo.
- Kawashita, K., Mahiques, M.M. de and Ulbrich, H., 1984. Idades Rb/Sr de nefelina sienitos do anel norte do maciço alcalino de Poços de Caldas, MG-SP. -23° *Cong. Bras. Geol.*, Resumos e Breves Comunicações, 244-245 (Ed. Soc. Bras. Geol.), Rio de Janeiro.

- Miranda Filho, M.C. de, 1983. Síntese do modelo geológico-estrutural da Mina de Caldas (modelação e projeto de lavra, parte I), 44 p, *NUCLEBRÁS, Poços de Caldas*.
- Ulbrich, H.H.G.J., 1984. A petrografia, a estrutura e o quimismo de nefelina sienitos do Maciço Alcalino de Poços de Caldas, MG-SP. *Tese de Livre Docência (inéd.)*, 2 vols., Inst. Geociências, USP, São Paulo.

## **Appendix 6**

### **Mineralogy and geochemistry of redox front I (RFI).**

# Contents

	page
1. Introduction	413
2. Field observations and sampling	413
3. Macroscopic descriptions and sample preparation	415
3.1. Macroscopic descriptions	415
3.2. Sample preparation	419
4. Mineralogy and petrography	419
4.1. Non-mineralised rocks	419
4.2. Mineralised rocks	422
4.3. X-ray diffraction (XRD) studies	426
5. Rock physical parameters	428
6. Geochemistry	429
6.1. Sample preparation and analysis	429
6.2. Geochemistry of sample set I (large-sized samples)	433
6.3. Geochemistry of sample set II (main XRF samples)	434
6.3.1. RFI phonolites: magmatic composition and hydrothermally altered potassic rock	435
6.3.2. RFI oxidised and reduced phonolites	444
6.3.3. RFI redox front processes	446
7. Summary	460
8. References	462
APPENDICES:	
Appendix 6:1: PLATES 6:1-1 – 6:1-9	465
Appendix 6:2: Rock chemical data for RFI	477

## **Appendix 6**

### **Mineralogy and geochemistry of redox front I (RFI).**

**H.D. SCHORSCHER**

Universidade de São Paulo, Instituto de Geociências-DMP, C.P. 20 899,  
014 98 São Paulo (Brazil).

#### **1. Introduction**

Redox front I (RFI) was sampled from the Osamu Utsumi uranium mine (open pit, coordinates 8.2BJ.61). Two sample sets were prepared for distribution; one set for measurements of natural Pu and Tc, and the other for radiochemistry and global geochemistry.

Mineralogical, petrographic and geochemical studies were carried out at the University of Bern using routine XRF major and trace element analysis, together with the determination of rock physical parameters.

#### **2. Field observations and sampling**

RFI constitutes a complete profile across oxidised phonolite, the redox front *sensu stricto* and the reduced phonolite. On the reduced side, about 10 cm away from the redox front, a zone of secondary nodular U-mineralisation begins. This zone is about 30 cm wide and grades away from the front, accompanied by the disappearance of U-nodules into the reduced country phonolite.

The phonolite is an extremely fine-grained, almost aphanitic rock containing only subordinate coarser components (phenocrysts and microxenoliths). The oxidised phonolite is a light yellow/brown colour and the reduced phonolite is light to medium grey in colour.

The total width of the exposed profile was about 3 metres. Sampling was conducted systematically through the oxidised portion, the redox front, and included about 50 cm of the adjacent reduced phonolite, which contained the zone of secondary U-mineralisation. Following this, two sampling intervals of about 35 and 100 cm were selected within the reduced country phonolite further away from the redox front. Figure 6-1 gives a schematic view of the original outcrop situation and of the approximate spacial

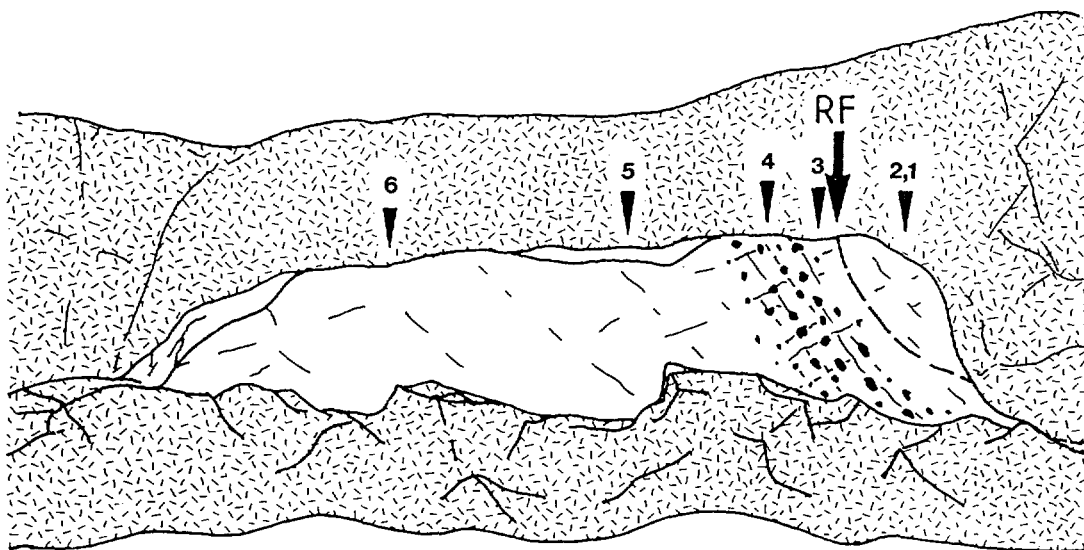


*Figure 6-1. Schematic view of the original outcrop situation at the RFI sampling site (scale 3 m long). Indicated are the approximate positions of the redox front (RF) and of the sampling locations RFI 1 to 6. Oxidised rocks occur on the right-hand side of the redox front and reduced rocks on the left. The zone of maximum U-mineralisation is indicated by black dots representing pitchblende nodules (Osamu Utsumi uranium mine, coordinates: 8.2 BJ.61, view towards the E).*

and structural relationships of the collected samples. The individual samples were medium-sized, weighing between 8 and 15 kg each.

### **3. Macroscopic descriptions and sample preparation**

#### **3.1. Macroscopic descriptions**

Detailed sample descriptions have been carried out and the various textural features illustrated in Plates 6:1-1 to 6:1-6 (Appendix 6:1); summarised sample descriptions and radioactivity measurements are contained in Table 6-I. Briefly, the RFI rocks suffered hydrothermal and supergenic alteration, following the early magmatic genetic stage; the supergene alteration occurred under reducing conditions or reducing conditions followed by oxidising conditions. The reduced RFI rocks furthest from the redox front (Fig. 6-1, samples RFI-5 and -6; Plates 6:1-5 and 6:1-6) have best preserved the primary magmatic and subsequent hydrothermal properties.

The main host rock is a very fine-grained, almost aphanitic phonolite of light to medium grey colour. It is normally only weakly porphyritic and microxenolithic (Plate 6:1-5), although in sample RFI-6 (Plate 6:1-6) there occurs one larger nepheline syenite xenolith. Phenocrysts consist of pseudoleucite, alkali feldspar and (pseudomorphosed) nepheline; microxenoliths of nepheline syenite and phonolite fragments also occur.

Hydrothermal effects include mainly the porous leaching of pseudoleucite phenocrysts, (micro-)xenoliths of nepheline syenites (Plate 6:1-6) and coarser-grained phonolites, and the disseminated pyritisation of the rocks and fracture planes.

The supergenic processes led to the development of the redox fronts which are locally associated with secondary U-mineralisations occurring on the reduced sides, and generally associated with the precipitation of hydrous ferric oxides (HFO) on the oxidised sides of the fronts.

The RFI redox front is easily recognisable due to the sharply developed colour contrast between the HFO-bearing oxidised and pyrite-bearing reduced rocks (Plates 6:1-1 and 6:1-2). The secondary supergenic U-mineralisation concentrates in the reduced rocks (Plates 6:1-3 and 6:1-4), forming a zone of variable width (20 – 30 cm) extending almost parallel to the redox front.

The mineralised zone, however, starts only some 5 to 10 cm ahead of the HFO precipitation front located inside the pyrite domain (Plate 6:1-3). The U-mineralisation consists of black coloured aggregates of cryptocrystalline oxides occurring either as

TABLE 6-I  
Summarised macroscopic petrography of RFI samples (see Fig. 6-1 for sample location).

Current no.	Sample code	Sample description	Radioactivity cps above bg	Refer to PLATES in Appendix 6:1
1	RFI-1	Oxidised, light-yellow/brown in colour, very fine-grained microporphyritic and microxenolithic phonolite. The sample extends from about 30 cm in the host rock to the redox front. It shows a homogeneous and oscillatory zoned hydrous ferric oxide (mainly limonite) distribution, and contains bleached, whitish coloured residual nodules resulting from pitchblende dissolution.	30	
2	RFI-2	Rock composed mainly of oxidised and minor reduced phonolite, including the redox front. The sample extends from about 25 cm before the redox front to about 10 cm into the reduced phonolite, and represents the physical continuation of sample RFI-1. Only the reduced phonolite differs, being light-grey in colour, characterised by finely disseminated pyrite and is free of HFO minerals.	30 (10 cm before RF); 50 (Zone rich in HFO close to RF); 50 (Reduced side close to RF);	6:1-1; 6:1-2
3	RFI-3	Rock composed mainly of reduced phonolite, minor oxidised phonolite, including the redox front. The reduced phonolite is characterised by a 10 cm zone immediately adjacent to the redox front which is free of nodular U-mineralisation. This zone soon gives way to the appearance of pitchblende nodules and eventually to the zone of maximum mineralisation.	50 (Zone of 10 cm near RF); 95 (Transition to U-mineralised zone);	6:1-3

TABLE 6-I (contd.).

Current no.	Sample code	Sample description	Radioactivity cps above bg	Refer to PLATES in Appendix 6:1
4	RFI-4	Reduced phonolite selected from zone of maximum secondary (redox front-related) U-mineralisation. Pitchblende nodules of various dimensions, forms and internal textures are always controlled by fracture systems. The pitchblende nodules are commonly richer in pyrite than the enclosing reduced phonolite. The reduced rock portions consists of a very fine-grained microporphyritic and -xenolithic phonolite similar to that described above. The sample represents the profile portion which grades away from the redox front, accompanied by the disappearance of pitchblende nodules, into the normal (macroscopically non-mineralised) reduced country phonolite.	120 (Zone of max. U-mineralisation);	6:1-4
5	RFI-5	Reduced country phonolite (macroscopically non-mineralised), collected about 35 cm from sample RFI-4 within a homogeneous sequence of rock composition.	15 (Reduced country phonolite);	6:1-5
6	RFI-6	Reduced country phonolite (macroscopically non-mineralised) containing a major xenolith of reduced nepheline syenite. The sample was collected about 1 m from sample RFI-5 in a sequence of macroscopically homogeneous phonolites.	15 (Reduced country phonolite);	6:1-6

nodular concretions of rounded, elliptical or, more rarely, irregular forms of pitchblende (of submillimetric to centimetric dimensions and sometimes showing zoning structures; Plates 6:1-3 and 6:1-4), or as very fine, normally submillimetric coatings on fracture surfaces (Plate 6:1-3). The secondary U-mineralisations are always enriched in pyrite compared to the host (reduced) rocks.

Genetically and structurally it is significant that the formation and preferential development of both types of secondary U-mineralisation are controlled by fractures/fracture systems (Plates 6:1-3 and 6:1-4).

Within the 5 – 10 cm zone of reduced rocks closest to the HFO front, the progressive and normally complete dissolution of the U-mineralisation still occurs under the continuing presence of pyrite. In the oxidised rocks, secondary U-oxide mineralisation is absent, except for rare cases of preserved relicts that survived (in association with pyrite) in reducing micro-environments entirely included by the oxidised rocks. The total dissolution of secondary U-mineralisation results in bleached, white-coloured, pyrite-free rock portions that precisely demarcate the original extent of the mineralisation (Plates 6:1-1 and 6:1-2). It is important to note that the precipitation of HFO minerals (from the pyrite oxidation) was not coeval with U-oxide dissolution. It seems that the higher pyrite contents of the U-nodules (this report; Appendix 1, Fig. 1-13) and their dissolution, leading to a low pH acidic environment, favoured the fairly complete removal of the originally indigenous nodule (Blanchard, 1968).

In the oxidised rocks, similar magmatic and hydrothermal features were developed as described for the reduced phonolites. However, these were modified and less well preserved, due particularly to the oxidic-supergenic overprinting. The latter resulted in higher rock porosities and permeabilities due to general pyrite dissolution that was only partially compensated for by the overall HFO precipitation. These tend to be distributed homogeneously to inhomogeneously throughout the rocks. In the RFI oxidised rocks the HFO distribution is irregular, with some rock portions showing homogeneously dispersed HFO and others showing millimetrically fine rhythmic zoning (Plates 6:1-1 and 6:1-2). The origin of the rhythmic zoning is not known but may be related to seasonal oscillations of the water table and/or to climatic changes. Former secondary U-oxide mineralisations can be recognised by matching areas of bleached rock (Plates 6:1-1 and 6:1-2). However, the distribution of radioactivity, as shown by scintillometry, is irregular in the oxidised rocks. Higher radioactivity occurs in the rock portions richer in HFO, indicating the fixation of (mainly) U to the Fe-oxyhydroxides, probably by co-precipitation.

### **3.2. Sample preparation**

Detailed macroscopic studies determined the samples selected for the mineralogical and geochemical studies. A total of 10 thin sections, 5 polished sections and 7 polished thin sections were prepared for light-optical, petrographic and ore microscopy. Selective powder samples for complementary mineralogical XRD studies were extracted from the bulk rocks, together with other features of interest such as secondary nodular U-mineralisations and their dissolution-bleached equivalents.

For geochemical studies two representative sample sets were selected; large-sized samples (decimetric) of the major zones distinguishing the RFI front, and smaller, more densely sampled sets (centimetric) to better define the small-scale variations. Finally, a set of samples for determining rock physical parameters was selected. Table 6-II presents sample details and the nature of the performed studies.

## **4. Mineralogy and petrography**

### **4.1. Non-mineralised rocks**

The main phonolites of the RFI profile are quite homogeneous, extremely fine-grained (almost aphanitic) and contain only subordinate amounts of microphenocrysts and microxenoliths. The mean grain-size of the phonolite was estimated from the major constituents, i.e. sanidine laths and prisms, and ranges from 0.02 – 0.04 mm. These have survived hydrothermal and supergene processes without any major textural alteration. The other major silicate minerals comprise sericite/illite (white micas) and kaolinite and are products of hydrothermal replacement. Semi-translucent minerals include Ti-oxides (rutile) in the reduced rocks and HFO minerals (mainly limonite) and Ti-oxides in the oxidised rocks. Opaque minerals consist mainly of cube-shaped pyrite microcrystals that occur exclusively in the reduced rocks; the pyrites are free of inclusions and are freshly preserved. Due to the extremely fine grain-size of the RFI rocks, volumetric estimates are problematic. However, the best possible approximations are given in Table 6-III, which considered the original magmatic, hydrothermal and supergene minerals.

Textural evidence shows that the main RFI phonolites are of very shallow subvolcanic to extrusive origin. The low zircon contents indicate that these phonolites were not affected by higher grade hydrothermal U-Zr-REE mineralisation.

TABLE 6-II  
Sample details and studies performed.

Number of original sample	Sample splits prepared according to petrographic zones		Geochemistry: analytical sets and nos.			Other studies			Refer to PLATES in Appendix 6:1
	No.	Petrography	I-various methods	II-Univ. Bern XRF	Cd-AAS	Rock physical parameters	X-ray diffraction	Optical mineralogy, petrography	
RFI-1	1A	Oxidised rock: 25-15 cm from redox front (2 identical splits)	03 -	- RFI-1A	03 2	- RFI-1A	I-A I.3	+ +	- -
	1B	Oxidised rock: 15-5 cm from redox front with bleached nodules	-	RFI-1B	1, 3 <sup>1)</sup>	RFI-1B	I-B I.1 I.2	+	-
	1C	Oxidised rock: 5 cm adjacent to redox front	-	RFI-1C	-	RFI-1C	-	+	-
	1D	Reduced rock: ≤ 3 cm adjacent to redox front	-	-	-	-	-	+	-
RFI-2	2A	Oxidised rock: 25-10 cm from redox front, with bleached nodules	-	-	1, 3 <sup>1)</sup>	-	-	+	-
	2B	Oxidised rock: 10 cm adjacent to redox front	04	-	04 -	-	-	+	6:1-1, 6:1-2
	2C	Reduced rock: 0- ~ 10 cm adjacent to redox front, non-mineralised	-	-	4	-	II I.4	+	6:1-1, 6:1-2
RFI-3	3A	Oxidised rock: ~ 3 cm adjacent to redox front	-	-	-	-	-	+	6:1-3
	3B	Reduced rock: non-minerali- sed zone of ~ 10 cm adjacent to redox front (2 identical splits)	05 -	- RFI-3	05 5	- RFI-3	I.5 -	+ +	6:1-3 6:1-3

TABLE 6-II (contd.).

Number of original sample	Sample splits prepared according to petrographic zones		Geochemistry: analytical sets and nos.			Other studies			Refer to PLATES in Appendix 6:1
	No.	Petrography	I-various methods	II-Univ. Bern XRF	Cd-AAS	Rock physical parameters	X-ray diffraction	Optical mineralogy petrography	
RFI-3 (contd.)	3C	Reduced rock: 0- ≤ 5 cm of mineralised zone with abundant U-macronodules	-	-	-	-	III	+	6:1-3
RFI-4	4A-1	Reduced rock: mineralised zone with U-micronodules	-	RFI-4A-1	-	-	-	+	-
	4A-2	Reduced rock: mineralised zone without U-nodules	-	RFI-4A-2	-	-	-	+	-
	4B	Reduced rock: max. mineralised zone with abundant U-macronodules (2 identical splits)	06 -	- RFI-4B	06 6, 7	- RFI-4B	- 1.6 1.7	+ +	6:1-4 6:1-4
	4C	Reduced rock: transition to non-mineralised phonolite	-	-	-	-	-	+	-
RFI-5	5A	Reduced phonolite, non-mineralised	-	RFI-5A	-	RFI-5A	-	+	6:1-5
	5B	Reduced phonolite, weakly mineralised (2 identical splits)	07 -	- RFI-5B	07 -	- RFI-5B	- -	+ +	- -
RFI-6	6A	Reduced phonolite, non-mineralised	-	-	-	-	-	+	6:1-6
	6B	Reduced nepheline syenite xenolith	-	RFI-6B	-	RFI-6B	-	+	6:1-6

<sup>1)</sup>Mixed samples of RFI-1B and RFI-2A.

## 4.2. Mineralised rocks

The phonolites of the mineralised zone (Plates 6:1-3 and 6:1-4) are identical in composition with the non-mineralised rocks (Table 6-III), except for the pitchblende nodules and their bleached equivalents in the case of oxidised, formerly mineralised phonolites (Plates 6:1-1 and 6:1-2). The pitchblende nodules consist of cryptocrystalline U-oxides precipitated along grain boundaries and in (micro-)pores and interstices of the rock. These precipitations form intergranular films and aggregates, causing partial to total pore fillings. The U-oxides are accompanied by the precipitation of a second generation of pyrites, but only in the inside of the nodules. Both processes effectively diminish the microporosity of the reduced rocks. The second generation pyrites are frequently coarser-grained than the earlier varieties and may even include them. Both pyrite generations are freshly preserved and show no differences in colour or reflectivity. The substitution of rock-forming minerals by pitchblende and/or second generation pyrites could not be verified microscopically. Doubtless there exists a growth process of the nodules. This can be described, based on mineralogical-textural grounds, as originating from some point source and subsequently being followed by centrifugal spreading and growth controlled by fracture planes and grain boundaries, and the infiltration and the filling of micropores with U-oxides and pyrites. Regular (concentric) and irregular zoned U-nodules are products of variable densities/concentrations of U-oxide precipitation (Plates 6:1-3 and 6:1-4). The reasons for the variable patterns of the U-oxide precipitation within isotropic igneous rocks are unknown and difficult to explain by purely inorganic processes.

In general, the pitchblende nodules can be considered to consist of cryptocrystalline U-oxides (see item 4.3, XRD studies), with crystallites dominating below the limit of microscopic resolution (magnification of about 1200 x). Aggregated masses of U-oxides are optically isotropic. The U-oxides are precipitated together with a second pyrite generation mainly available in natural open spaces (grain boundaries, rock pores, interstices) of the reduced rocks without any microscopically recognisable substitution of the rock-forming minerals. The sizes of the nodules range from microscopic (and even submicroscopic) dimensions, as a lower limit, to a maximum of a few centimetres. The nodular forms suggest either inorganic growth processes, e.g. ovoidal concretions or biogenic processes. The microtextures and mineral parageneses are interpreted as favouring the biogenic hypothesis. The nodules of the active redox fronts can be termed first generation nodules and are distinct in nature and origin from the massive secondary U-nodules described elsewhere. (Appendix 1).

During the advancement of the redox front, the pitchblende nodules of the mineralised rocks suffered dissolution still under reducing conditions, due to the continued stability of pyrite. This resulted in pitchblende-free zones directly adjacent to the redox fronts on the reduced side. The widths of these zones can vary from millimetres (or even submillimetres) to centimetres, as in the case of RFI. For comparison, an example of millimetre dimensions from another redox front is shown in Plate 6:1-7. These zones are also pyrite-bearing but normally distinctly white-coloured (due to the dissolution of black U-oxides) when compared to the adjacent mineralised (grey) and oxidised (yellowish-brown) rocks. Their compositions proved to be similar to those of the adjacent reduced rocks free of U-oxides, and they should not be confused with the clay mineral (e.g. kaolinite)-enriched zones. Plates 6:1-8 and 6:1-9 show pitchblende dissolution using detailed cathodoluminescence images.

Further advancement of the redox front finally leads to the complete oxidation and transformation of the formerly U-mineralised reduced rocks into oxidised varieties. Macroscopically, oxidation refers only to the precipitation of HFO minerals (mainly limonite) that give the oxidised rocks their typical yellowish-brown colouration (Plates 6:1-1, 6:1-2, 6:1-3 and 6:1-7). This oxidation process is already seen in the U-oxide-free rocks as a function of the availability of low pH solutions resulting from the oxidation of pyrite, which forms a variety of ferrous and ferric sulphates. In the presence of low sulphate concentrations all the oxidised Fe-pyrite is reprecipitated in situ as indigenous limonite, ideally without any pseudomorphism of the former pyrite microcrystals. At higher sulphate concentrations, mobilisation, oxidation and limited transport takes place, and reprecipitation as limonite occurs only after adequate dilution and hydrolysis. Limonite can be precipitated as new forms, independently of the former pyrite distribution, as homogeneous or inhomogeneous pigmentations. This generally affected the oxidised rocks, explaining their higher porosity resulting from pyrite dissolution, which was only incompletely compensated for by the reprecipitation of the HFO minerals (limonite). At highest original pyrite contents which have consequently resulted in the highest sulphate concentrations, all of the former Fe-pyrite is removed. Reprecipitation takes place elsewhere after sufficient transport has occurred to permit adequate dilution and hydrolysis. This is the case with the bleached nodules remaining from the final dissolution of the former pitchblende nodules (Plates 6:1-1 and 6:1-2), which contained a very high content of original pyrite. The bleached nodules achieve the highest porosity through these processes since pyrite dissolution is not compensated for by HFO mineral precipitation. Microscopically, the bleached nodules contain all the rock-forming minerals comprising the enclosing oxidised rocks, and are characterised by

TABLE 6-III

Modal compositions of RFI non-mineralised reduced and oxidised phonolites (numbers in brackets refer to totally replaced minerals).

Minerals	Vol.% Mean grain-size in mm Origin	Observations
Alkali feldspar phenocrysts	1 – 2 0.1 > 5 magmatic	Former micropertthitic orthoclases showing alkali exchange and indicating structural readjustment. Fluid inclusions and weak kaolinisation are also present. Pyrite and HFO mineral inclusions occur in both the reduced and oxidised rocks.
Pseudoleucite phenocrysts	tr. – 1 0.5 – > 20 magmatic	Pseudomorphs composed of alkali feldspars, sericite/illite, kaolinite, pyrite and containing HFO minerals.
Nepheline phenocrysts	(tr. – 1) (0.1 – 3) magmatic	Replaced kaolinite, sericite/illite, pyrite and containing HFO minerals.
Aegirine-augite phenocrysts	(0 – tr.) (0.1 – 2) magmatic	Replaced by cryptocrystalline aggregates of TiO <sub>2</sub> minerals, kaolinite, unidentified clay minerals (? smectites), pyrite and containing HFO minerals.
Nepheline of the groundmass	(~ 10) (~ 0.02) magmatic	Replaced by kaolinite, sericite/illite, pyrite and containing HFO minerals.
Sanidine laths and prisms of the groundmass	55 – 65 0.02 – 0.04 magmatic	The main magmatic minerals show evidence of alkali exchange and structural readjustment. Some kaolinisation also occurs.
Aegirine-augite of the groundmass	(1 – 3) (0.01 – 0.03) magmatic	Replaced by cryptocrystalline aggregates of TiO <sub>2</sub> minerals, kaolinite, unidentified clay minerals (? smectites), pyrite and containing HFO minerals.
Pyrite	3 – 6 0.01 – 0.04 hydrothermal	Idiomorphic microcrystals finely disseminated only in reduced rocks.

TABLE 6-III (contd.).

Minerals	Vol.% Mean grain-size in mm Origin	Observations
Kaolinite	10 – 15 < 0.01 hydrothermal (and supergene)	Replacement minerals of nepheline, alkali feldspars, aegirine-augite.
Unidentified clay minerals (? smectites)	tr. – 1 < 0.01 hydrothermal (and supergene)	Replacement minerals of aegirine-augite.
TiO <sub>2</sub> minerals (? rutile)	tr. – 1 < 0.04 hydrothermal	Replacement mineral of groundmass aegirine- augites, present as cryptocrystalline aggregates.
Sericite/illite	5 – 10 < 0.02 hydrothermal	Replacement minerals of mainly nepheline/ kaolinite from nepheline.
Zircon	tr. 0.01 – 0.04 hydrothermal	Hydrothermal mineral sometimes altered to baddeleyite.
HFO minerals (limonite)	~ 5 < 0.01 supergene	Clouded or rhythmically zoned distributions of cryptogranular aggregates forming pigmentations and impregnations. Only occurs in the oxidised rocks.
Microxenoliths	1 – 3 0.5 – > 50 magmatic	Composed of angular fragments of phonolites and nepheline syenites of leucocratic to hololeucocratic composition included/ surrounded by a weakly flow-oriented RFI phonolite.

the same textures, except for the HFO minerals. The observations of pyrite dissolution and HFO mineral reprecipitation in the RFI rocks are in very good agreement with the descriptions and genetic interpretations of Blanchard (1968) which formed the basis for the discussion above.

### 4.3. X-ray diffraction (XRD) studies

Initial X-ray work was carried out at Paulo Abib Engenharia S.A., São Paulo, and completed using the equipment at the University of São Paulo (USP). Semiquantitative XRD analyses using LiF as an internal standard were run at the University of Bern by N. Waber. The XRD results of selected samples from RFI are shown in Table 6-IV. Textured preparations refer to powder preparations with planar orientation. Most samples were run in three laboratories, and with both planar and non-oriented powder preparations. The equipment at USP could only be used at  $2\theta$  angles  $\geq 5^\circ$ ; therefore, smectite peaks could not be observed in these runs. In addition, for some samples, the analysed alkali feldspar peak ( $d \sim 3.25 \text{ \AA}$ ) was more intensive than the chosen full scale deflection (of 1,000 cps). These peaks could not be measured and are therefore indicated in the table as not measurable (n.m.).

As the differences between duplicate runs (and runs made in different laboratories) were larger than the microscopically observed mineralogical variability, numerical (semi-)quantitative interpretations were avoided. The LiF ( $d \sim 2.01 \text{ \AA}$ ) peak intensity (Table 6-IV) refers to an admixture (internal LiF standard) in the weight proportion 10:1 (10 samples, 1 LiF) and can serve as an estimate for the analytical conditions of these runs.

Some general conclusions from the X-ray results include the greater presence of smectites in the RFI samples than expected from the microscopic work (probably in the range of 3 – 6 vol.%). The latter indicated the presence of unidentified clay minerals (probably smectites) in trace amounts of 1 vol.% aggregated into pseudomorphs after aegirine-augites. The measured smectites are probably present as cryptocrystalline (submicroscopic) finely disseminated individual grains.

The illite/sericite ( $d \sim 10 \text{ \AA}$ ) peak is always significantly weaker than the kaolinite ( $d \sim 7 \text{ \AA}$ ) peak, supporting the relatively higher abundance of the latter mineral (Table 6-II). Complementing, and to some extent modifying, the microscopic results, one observes the highest kaolinite/illite peak intensity relationships and also the absolutely lowest illite peak intensities in the pitchblende nodules and bleached nodules. This

TABLE 6-IV  
X-ray diffraction data of selected RFI samples.

Sample no. (split no.)	Run no.	Lab.	Preparation	Minerals: Peak heights (in mm) > background						Sample petrography
				Smectite d~15 Å	Illite d~10 Å	Kaolinite d~7 Å	Alk. feldspar d~3.25 Å	Uraninite d~3.10 Å	LiF d~2.01 Å	
RFI-I (1A)	I-A	PA	textured	11	12	37	n.m.	—	—	Oxidised bulk rock powders.
	I-A	USP	idem	—	9	17	135	—	—	
	I.3	Be	idem	6(?)	10	19	n.m.	—	48	
	I.3	Be	non-oriented	3(?)	8	12	140	—	38	
RFI-I (1B)	I-B	PA	textured	13	11	44	n.m.	—	—	Bleached nodule, selectively extracted powders.
	I-B	USP	idem	—	8	22	210	—	—	
	I-1	Be	idem	7(?)	3(?)	16	190	—	32	
	I.1	Be	non-oriented	10(?)	—	10	110	—	27	
	I.2	Be	textured	10(?)	3(?)	22	n.m.	—	41	
	I.2	Be	non-oriented	3(?)	2(?)	17	135	—	34	
RFI-II (2C)	II	PA	textured	9	15	28	n.m.	—	—	Reduced bulk rock (powder) adjacent to redox front.
	II	USP	idem	—	14	24	137	—	—	
	I.4	Be	idem	5(?)	4(?)	15	194	—	41	
	I.4	Be	non-oriented	—	8	13	108	—	34	
RFI-III (3B)	I.5	Be	textured	—	10(?)	21	176	—	45	Reduced bulk rock (powder) from centre of non-mineralised zone adjacent to the redox front.
	I.5	Be	non-oriented	4(?)	10	15	128	—	41	
RFI-III (3C)	III	PA	textured	3(?)	2(?)	8(?)	47	85	—	Pitchblende nodule of mineralised zone, selectively extracted.
	III	USP	idem	—	—	10	55	45	—	
RFI-IV (4B)	I.6	Be	textured	3(?)	—	12	88	70	29	Pitchblende nodule; Reduced bulk rock (powder) of mineralised zone adjacent to pitchblende nodule.
	I.7	Be	textured	2(?)	—	14	160	—	38	
	I.7	Be	non-oriented	3(?)	3(?)	12	125	—	36	

Abbreviations:

Lab = Laboratories

PA = Paulo Abib Eng. S.A.

USP = University of São Paulo

Be = University of Bern

n.m. = not measurable

— = not observed

(?) = uncertain peak identification

indicates that the U-oxide precipitation and dissolution, i.e. the pitchblende nodule formation and later destruction (with release of low pH sulphate concentrations), exercised some preferential attack on the mica mineral.

Alkali feldspars are the most abundant minerals of the RFI rocks and consist texturally of typical sanidine laths and prisms often of very fine grain-size (Table 6-III). Chemically, however, they are very pure K-feldspars (see section 6). These characteristics, together with the XRD patterns, indicate that crystal chemical exchange reactions affected the primary magmatic sanidines, substituting  $\text{Na}^+$  for hydrothermal  $\text{K}^+$  along with structural modification. These reactions produced the presently observed very pure K-feldspars of intermediate structural state and triclinicity (between high and low temperature). Similar processes were reproduced experimentally and confirmed using stable isotope studies by O'Neil and Taylor (1967) under P-T conditions that permit extrapolation/comparison with the "potassic rock" hydrothermal processes of Poços de Caldas (Waber *et al.*, this report).

The main U-minerals of the pitchblende nodules are cryptocrystalline U-oxides similar to those described by Barrington and Kerr (1961; referenced in the ASTM-index under No. 13-225) and others described by Swanson and Fuyat (1953). A comparison of the main X-ray peaks is shown in Table 6-V. The uraninite of the RFI pitchblende nodules, however, furnished broad X-ray lines indicating low crystallinity, probably allied with partial oxidation of the  $\text{UO}_2$  to  $\text{UO}_3$  (Table 6-V, column PH/HHW).

## 5. Rock physical parameters

Rock physical properties of RFI selected minor samples (see also section 6) and of the regional phonolites and nepheline syenites (Schorscher and Shea, this report series; Rep. 1) were determined by N. Waber (Univ. Bern). Results are shown comparatively in Table 6-VI. The measurements confirm the microscopic observations regarding the higher porosity of the oxidised RFI rocks when compared with the reduced non-mineralised rocks (Table 6-VI, sample no.: RFI-1A, B, C and RFI-5A, -6B; means 1 and 3).

Sample nos. RFI-4B and -3 are of reduced phonolites from (respectively) the zone of maximum U-mineralisation and the zone free of U-mineralisation due to dissolution adjacent to the redox front. They further support the results of the XRD studies which indicated that the supergene reducing processes of formation and subsequent dissolution

TABLE 6-V

X-ray diffraction data of uraninite from RFI pitchblende nodules compared to literature data.

a		b		RFI pitchblende		
d(Å)	Int.	d(Å)	Int.	d(Å)	Int.	PH/HHW
3.090	10	3.16	10	3.12	10	8.5
2.686	5	2.74	5	2.70	5	2.9
1.900	5	1.93	5	1.91	5	2.9
1.62	4	1.65	5	1.63	5	3.5
7 additional peaks down to d = 1.04 Å		5 additional peaks down to d = 1.05 Å		Interval not studied		

a = Midnite Mine (Barrington and Kerr, 1961)

b = Swanson and Fuyat (1953)

PH/HHW = Peak height to half height width ratio

of the pitchblende mineralisations occurred with partial silicate mineral replacement, causing a moderate elevation of the porosities (not observed microscopically).

Comparison of the RFI rocks with the regional rocks (Table 6-VI), for example in terms of their mean values (means 4 and 5), reveal strong differences in their global rock densities and porosities, even though they have identical grain densities. This indicates that the hydrothermal (reducing) potassic rock-forming and supergene (reducing and oxidising) processes compensated for the incurred porosity formation by precipitation of denser mineral phases such as pyrites in the reduced rocks and HFO minerals in the oxidised rocks. A graphic representation of the variation of the rock physical parameters of the RFI samples is shown on the scale profile of the redox front illustrated in Figure 6-2.

## 6. Geochemistry

### 6.1. Sample preparation and analysis

Two main representative sample sets were prepared for geochemical studies: one from large-sized homogeneous parts of the original samples and one from selected minor

TABLE 6-VI

Rock physical properties of selected RFI samples and regional alkaline rocks of the Poços de Caldas complex.

Sample no.	Density (Hg), global	Grain (solids) density	Porosity	Rock types
RFI-1A	2.17	2.62	17.1	RFI oxidised phonolite, ~ 20 cm from redox front;
RFI-1B	2.20	2.62	15.9	RFI oxidised phonolite, 15 to 5 cm from redox front;
RFI-1C	2.18	2.65	17.8	RFI oxidised phonolite, 5 to 0 cm from redox front, rich in HFO minerals;
RFI-3	2.17	2.64	17.8	RFI reduced phonolite, 0 to 10 cm from redox front, zone without U-nodules;
RFI-4B	2.20	2.61	15.5	RFI reduced phonolite (without U-nodules) of zone of max. U-mineralisation;
RFI-5A	2.35	2.59	9.4	RFI reduced phonolite, ~ 1 m from redox front (variety 1);
RFI-5B	2.26	–	–	RFI reduced phonolite, ~ 1 m from redox front (variety 2);
RFI-6B	2.33	2.61	10.6	RFI reduced nepheline syenite xenolith, ~ 2 m from redox front;
PDC-PH-02B	2.62	2.66	1.6	Regional nepheline syenite – hypabyssal;
PDC-I1-04	2.57	2.62	1.8	Regional phonolite – subvolcanic;
PDC-PH-05	2.59	2.61	0.6	Regional phonolite – volcanic;
PDC-I1-06	2.50	2.59	3.5	Regional nepheline syenite – plutonic;
PDC-I1-07	2.49	–	–	Regional nepheline syenite – plutonic;
PDC-PH-08	2.59	–	–	Regional phonolite – volcanic;
PDC-I1-01	2.55	–	–	Regional nepheline syenite – hypabyssal;
means 1	2.18	2.63	16.93	RFI oxidised rocks;
means 2	2.19	2.63	16.65	RFI reduced, mineralised and related rocks;
means 3	2.31	2.60	10.00	RFI reduced non-mineralised rocks;
means 4	2.23	2.62	14.87	RFI rocks, all;
means 5	2.56	2.62	1.88	Regional rocks, all.

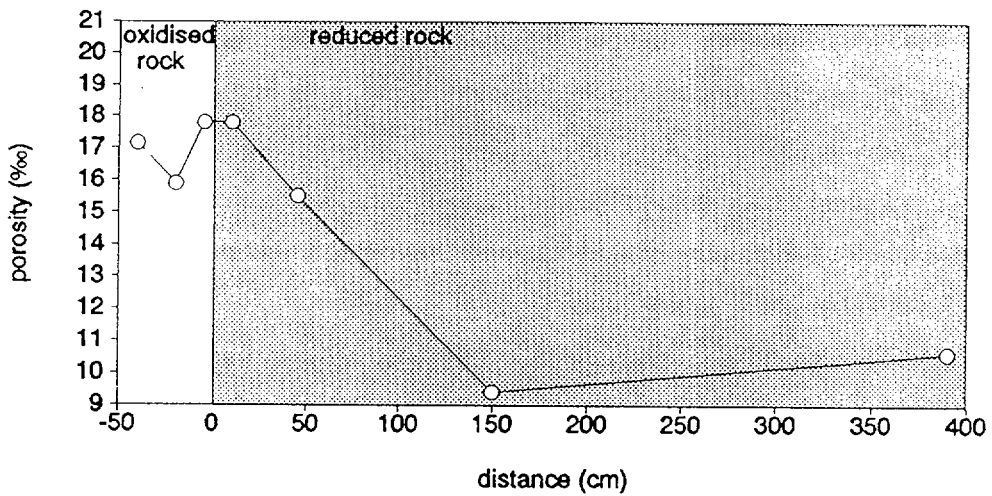
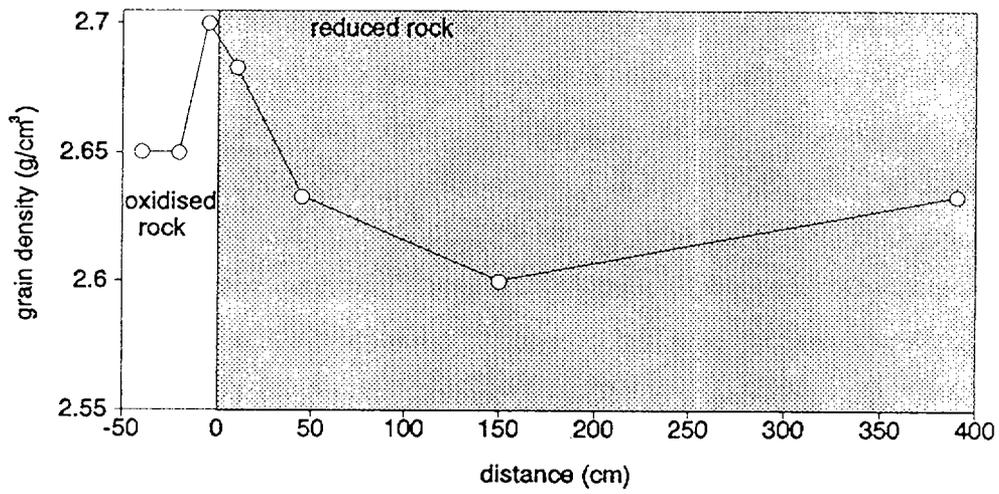
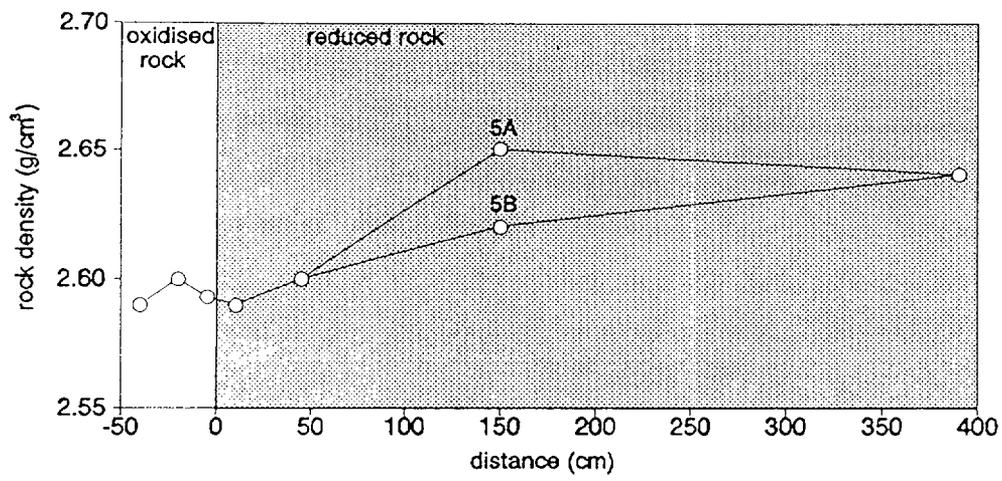


Figure 6-2. RFI redox front: distribution of rock physical properties.

portions cut out of the original samples (based on specific mineralogical, petrographic and metallogenetic characteristics). From these, as an additional detail, specific powder samples were removed by drilling for complementary geochemical (and mineralogical) analysis. Details of the different sample sets and the analytical work performed are presented in Tables 6-I and 6-II, and the chemical data are listed in Appendix 6:2.

Geochemical sample set I (Table 6-II) comprises five large-sized representative samples (750 – 1350 g) from the main mineralogical-petrographic zones of RFI. Major and trace element studies (by routine XRF analysis; University of Bern), determination of  $\text{Fe}^{3+}_{\text{tot}}$ ,  $\text{Fe}^{2+}$ , S and Lost On Ignition (LOI) using classic methods, analysis of Mo by Atomic Absorption (AAS); work performed at Paulo Abib Engenharia S.A., São Paulo), and determination of Cd by AAS (work done by R. Mader, University of Bern) were carried out on the samples. Figures 6-4, 6-6 and 6-13 show the distribution of  $\text{Fe}^{3+}$ , S, LOI and Mo across the redox front. The geochemistry of Cd will be discussed later together with complementary data. Analytical problems arose during the determination of  $\text{Fe}^{2+}$ , probably due to the presence of uranium. Thus, even the reduced rocks with abundant pyrite showed below-detection-level amounts of FeO (<0.2 wt.%; Appendix 6:2; Table 6:2-I).

Geochemical sample set II (Table 6-II) comprises 10 samples selected from the original specimens in an attempt to further subdivide the main zones of the redox front, and also to consider the internal compositional and textural variations of the original samples. To accomplish this, the original sample RFI-1 was subsampled (1A, 1B, 1C) from the redox front (Table 6-II), progressing into greater HFO mineral contents as indicated by the more intensive yellowish-brown colouration.

The original sample RFI-4 was also subsampled (4A-1, 4A-2, 4B) to show different degrees of U-mineralisation. Sample RFI-4 represents the zone of maximum U-mineralisation and the subsamples prepared represent reduced types a) containing pitchblende micronodules (4A-1), b) devoid of macroscopically recognisable pitchblende nodules (4A-2), and c) of maximum U-content with abundant pitchblende macronodules (4B). Subsampling of RFI-5 resulted in sample 5A (non-mineralised) and 5B (contains pitchblende micronodules).

Sample RFI-6 was subdivided according to its lithological composition into sample 6A (reduced non-mineralised phonolite country rock) and 6B (reduced nepheline syenite xenolith). However, only 6B was analysed. The analytical results are presented in Appendix 6:2 (Table 6:2-II).

The mean geochemical variation of the respective elements in the regional (hydrothermally altered non-potassic) rocks, the borehole F1 reduced rocks and the

borehole F1 oxidised rocks were considered. Only in the case of Hf had comparative values for borehole F4 rocks to be used – i.e. oxidised phonolites and nepheline syenites (sample nos. 19-1A, 22-1A, 39-1A) and reduced nepheline syenite xenolith (sample nos. 413-1A-A; -1A-B; 1A-C; 1A-D; 1A-E), respectively, since borehole F1 rocks were not analysed for this element.

Concerning samples RFI-1A, -3B, -4B, -5B, and the S,  $\text{Fe}_2\text{O}_{3\text{tot}}$ , and LOI analysed by both laboratories (Paulo Abib Engenharia S.A., São Paulo and the University of Bern), one can see quite a good agreement of results, bearing in mind the different methods used and that the two sample sets were not homogenised splits, but simply from adjacent parts of the same original samples (Figs. 6-2, 6-6 and 6-4; Appendix 6:2, Tables 6:2-I and 6:2-II). This is particularly important in the case of sample RFI-4B, where the split analysed by the Paulo Abib laboratory was free of pitchblende nodules (analysis no. 06, Appendix 6:2; Table 6:2-I), in contrast to the split analysed by the University of Bern (analysis RFI-4B, Appendix 6:2, Table 6:2-II) which represented the maximum U-mineralisation, i.e. particularly rich in pitchblende macronodules (Appendix 6:1, Plate 6:1-4). This fact explains, for instance, the almost proportional differences in the  $\text{Fe}_{\text{tot}}$  and S results by a factor of 2.

## 6.2. Geochemistry of sample set I (large-sized samples)

Figures 6-6 and 6-4 show the stepwise and proportional decrease of S and  $\text{Fe}_{\text{tot}}$  from the reduced rocks (analysis no. 07; sample RFI-5B) towards the redox front (on its reduced side), corresponding, most probably, to the formation and partial removal in solution of Fe-sulphates from pyrite (even though dissolution of pyrite could not be positively confirmed microscopically). The mobilisation and release into solution of Mo (Fig. 6-13) is anomalous, apparently occurring as a continuous (one-stage) process in the near-vicinity of the redox front on the reduced side. This further supports the existence of specific Mo-minerals (probably sulphides) in the reduced rocks rather than its presence as a minor constituent (up to  $\leq 1.500$  ppm) in pyrite. However, it must be mentioned that molybdenite ( $\text{MoS}_2$ ) has not been observed in the RFI rocks (either due to cryptocrystallinity or to its non-existence) and that the less likely jordisite (amorphous  $\text{MoS}_2$ ) may in fact have been overlooked. In the field, one very frequently observes the presence of a blue Mo-mineral, most probably ilsemanite (Mo-hydrous oxide), in the presence of pyrite, i.e. only in the reduced rocks exposed to weathering. Ilsemanite is, according to Ramdohr (1975), most readily formed from the weathering of jordisite by

rapid oxidation (even in mineral collections). At the Osamu Utsumi mine the formation of the blue Mo-mineral was observed on drillcores of reduced rocks within time spans of only a few days. Jordisite is considered here as the more probable Mo-mineral phase in the reduced RFI rocks, even if the formation of the blue Mo-mineral in the studied rocks was not observed. With respect to jordisite being a paragenetic mineral forming part of the hydrothermal U-Zr-REE-mineralisation at the mine, there are some reservations. For example, jordisite is a very low temperature mineral (Ramdohr, 1975). From the oxidised side of a zone located outside the direct influence of the redox front, Mo-values may again reach up to half of the original content of the reduced rocks, and may have been fixed mineralogically by coprecipitation onto HFO-minerals of low crystallinity (mainly limonite).

### 6.3. Geochemistry of sample set II (main XRF samples)

The main major and trace element (XRF-) data-sets of the RFI redox front (Appendix 6:2; Table 6:2-II) are compared globally with other equivalent oxidised and reduced potassic rocks of the Osamu Utsumi mine, and with the regional rocks (unaffected by the potassic rock hydrothermal alteration) and related Zr-REE-U-mineralisation (Waber *et al.*, this report). In addition, the specific geochemical processes related with the development of the redox front are also discussed.

The XRF analytical data for RFI were recalculated to obtain mean values for the oxidised and reduced non-mineralised rocks ( $U \leq 210$  ppm) and for the reduced mineralised rocks ( $U > 210$  ppm). These are compared and related to one U-mineralised oxidised rock from the RFI front ( $U = 861$  ppm, sample RFI-3), and to the mean values for borehole F1 oxidised and reduced rocks and the regional rocks (Appendix 6:2; Table 6:2-III). The non-mineralised reduced rocks were considered first, to try and reconstruct the character of the magmatic and superimposed hydrothermal geochemistries of the RFI rocks. It should therefore be remembered that these were initially classified mineralogically and petrographically as very fine-grained hololeucocratic volcanic phonolites containing subordinated phenocrysts of alkali feldspar, pseudoleucite, nepheline and aegirine-augite, and (micro-)xenoliths of phonolites and nepheline syenites, i.e. unsaturated alkaline rocks (section 4).

### 6.3.1. RFI phonolites: magmatic composition and hydrothermally altered potassic rock

#### Major elements

When comparing the major elements (and corresponding mean values) of the non-mineralised RFI rocks with the equivalent mean values for the reduced borehole F1 rocks (Appendix 6:2; Tables 6:2-II and 6:2-III), the similarities in  $\text{TiO}_2$ ,  $\text{Al}_2\text{O}_3$  and LOI contents, and the overall low and very low contents of Mn, Mg, Ca and P (-oxides), are easily observed. Differences include higher  $\text{SiO}_2$  and  $\text{K}_2\text{O}$  contents in the RFI rocks and the higher  $\text{Fe}_2\text{O}_{3\text{tot}}$  and  $\text{Na}_2\text{O}$  contents of the borehole F1 rocks;  $\text{Na}_2\text{O}$ , in particular, is almost entirely absent in the RFI rocks. These differences are similar when compared to the equivalent borehole F4 rocks and to the redox fronts II, III and IV sampled and analysed by Waber *et al.* (this report; section 9).

In comparison with the regional rocks (Appendix 6:2; Table 6:2-III) it becomes evident that all the above observed differences (of the RFI and borehole F1 reduced rocks) not only continue to exist, but reach maximum values. Additionally, the regional rocks also show minor but significant MnO and MgO contents and much lower LOI. If the RFI reduced non-mineralised rocks are plotted together with the regional rocks in a total alkali-silica (TAS) diagram (Le Maître, 1984) and compared with the borehole F1 rocks (Waber *et al.*, this report), all rocks are observed to lie in the phonolite (unsaturated) field. The RFI rocks, however, plot near the divide with the field of more (silica) saturated rocks (alkali trachytes and trachytes), in contrast to the regional rocks which plot in the opposite, more unsaturated part of the phonolite field. The borehole F1 rocks cover the main part of the phonolite field and the calculated means of the reduced non-mineralised varieties lie at the centre. Bearing in mind the reconstructed magmatic mineralogy of the RFI rocks (see section 4; Table 6-III) and the chemistry of the mineralogically similar regional rocks (particularly of the regional phonolites), it becomes evident that the original RFI rocks were certainly more leucocratic (Fe-Mg mineral poor) and their chemical composition is mainly a product of the “potassic rock” hydrothermal alteration. This imposed on the original rocks the progressive and ultimate total loss of  $\text{Na}_2\text{O}$ , the equally complete loss of CaO, MnO and MgO, and the partial loss of  $\text{Fe}_2\text{O}_{3\text{tot}}$  (while the preserved Fe was almost completely reduced to the divalent state and reprecipitated mainly as pyrite). The  $\text{Na}_2\text{O}$  loss was not entirely compensated by the addition of  $\text{K}_2\text{O}$ ; there also occurred moderate to substantial enrichments of  $\text{SiO}_2$  and  $\text{Al}_2\text{O}_3$ , whereupon nephelines underwent partial alteration to illite/sericite and kaolinite (causing  $\text{SiO}_2$  and K gains, but total-alkali losses at  $\sim$  constant  $\text{Al}_2\text{O}_3$ ) and the main

magmatic sanidines suffered alkali exchange reactions (Na by K), structural readjustments, and incipient kaolinisation (which caused increases in K and  $\text{Al}_2\text{O}_3$  and important Na and minor  $\text{SiO}_2$  loss). The almost total loss of CaO, MgO and MnO, and the partial loss of  $\text{Fe}_2\text{O}_{3\text{tot}}$ , are explained by the argillation of magmatic Fe-Mg minerals, mainly of aegirine-augites, through the formation of pseudomorphs comprising mixtures of clay minerals (kaolinite, smectite), pyrite and Nb-Fe-rutile (with consequent losses in variable proportions of Na, Ca, Mg, Fe, Mn, Si). Possibly, there also occurred the dissolution of minor magmatic plagioclase feldspar and of the minor anorthite components of ternary magmatic (alkali-) feldspars.

$\text{TiO}_2$  is present in the RFI and borehole F1 rocks in similar amounts, somewhat lower, however, than in the regional rocks. Magmatic Ti occurs in these rocks in rare oxidic ore minerals, but mainly as a minor element in the clinopyroxenes. (Giannettite is a pneumatolytic Ti-bearing mineral of the regional rocks, hydrothermally unstable, but less frequent in phonolites.) These have been generally referred to as aegirine-augites, but even the groundmass clinopyroxenes of the volcanic phonolites show compositional zoning. This is particularly well developed in the case of the coarser phenocrysts and nepheline syenite regional rocks (Schorscher and Shea, this report series; Rep. 1), ranging from sodi-augitic centres to almost pure aegirine rims. Ulbrich (1983) and Ulbrich *et al.* (1984) reported microprobe analyses of the clinopyroxenes of various nepheline syenites from Poços de Caldas with  $\text{TiO}_2$  contents ranging from 0.5 wt.% in the centres to 5 wt.% at the aegirine borders. Due to its geochemical immobility, Ti reprecipitates (hydrothermally) in situ as  $\text{TiO}_2$ - (rutile-) minerals, pseudomorphing the clinopyroxenes.

### Minor and trace elements

To discuss the original magmatic and superimposed hydrothermal trace element geochemistry of the RFI non-mineralised, reduced phonolites is more problematic, even if the equivalent borehole F1 rocks are also included for comparison (Appendix 6:2; Tables 6:2-II and 6:2-III). For instance, the trace element geochemistry of the borehole F1 rocks (Waber *et al.*, this report) showed that macro- and microscopically they are very similar, and that in the core profile more or less contiguous rocks showed abrupt differences in their trace element contents, in some cases by factors of 2 to >10. This has a major influence, for instance, upon mean values, even in the case where quite a high number of analysed samples are petrographically similar. In the case of RFI, and similarly with the RFII, III and IV redox fronts, the numbers of analysed samples are

relatively low and the interval between the individual samples comparatively high. The occurrence and influence of individual samples of anomalous geochemistry in these types of populations is evidently possible and marked. Therefore, to avoid misinterpretation, the nature/origin of these geochemical anomalies in the redox front samples, i.e. whether primary-magmatic, hydrothermal or redox front-related supergenic, must initially be well characterised.

For RFI samples, RFI-3, RFI-4A-2, RFI-5A and RFI-6B (Appendix 6:2; Table 6:2-II) were considered to represent the mean composition of the reduced non-mineralised (U <210 ppm) RFI rocks (Appendix 6:2; Table 6:2-III). However, even though microscopically the first three (phonolite) samples can be considered as similar, the fourth sample, a nepheline syenite xenolith, was also included, even though of different chemistry. Only in the case of Ba were two mean values calculated for both RFI (reduced non-mineralised) and regional rocks: one comprising all the rocks (nepheline syenites and phonolites), the other only the phonolites.

The RFI reduced non-mineralised rocks are compared to the equivalent borehole F1 rocks and to the regional rocks in order to establish their possible primary magmatic and hydrothermal trace element geochemical characteristics (Appendix 6:2; Table 6:2-III).

#### *Elements Ba, Rb, Th, U, V and Zn*

These elements are systematically enriched in the reduced, non-mineralised RFI and borehole F1 rocks, when compared with the regional rocks. In the case of Ba, two mean values are given for RFI and regional rocks (Appendix 6:2; Table 6:2-III). The initial (higher) means include in both cases all the rocks (phonolites and nepheline syenites) and the second only the extremely fine-grained, volcanic phonolites. This was necessary because, in the case of the regional rocks, there exists a very characteristic, strong fractionation of Ba between the fine-grained phonolites (means: 50 ppm) and the coarse-grained nepheline syenites of hypabyssal to subvolcanic and plutonic origin (means: 387 ppm). Similarly, in the case of the RFI rocks, the nepheline syenite (Appendix 6:2; Table 6:2-II; sample RFI-6B) has a much higher Ba content than the means of the associated volcanic phonolites. Therefore in this case, the means of the RFI volcanic phonolite are considered more representative and should be compared with the equivalent means of the regional phonolites for the appropriate estimation of the Ba-enrichment factor. For the RFI and regional phonolites this is ~7.

Such evident fractionation was only observed in the case of Ba. Furthermore, the petrographic variability of borehole F1 shows that it includes predominantly subvolcanic

to hypabyssal rock types, and only minor well-defined plutonic and shallow volcanic rock types. Therefore, the mean values for all the rocks, rather than the partial means from minor lithological subgroups, were used for the other comparisons, including Ba from the borehole F1 and regional rocks. Its enrichment factor in this case is lower (~2.5). One mineralogical reason for the enrichment of Ba in the hydrothermally altered rocks could be the inclusion of a complementary celsian component during the alkali exchange reactions of the feldspars. This interpretation is supported by Ulbrich (1983) and Ulbrich *et al.* (1984) who have described the erratic presence of low Ba contents, similar to those of CaO ( $\leq 0.36$  wt. %), in the alkali feldspars of nepheline syenites from Poços de Caldas. In addition, barite is known in hydrothermally altered rocks from the Osamu Utsumi mine, and its existence as a minor finely-dispersed mineral in these rocks could not be totally excluded.

The enrichment of Rb by a factor of 1.7 in RFI and 1.9 in the borehole F1 rocks corresponds quite well to the K<sub>2</sub>O enrichment factors (1.7 and 1.6 respectively). This process, too, is mineralogically related to the hydrothermal alkali exchange reactions of the feldspars and, to a lesser extent, to the hydrothermal sericite/illite formation in the pseudomorphs resulting from nepheline.

Thorium has higher mean values in the RFI and borehole F1 rocks than in the regional varieties. The borehole F1 mean value, moreover, lies within the range of data published from various global alkaline intrusive complexes (Roger and Adams, 1978). However, based on the few analysed regional rocks in the Poços de Caldas complex it is difficult to decide whether the Th means of borehole F1 really represent a weak hydrothermal enrichment, or whether the Th mean value of the regional rocks represents unusually Th-poor rocks. The RFI rocks are quite clearly Th-enriched with respect to the borehole F1 rocks by a factor of 2, and to the regional rocks by a factor of 6. The attempt to correlate Th with another trace element for the four individual RFI samples yielded at best a reasonably good positive linear correlation with Zr. If the borehole F1 and regional rock mean values are included, they lie quite close to each other, but are still totally isolated from the correlation line.

This tends to indicate that the Th-contents of the borehole F1 rocks probably represent low or unmodified magmatic values, while those of the RFI reduced non-mineralised rocks are of hydrothermal origin. Specific Th-minerals were not observed. Microprobe analysis of hydrothermal zircons from the borehole F1 rocks indicated the presence of Th in zircons from the potassic rocks of the mine (Waber *et al.*, this report, Appendix 3). Giannettite, however, is the main Zr-bearing mineral in the regional rocks.

Uranium is enriched in both RFI and borehole F1 rocks in relation to the regional rocks, where the U-content was consistently below the XRF detection limit (<5 ppm); the respective mean values for the RFI and borehole F1 reduced non-mineralised rocks are 146 and 32 ppm U. No systematic variation and/or correlation of U with other elements could be observed from the RFI means. Therefore, the higher U-enrichment of the RFI rocks compared to the borehole F1 rocks is considered to be due to complex processes related to superimposed hydrothermal and reducing redox front mechanisms. The borehole F1 means are considered to represent the mean U-content of the reducing hydrothermal potassic rock-forming process, and not the associated higher grade U-mineralisation. Higher grade, truly hydrothermal (deep-seated) U-mineralisations were only analysed recently in samples from borehole F4. These were found to consist of minor U-oxides associated mainly with zircon, baddeleyite and pyrite (Waber *et al.*, this report; Appendix 1). Analyses show mostly a positive U – Zr correlation, even though there were some variable correlation factors in each of the studied examples. This may indicate the inhomogeneity of the hydrothermal U-mineralising fluids that acted in restricted locations at the Osamu Utsumi site during the more general hydrothermal alteration which gave rise to the potassic rocks.

Specific U-minerals were not identified in the studied RFI and borehole F1 rocks, although it is believed that finely dispersed rare U-oxides may be present. Vanadium shows a mean value of about 70 ppm in the regional rocks, where it is bound to the aegirine-augites. The mean V values of the RFI and borehole F1 reduced, non-mineralised rocks (about 3 times that of the regional rocks) are practically identical with one another. Thus, V has not only an early magmatic origin, but can also be related to the hydrothermal potassic rock-forming process, independent of the grade of U-mineralisation. Specific V-bearing minerals were not identified in the RFI or borehole F1 rocks although they may be present in minor or trace amounts in the sericites/illites.

Zinc shows a somewhat similar behaviour to V; it already occurs in quite high amounts in the regional rocks (means of 168 ppm), bound to the silicate minerals (mainly pyroxenes). In the course of the hydrothermal alteration it becomes enriched, attaining practically identical mean values (about 220 ppm) in the RFI and borehole F1 rocks. Here it is present as fine sphalerite; no relationship with the U-mineralisation was observed.

Strontium occurs in the regional rocks in concentrations typical for worldwide nepheline syenites (1,000 – 3,000 ppm; Goldschmidt (1954)), with a mean content of 1,913 ppm. Much lower contents and mean values are found in the hydrothermally altered (non-mineralised) RFI (626 ppm) and borehole F1 rocks (181 ppm), being reduced respectively by factors of ~3 and >10. Similarly, lower Sr mean values (than those of the regional rocks) are found in the borehole F4 reduced (non-mineralised) rocks and in the RFII, III and IV reduced non-mineralised rocks. The hydrothermal Zr – U – REE mineralised rocks of borehole F4 may achieve higher Sr contents than the regional rocks, thus showing that an Sr-enrichment occurred during the high-temperature hydrothermal mineralising processes. However, the Sr enrichment factors vary strongly, not only between different occurrences but also within individual mineralised zones.

The redox front-related U-mineralisations show no relationships with Sr. It is known that the typical alkaline (magmatic) minerals of feldspathoidal (alkaline) rocks such as nepheline, leucite, orthoclase and sanidine may contain quite high amounts of Sr (Goldschmidt, *op. cit.*). Ulbrich (*op. cit.*) and Ulbrich *et al.* (*op. cit.*) confirmed SrO contents of up to  $\geq 1$  wt.% in nepheline syenite alkali feldspars from Poços de Caldas. Sr contents are lower in the case of equivalent hydrothermal minerals, for instance in low-temperature K-feldspars or in mica minerals resulting from the replacement of feldspathoids. This may explain the observed reduction of Sr in the studied RFI and borehole F1 rocks as being due to the associated processes of low-temperature (hydrothermal) alkali exchange reactions of the feldspars and the replacement of feldspathoids. The differences between RFI and borehole F1 rocks (and the other reduced non-mineralised rocks) are thought to reflect primary magmatic variations.

Lead occurs in very low concentrations near, or even below, detection level (<6 ppm), in both the regional (non-altered) and borehole F1 reduced (non-mineralised) rocks; higher contents (mean value = 47 ppm Pb) were found in the RFI rocks. These may be related to the magmatic and hydrothermal variations, but also, at least in part, to the higher U-contents of the studied RFI rocks. No Pb or Pb-bearing minerals were found in the discussed rocks. The occurrence of galena associated with the hydrothermal U-mineralisation has been mentioned in Urânio do Brasil internal reports, but has not been confirmed in this study of the high-grade hydrothermal U-mineralisation.

Niobium occurs in the regional rocks in normal concentrations (mean: 249 ppm) for alkaline rocks of these types, and also shows similar concentrations in the borehole F1

(226 ppm) and RFI rocks (277 ppm). In the regional rocks, Nb is thought to substitute mainly for Ti in the magmatic clinopyroxenes and probably in giannettite as well. In the hydrothermally altered rocks (borehole F1 and RFI) it is known to occur in the TiO<sub>2</sub>-(rutile-)minerals that form complex pseudomorphs after clinopyroxenes (Waber *et al.*, this report; section 5). In the borehole F1 rocks an almost perfect correlation of Ti and Nb can be observed (Waber *et al.*, *op. cit.*).

Zirconium and hafnium will be discussed together. The former shows similar mean concentrations (of 965 and 929 ppm respectively) in the regional and borehole F1 rocks, reduced by about half in the RFI rocks (means = 445 ppm). Hafnium was only analysed in the regional and RFI rocks, showing practically identical concentrations of 12 and 11 ppm. Hafnium is well known to substitute for Zr in Zr-minerals, but the main Zr-mineral species in the studied rocks are very different, consisting of giannettite in the regional rocks and zircon in the borehole F1 and RFI rocks. This, and the fact that hydrothermal zircons are normally richer in Hf than their magmatic equivalents, may explain the differences in the Zr/Hf ratios of the regional rocks (~80) and the RFI rocks (~40). Microprobe analysis of hydrothermal zircons of the borehole F1 reduced rocks showed consistently the presence of 1.0 – 1.5 wt.% of HfO<sub>2</sub>. The low total Zr contents in the RFI rocks, when compared with more than double the amount of Zr in the borehole F1 and regional rocks, are considered to be relicts of the primary magmatic geochemical character of the RFI phonolites.

Gallium was analysed only in the RFI and borehole F1 rocks, where it occurs in mean concentrations of 37 and 22 ppm in the reduced non-mineralised varieties. These are in fact low concentrations for nepheline-alkali feldspar rocks (Goldschmidt, *op. cit.*). As Ga analyses of the regional rocks of Poços de Caldas were not performed (and are unknown from the literature), the low contents of this element in the hydrothermally altered rocks (that tend to be richer in Al than the regional rocks and should therefore be also richer in Ga) are considered indicative either of the existence of alkaline magmas anomalously low in Ga at Poços de Caldas, or of a specific type of hydrothermal reducing alteration that enriched Al but leached Ga from the non-mineralised RFI and borehole F1 rocks.

#### *Some rare-earth (REE) and related elements: La, Ce, Nd, Y, Sc*

Routine XRF analyses do not yield very precise results for the REEs. These data should therefore be treated as semiquantitative and should only be used for the relative comparison of mean values.

In the regional, borehole F1 and RFI rock groups, the REE (mean) contents follow the natural sequence of abundance: Ce followed closely by La and, to a lesser extent by Nd. In addition, the total abundances of these elements in the regional and borehole F1 reduced non-mineralised rocks are quite similar (most probably lying within the limits of analytical uncertainties). In contrast, the RFI (reduced non-mineralised) rocks show individual and mean values significantly lower than those above (Appendix 6:2, Table 6:2-III); La and Ce are reduced by at least 5 to 6 times and Nd by more than 10 times.

The light REEs, La, Ce and Nd are expected to be fixed in the regional rocks in the clinopyroxenes, alkali feldspars and Zr-minerals (mainly giannettite). In the reduced borehole F1 rocks they are associated with the hydrothermal zircons (mainly Ce); however, in the hydrothermally exchanged alkali feldspars La, Ce and Nd are, if present at all, below the microprobe detection level (estimated  $\leq 500$  ppm).

The correlation of La, Ce and Nd with Zr is evident for the three compared groups, particularly if the analytical uncertainties are kept in mind. If the geochemical immobility of REEs is also considered, it may be concluded that the RFI phonolites were, in terms of their magmatic origin, strongly depleted in REEs (La, Ce and Nd), as they were in Zr. The hydrothermal reducing potassic rock alteration heat, judging from the comparison of regional and borehole F1 rocks, shows that only a very minor effect on these elements occurred, if at all.

Yttrium is similar to the REEs in showing the same concentrations in the regional and borehole F1 rocks, but is about 2 times less in the reduced non-mineralised RFI rocks. Yttrium should also be present in the regional rocks, mainly in the clinopyroxenes, and possibly in giannettite (and other rare metal silicates). In the borehole F1 rocks Y is most frequently found in crystallo-chemically significant amounts in zircons and zircon-baddeleyite intergrowths (Waber *et al.*, this report, section 5). This, however, would imply higher Zr-contents in the RFI rocks (where in fact they are diminished) or, alternatively, higher Y-contents in the RFI zircons. As such indications are however lacking, it is thought that the higher Y-contents of the RFI reduced rocks may somehow be related to their higher U-content. It is known that various hydrothermal U-mineralisations formed by alkali metasomatism are also associated with Y and heavy REE enrichment (for instance: Porto da Silveira, 1986; Porto da Silveira *et al.*, 1989).

Scandium was only analysed in the regional rocks and borehole F1 rocks. In the former, the mean values are below the XRF detection limit ( $< 1$  ppm), and in the borehole F1 reduced, non-mineralised rocks a value of 2 ppm was obtained. These very low values are within the expected limits for nepheline syenites (Goldschmidt, *op. cit.*).

### *Elements Cr, Ni, Co, Cu, F and S*

Cr, Ni, Co and Cu occur in the three rock groups in very low amounts, near or even below the XRF detection limit (Appendix 6:2; Table 6:2-III). Even Co, which in various hydrothermal U-occurrences is one of the typical elements, occurs in higher amounts at the Osamu Utsumi mine in only one (of the studied) hydrothermally mineralised intersections of borehole F4. In the RFI rocks all of these elements show very low total concentrations, which precludes any further interpretation.

Fluorine was analysed only in the regional and borehole F1 rocks with similar results (within the limits of analytical uncertainty). In the borehole F1 reduced non-mineralised rocks, F is most commonly present as rare fluorspar and may also still be a minor constituent in the hydrothermal white micas (sericite/illite). Fluorspar is also known from late pegmatitic to autohydrothermal veins of the regional rocks. Besides, F may be present in minor amounts in aegirine and giannettite and other rare metal silicates of the woehlerite group.

Sulphur as the sulphide ion is one of the important elements of the hydrothermal potassic rock (reducing) processes at the Osamu Utsumi site. It is typically high in the reduced RFI and borehole F1 rocks, where it is bound to the sulphidic ore minerals pyrite, sphalerite, (?)jordisite, (?)greenockite and others. The regional rocks are poor in S, where it should be present in cancrinite, sodalite and nosean.

### **Conclusions**

In conclusion, the RFI non-mineralised reduced phonolites must be considered as being derived from the original magmatic rocks that were typically low in Zr and La, Ce and Nd. Otherwise the trace element compositions for these types of unsaturated hololeucocratic nepheline- and pseudoleucite-bearing rocks are normal. The hydrothermal reducing potassic rock alteration led to the enrichment of Ba, Rb, V, Zn and S, independent of the grade of U-mineralisation. The enrichment of Th, Pb, Y, Zr and U occurred as both a direct and indirect consequence of the associated (hydrothermal) mineralising processes. In the case of U, some redox front-related supergenic-reducing enrichment also probably occurred. Strontium was lost in the course of hydrothermal alteration and Nb and Hf maintained concentration levels similar to those of the regional igneous rocks. The Zr/Hf ratio is however less in the RFI rocks due to their lower total Zr content and to their particularly Hf-rich hydrothermal zircons. Scandium, Cr, Ni, Co and Cu occur in very low total concentrations in both the regional magmatic and the hydrothermally altered RFI and borehole F1 rocks; this is considered

normal. Gallium and F were not analysed in the regional magmatic and the RFI rocks. The former shows concentrations lower than normal for magmatic nepheline-alkali feldspar rocks in the hydrothermally altered rocks, and the latter shows similar concentrations when compared to the borehole F1 and regional rocks.

### 6.3.2. RFI oxidised and reduced phonolites

The non-mineralised reduced RFI and borehole F1 rocks are compared here with the equivalent oxidised RFI and borehole F1 rocks. Comparisons are based on the mean values obtained for a total of 16 analysed individual samples (Appendix 6:2; Table 6:2-III) including the RFI rocks from samples RFI-1A and RFI-1B and the borehole F1 rocks.

Comparison of the major elements shows only minor systematic variations that include increasing  $\text{Al}_2\text{O}_3$  (and possibly  $\text{TiO}_2$  and  $\text{K}_2\text{O}$  contents) in the oxidised rocks;  $\text{SiO}_2$  diminishes very slightly and LOI more characteristically. Calcium, if present in the reduced rock, is almost totally eliminated. Among the other elements,  $\text{Fe}_2\text{O}_{3\text{tot}}$  shows insignificant variation and  $\text{MnO}$ ,  $\text{MgO}$  and  $\text{P}_2\text{O}_5$  maintain very low concentration levels. This is also the case for  $\text{Na}_2\text{O}$  in the RFI rocks. The apparent enrichment of  $\text{Na}_2\text{O}$  in the borehole F1 oxidised rocks is erroneous; the higher contents are due to the preservation of less altered perthitic K-feldspars in some of the oxidised rocks (Waber *et al.*, this report; Appendix 4).

These major element variations between reduced and oxidised RFI (and borehole F1) rocks may be largely explained by incipient oxidising lateritic weathering processes producing further kaolinisation ( $\text{Al}_2\text{O}_3$ -increase,  $\text{SiO}_2$ -decrease), pyrite oxidation (LOI reduction), HFO mineral precipitation (irregular  $\text{Fe}_2\text{O}_{3\text{tot}}$  redistribution), possible carbonate and fluorite dissolution (CaO decrease), and rock-solid volume reduction and residual enrichment of  $\text{K}_2\text{O}$  (in weathering-resistant white micas) and  $\text{TiO}_2$  (in rutile/hydrorutile minerals).

In comparison, the trace element variations show systematic but minor enrichments of Rb, partial depletion of Sr, strong depletion of Zn and S, and significant enrichment of Ga in the oxidised rocks. The REEs, La, Ce and Nd, were inert/immobile during the oxidising supergenic process. Ba and Nb show non-systematic variations and V is immobile, or only very slightly enriched, in the borehole F1 rocks, but strongly enriched in the RFI oxidised rocks.

Cr, Ni, Co, Cu and Sc (analysed only in the borehole F1 rocks) maintain very low total concentrations and F, analysed only in the borehole F1 rocks, is significantly diminished in the oxidised rocks.

Pb, Th, U, Y, Zr and Hf in the RFI rocks behaved differently from those in the borehole F1 rocks due to the higher grade of U-mineralisation of the former. Upon oxidation, a drastic reduction of Zr in the RFI rocks, and a consequent reduction of Hf, Y and Th, were also observed; similarly a decrease of U and Pb occurs.

In the borehole F1 rocks Zr and Y were generally immobile, and Pb, Th and U show higher concentrations in the oxidised than in the reduced rocks. However, the total concentrations of Pb, Th and U are within the range of these elements present in the oxidised RFI rocks.

The observed trace element variations further support the major element results, i.e. Rb enrichment is sympathetic with  $K_2O$ , Sr depletion with  $CaO$ ; Zn and S indicate the dissolution/oxidation of sphalerite and of all the other sulphide minerals. The enrichment of Ga is, as that of  $Al_2O_3$ , typical for lateritic weathering. This is confirmed by the immobility (within the restrictions of analytical uncertainties) of the REEs and also Ba and Nb, and by the enrichment of V.

Cr, Ni, Co, Cu and Sc are known to become enriched during lateritic weathering; however, their low availability during the incipient stages of the process may have resulted in their chemical uniformity. The decrease of F in the oxidised borehole F1 rocks is confirmed by the mineralogy, which points to the total dissolution of fluorite during oxidation of the rock.

Pb, Th, U, Y, Zr and Hf behave differently in the RFI and borehole F1 rocks. In the former, their behaviour corresponds to weathering dissolution with partial laterite reprecipitation of a hydrothermal low-grade radioactive mineralisation. This has also resulted in the partial dissolution of  $ZrO_2$ – $HfO_2$ -rich, Th- and Y-bearing hydrothermal zircons, and in the partial dissolution of (probably) U-oxide minerals and of (radiogenic) Pb. In the case of the borehole F1 rocks, Zr and Y remained inert and Pb, Th and U enrichment occurred from the considerably lower “protore” levels of the reduced rocks, to what may be considered the initial stages of their concentration, to form a lateritic geochemical anomaly in the oxidised rocks.

### 6.3.3. RFI redox front processes

#### Major and trace elements (XRF data)

The geochemical character of the RFI redox front is shown in Figures 6-3 to 6-13, and will be briefly discussed in comparison with the RFI non-mineralised, reduced and oxidised rocks mean values.

Four U-mineralised samples were included with the analysed RFI rocks. One (RFI-1C) typifies an oxidised U-mineralised zone directly adjacent to the redox front (of about 5 cm width). The others are from reduced samples RFI-4 and RFI-5; of these samples RFI-4A-1 and RFI-4B represent the zone of maximum U-mineralisation and samples with weak U-mineralisation respectively. Mineralisation is in the form of pitchblende micro- and macronodules. RFI-5B also represents a weakly mineralised sample with pitchblende micronodules, but its relationship to the redox front is not known and is therefore considered anomalous.

The oxidised U-mineralised zone (sample RFI-1C) shows, among the major elements (relative to the mean values of the respective RFI oxidised and non-mineralised rocks), a slight decrease in  $\text{SiO}_2$  and an increase in  $\text{Fe}_2\text{O}_{3\text{tot}}$  and LOI values. Of the trace elements, Zn, Co, Ni, La, Ce, Nd, Pb and, particularly strongly, U and S tend to be concentrated in the mineralised zone. Of the remainder, Y was slightly depleted and V enriched (but less than the means of the oxidised rocks) and the other elements remained within or very near to their mean values. Specific mineral phases that may be related to the observed geochemical anomalies could not be detected, except for HFO minerals (mainly limonite). These are known to coprecipitate available metals, e.g. REEs and U in lateritic deposits, but they do not explain the high S content. It is thought that possibly jarosite or similar  $\text{Fe}^{3+}$ -sulphates may also have formed, accounting for the S and trace element abundances (Bambauer *et al.*, 1988, 1989).

Of the redox fronts sampled and analysed by Waber *et al.* (this report), only RFII (in volcanic breccia) showed a comparable oxidised Fe – U – S enrichment, directly adjacent to the redox front. This and sample set I, without an oxidised U-mineralised zone (Figures 6-4 and 6-6), seem to indicate that the development of such a zone is either not a general feature of the redox fronts, or is restricted to very narrow zones (note that sample RFI-2B of sample set I is a few cm more distant from the redox front than sample RFI-1C of set II).

The reduced, non-mineralised zone directly adjacent to the redox front on the reduced side (sample RFI-3B) shows only weak geochemical variations when compared to the reduced non-mineralised rock.  $\text{Al}_2\text{O}_3$ ,  $\text{TiO}_2$ , Ga, V and Pb are enriched and Zr, Y, Th,

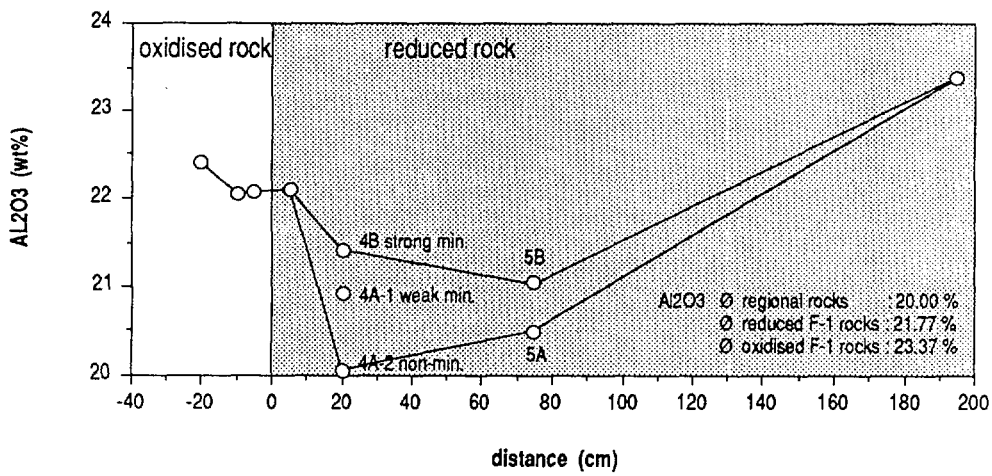
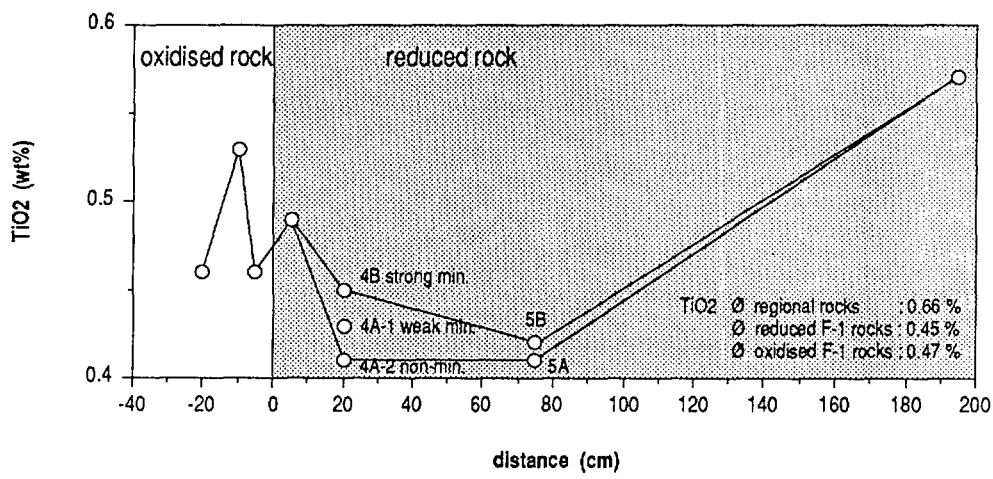
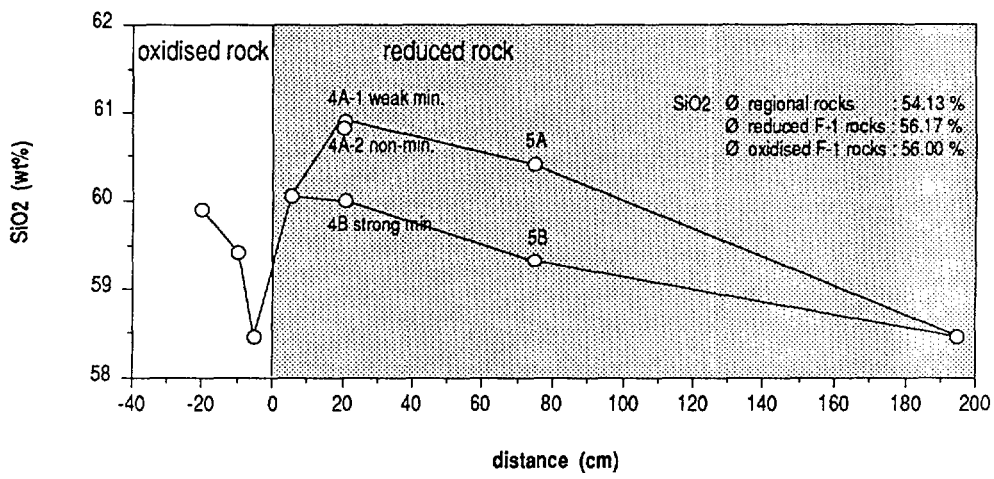


Figure 6-3. RFI redox front: geochemical distribution of selected elements/parameters.

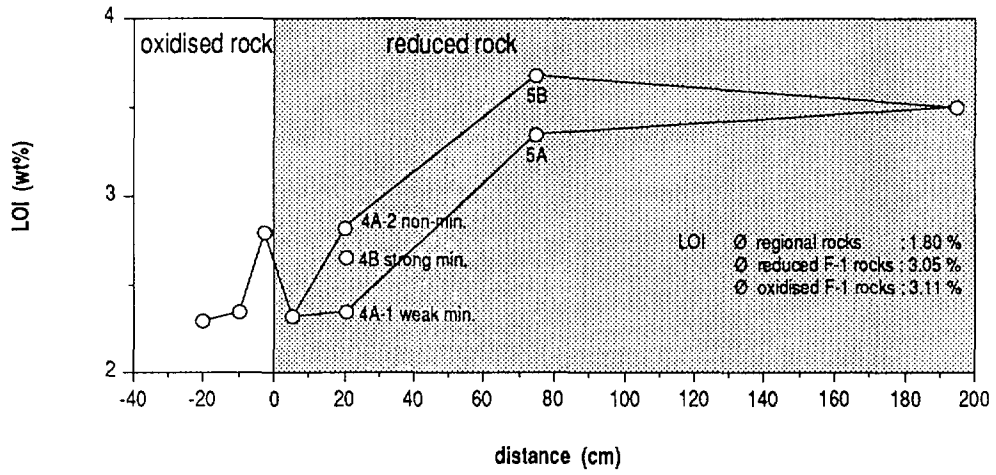
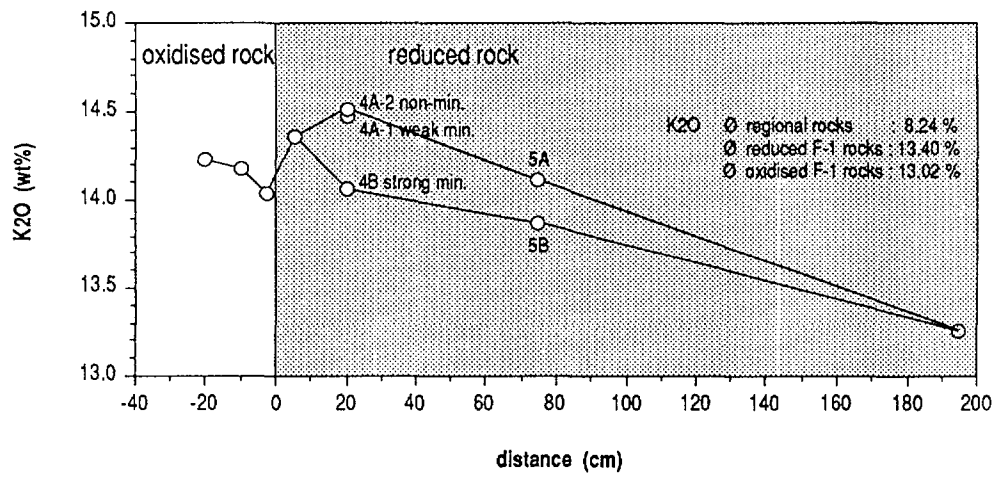
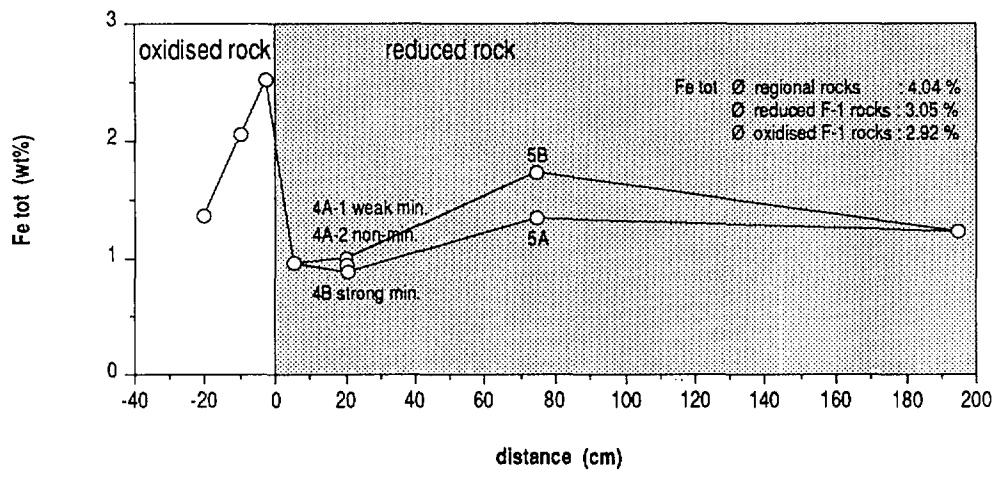


Figure 6-4. RFI redox front: geochemical distribution of  $Fe_2O_{3(tot)}$ ,  $K_2O$  and LOI.

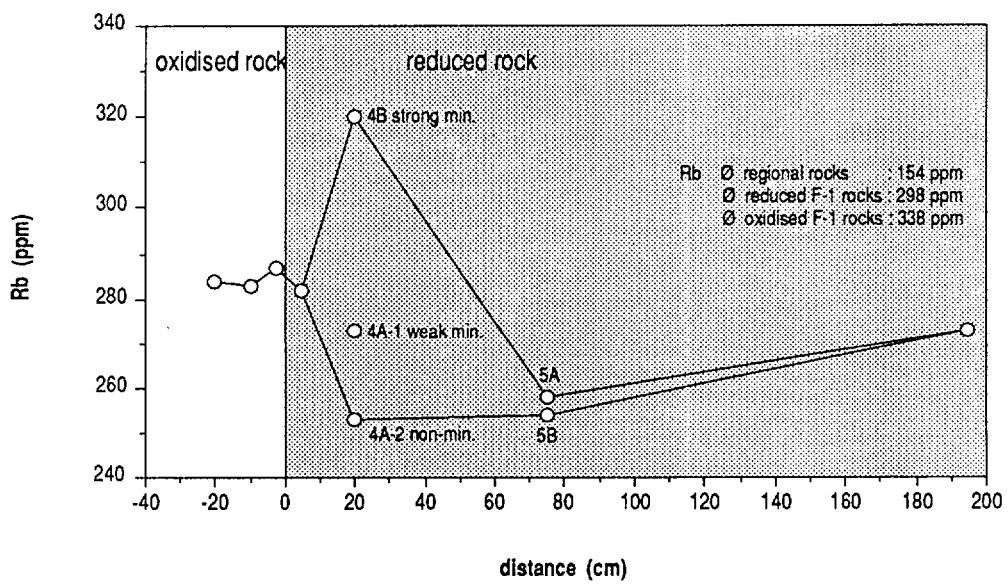
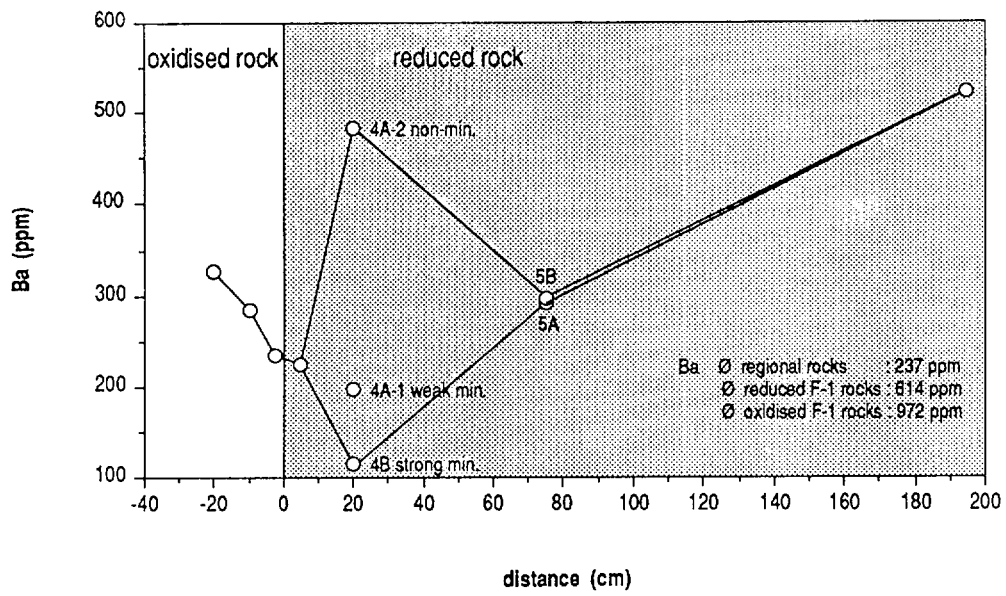


Figure 6-5. RFI redox front: geochemical distribution of Ba and Rb.

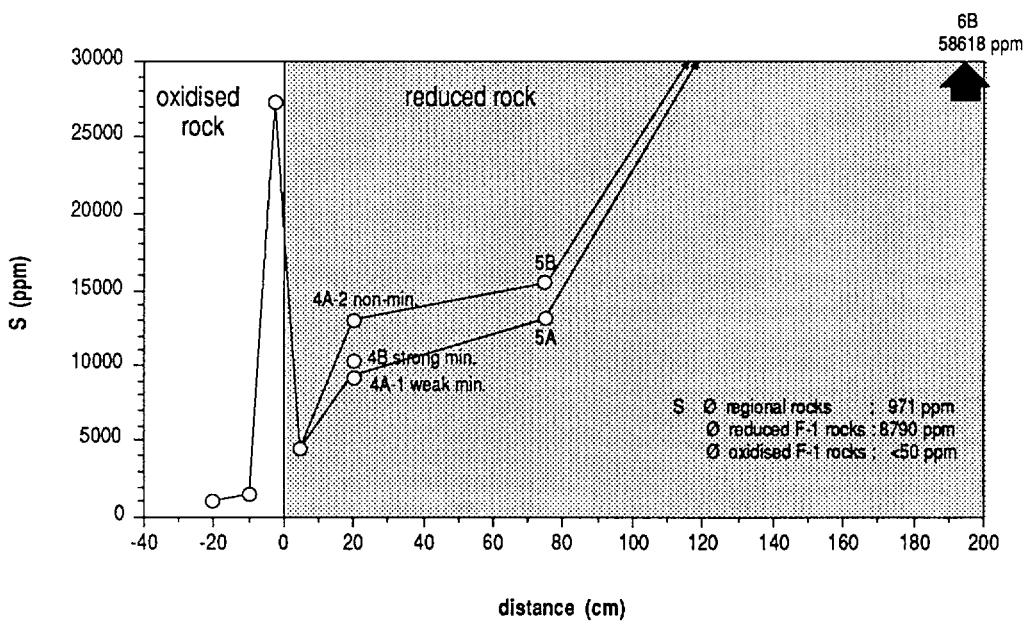
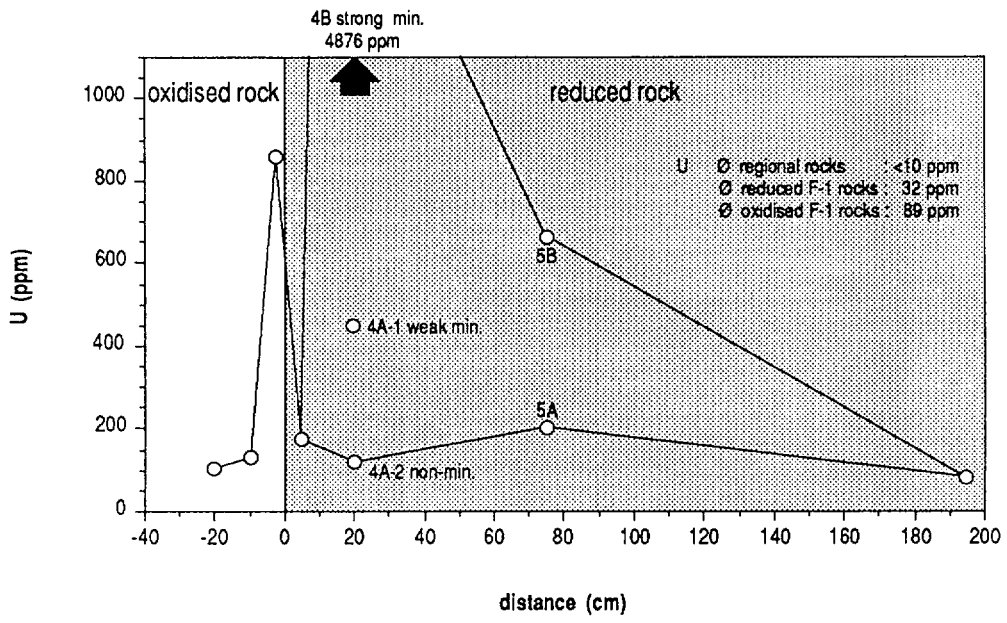


Figure 6-6. RFI redox front: geochemical distribution of U and S.

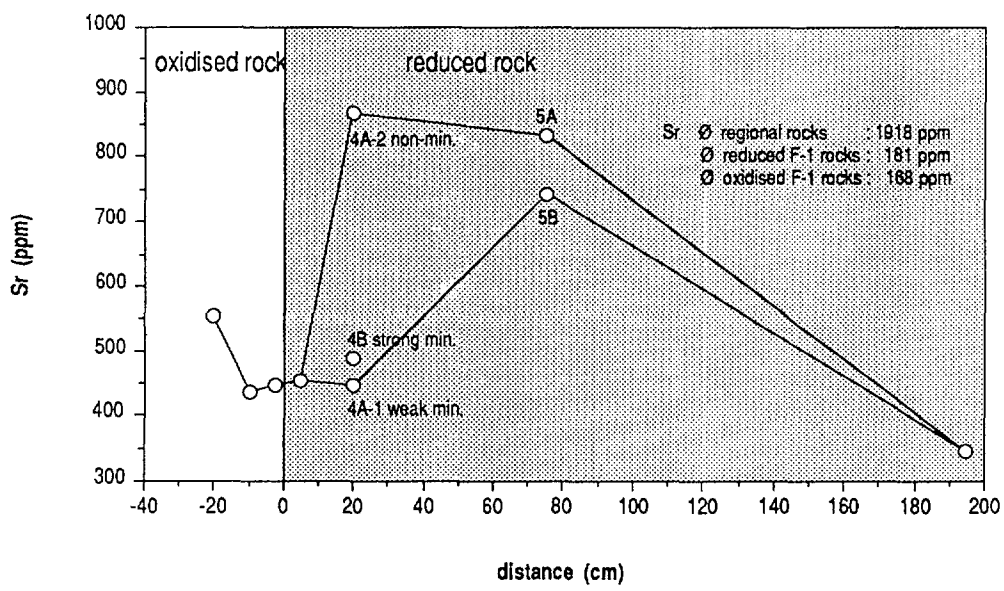
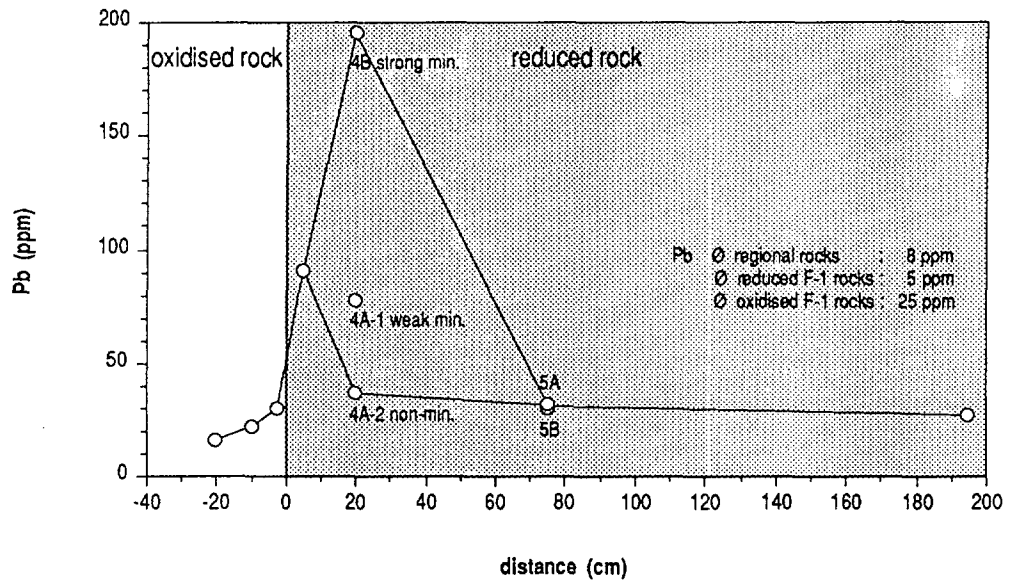


Figure 6-7. RFI redox front: geochemical distribution of Pb and Sr.

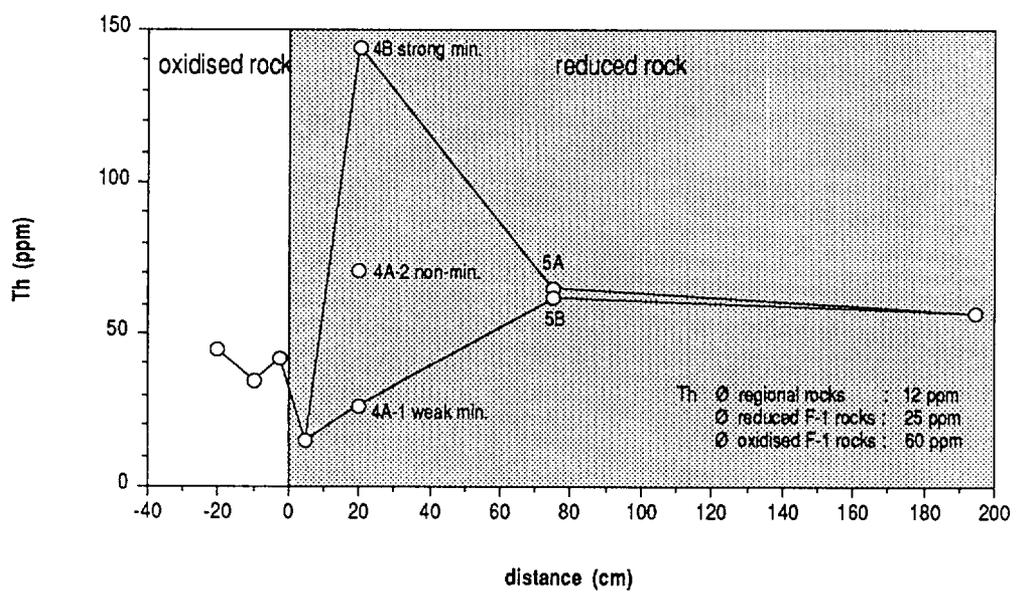
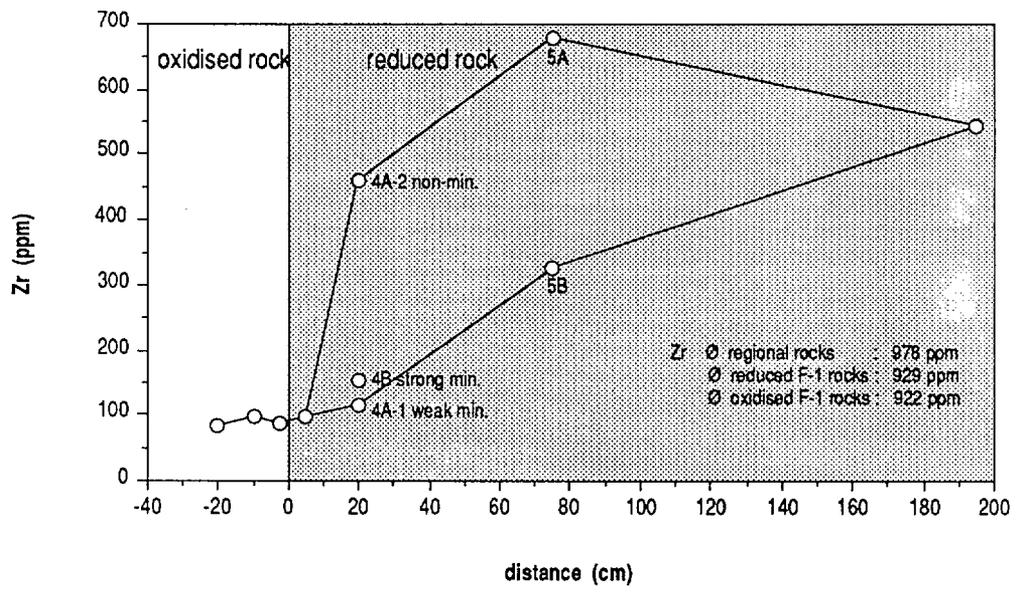


Figure 6-8. RFI redox front: geochemical distribution of Zr and Th.

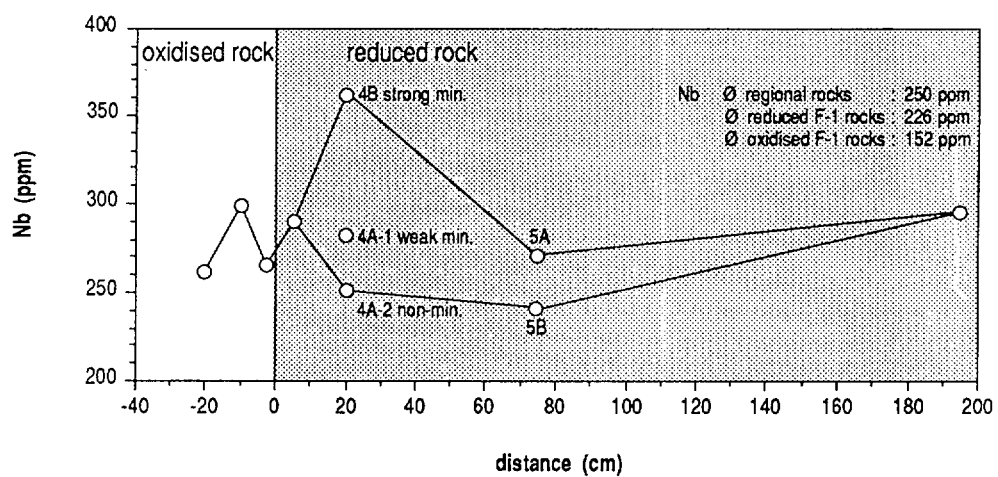
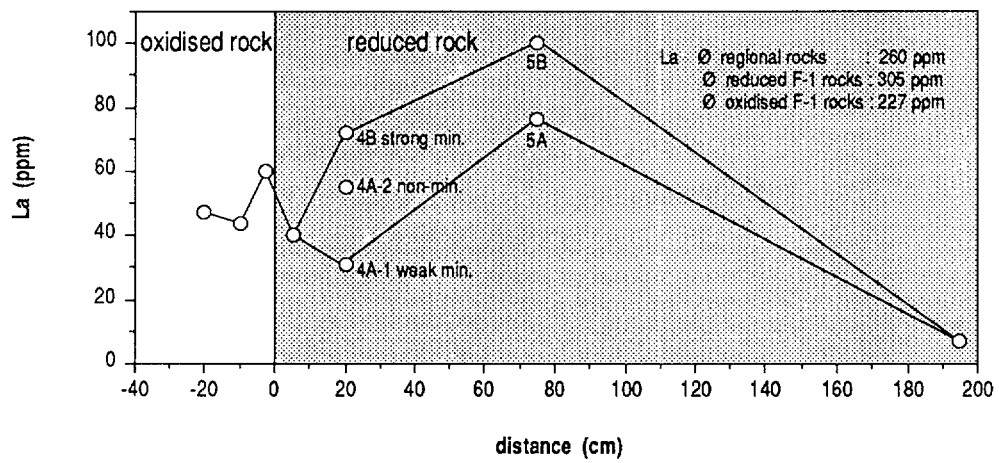
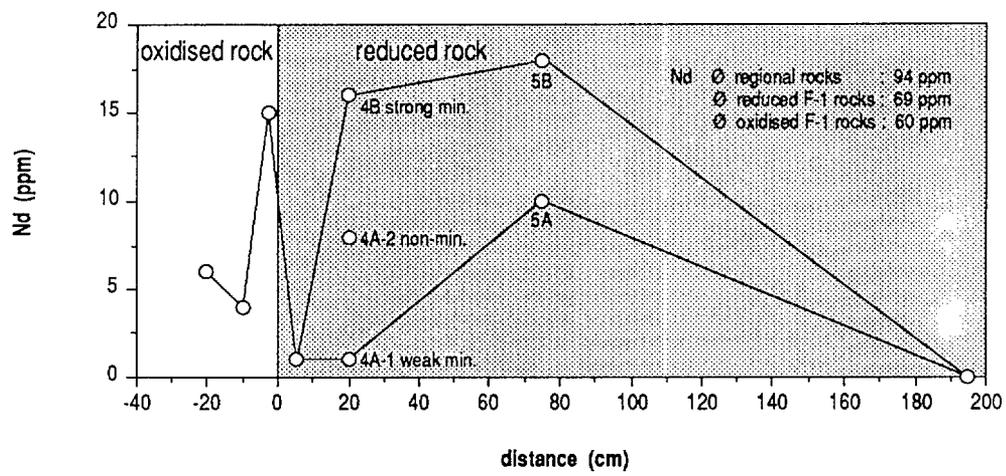


Figure 6-9. RFI redox front: geochemical distribution of Nd, La and Nb.

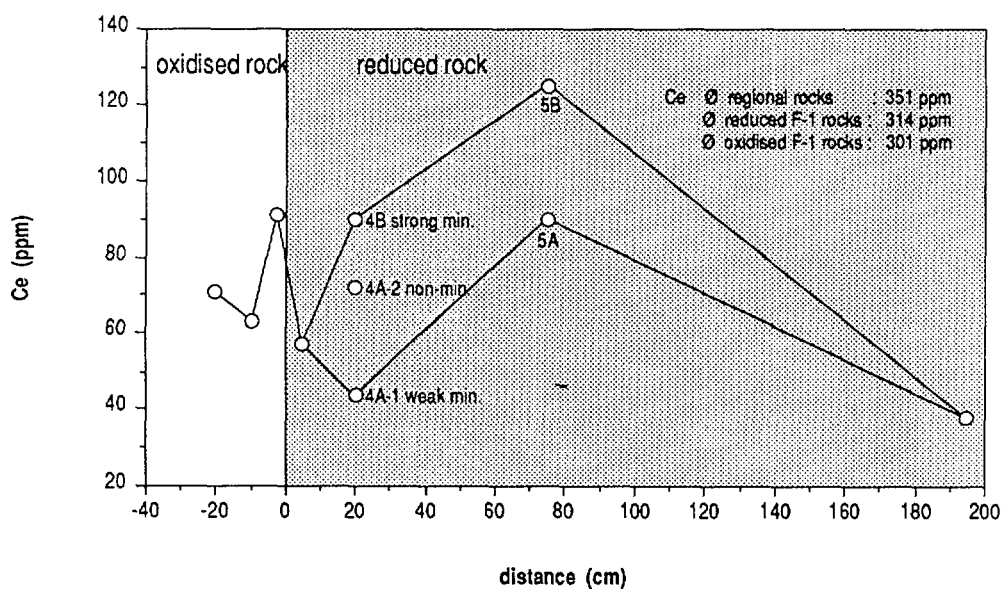
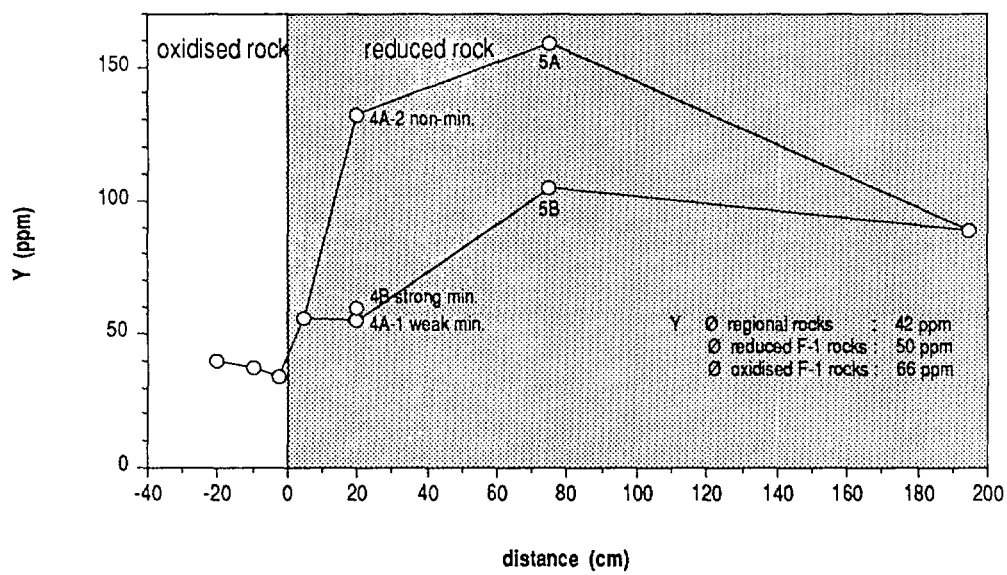


Figure 6-10. RFI redox front: geochemical distribution of Y and Ce.

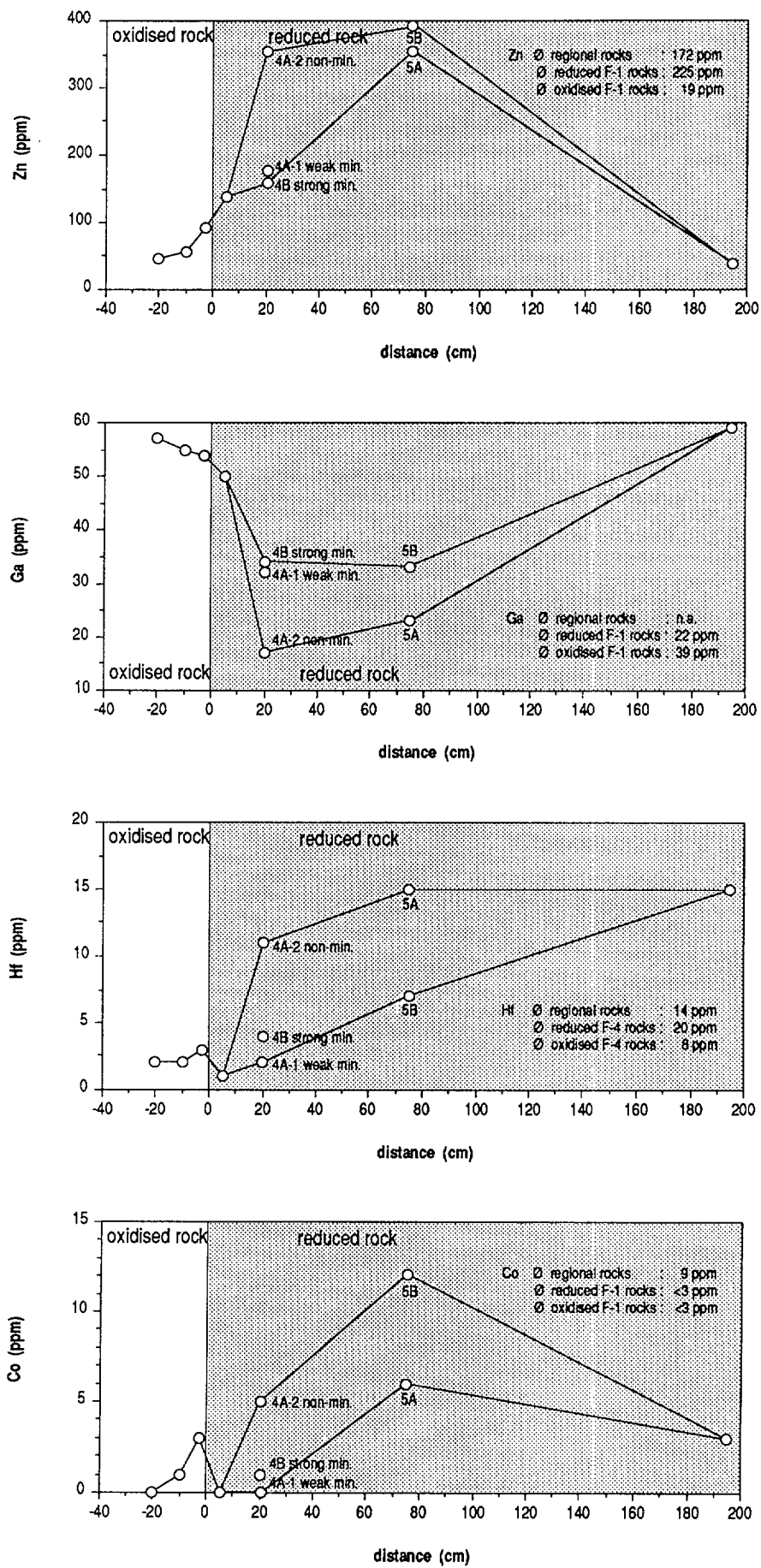


Figure 6-11. RFI redox front: geochemical distribution of Zn, Ga, Hf and Co.

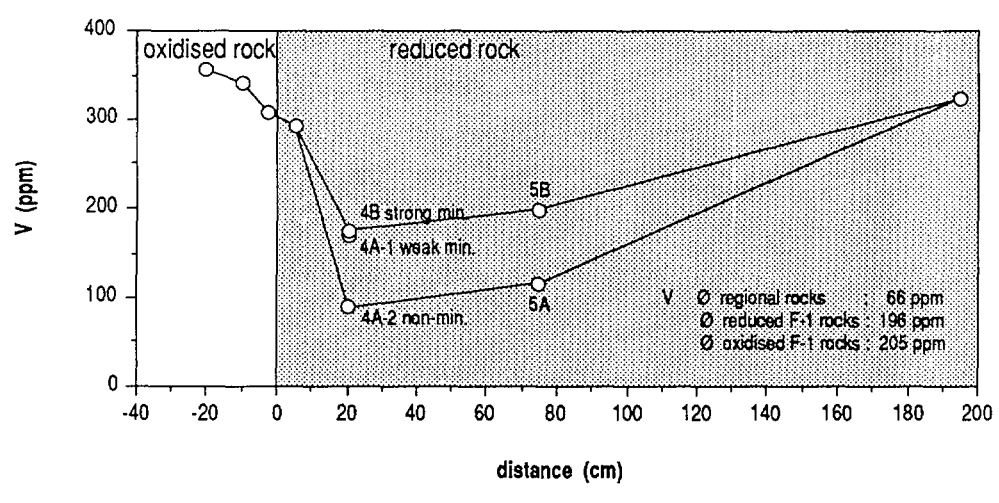
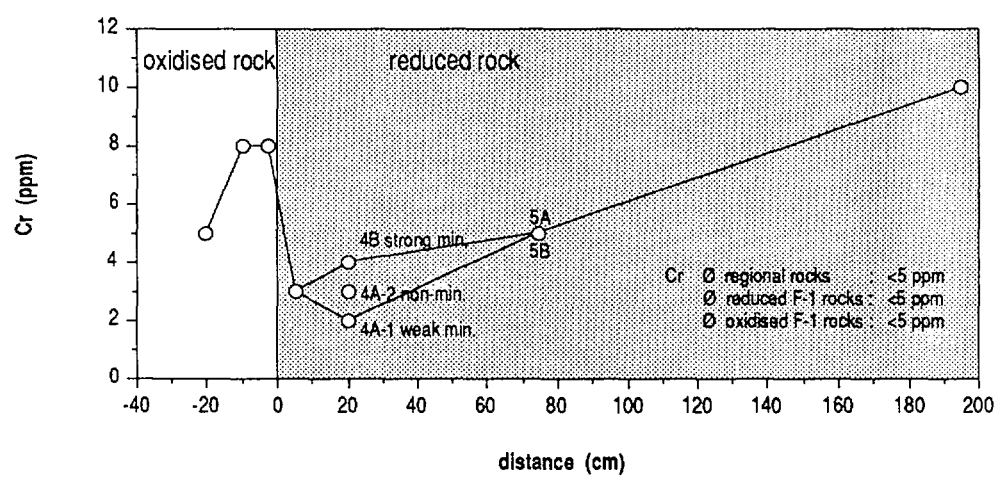
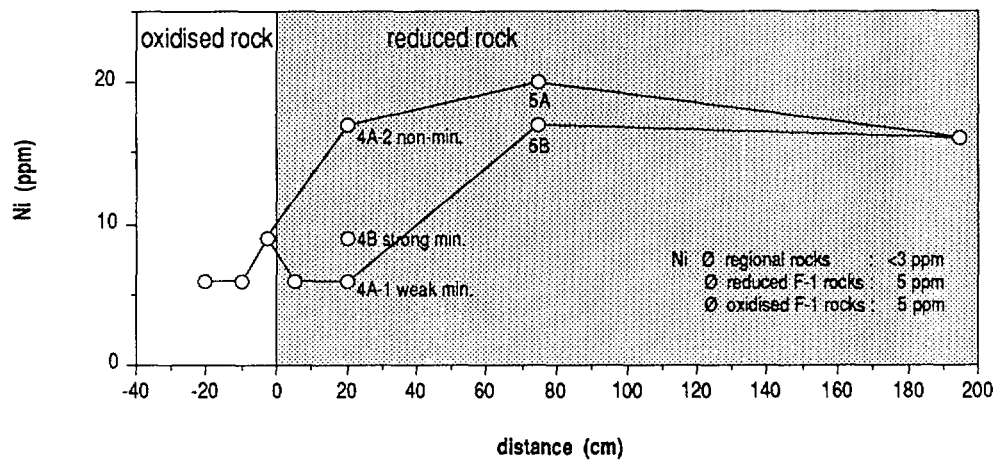


Figure 6-12. RFI redox front: geochemical distribution of Ni, Cr and V.

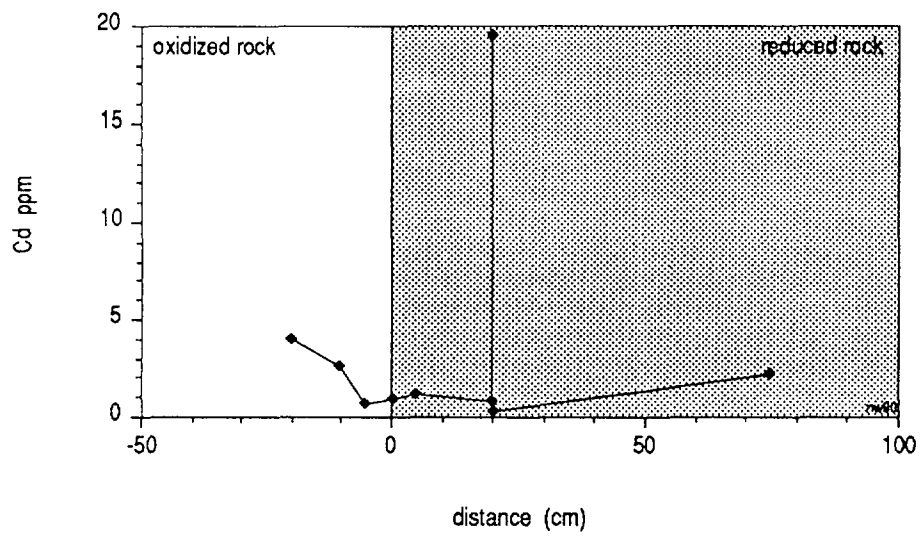
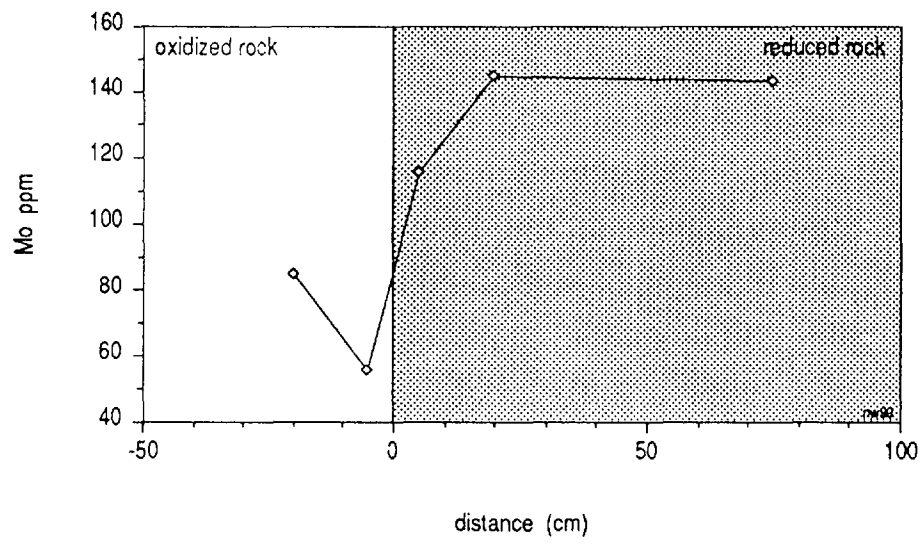


Figure 6-13. RFI redox front: geochemical distribution of Mo and Cd.

Hf, Zn, S and LOI are depleted; this is believed to be mainly due to redox front-related processes and not just the effect of natural rock compositional variations. However, sample RFI-3B is one of those included in the means of the RFI non-mineralised reduced rocks. The more mobile elements of the hydrothermal stage and of the redox front-related superimposed U-mineralisation were depleted, and the more immobile elements, including (?radiogenic) Pb, are enriched. The apparent mobility of Zr, Hf and, particularly, of Th and Y is surprising.

From the zone of maximum U-mineralisation, three subsamples representing different U-grades were analysed, including non-mineralised, weakly mineralised and strongly mineralised types (sample numbers RFI-4A-2; -4A-1 and -4B). They are considered together with samples RFI-5A and -5B of the non-mineralised and weakly mineralised reducing phonolites. It can be seen from the geochemical profiles that, of all the major and trace elements considered, only U precisely characterises the redox front-related U-mineralisation. Even Pb and Th are typically enriched in the highest grade U-mineralised rocks of RFI. In the low-grade (weak) U-mineralisations (samples RFI-4A-1 and -5B) both elements show insignificant variations, being either enriched or depleted in relation to the means of non-mineralised reducing rocks. Zr, Hf, Y and the analysed REEs show non-systematic variations with respect to the grade of the U-mineralisation related to the redox front, and most probably reflect just the rock compositional variations of magmatic and/or superimposed hydrothermal origin. However, this almost pure U-enrichment of the redox front mineralisation is characteristically very different from any of the hydrothermal (high-temperature) U-mineralisations. It characterises the redox front RFI, supported also by main and trace element geochemistry, as a low-temperature, geologically young (subrecent to recent) roll-front mineralisation.

### **The geochemistry of Cd**

The presence of the CdS greenockite in massive pitchblende nodules from the Urânio do Brasil collections in Poços de Caldas has already been noted. Unfortunately these massive pitchblende nodules were only found during the early stages of mining at Osamu Utsumi, and details of their location are only qualitative. However, it is known that they were collected from the open pit in the oxidised rocks, at a few metres to a few tens of metres above the main redox front, overlying reduced rocks in areas of the higher grade U-mineralisations.

The nature and possible genetic relationships between these massive “fossil” nodules and those of the (subrecent to recent) active redox fronts observed in the mine (1st generation nodules) were judged to be of considerable interest to the project. As a result, the selective Cd mineralogy and geochemistry of the nodules were investigated.

Two series of analyses were carried out at the University of Bern. The first sample series included the main RFI oxidised and reduced bulk rock samples (Table 6-II; analyses 03; 04; 05; 06 and 07) and one sample consisting of the massive pitchblende zone of a large nodule (no. Ku-6, Waber *et al.*, this report; Appendix 1). This sample series confirmed the extremely high Cd content of the massive pitchblende nodule (approx. 0.1% Cd), although it was not selective enough to reveal any systematic variations of Cd along the RFI profile. Consequently a second, more selective sample set was prepared from the RFI samples by drilling minor sample portions of:

- oxidised bulk rock (with HFO minerals) adjacent to a bleached nodule resulting from pitchblende – pyrite dissolution;
- bleached nodules from pitchblende – pyrite dissolution (without HFO minerals) from oxidised rock;
- reduced bulk rock directly adjacent to, and about 5 cm from, the redox front (in the middle of the non-mineralised reduced zone);
- pitchblende macronodule from the zone of maximum U-mineralisation, and
- reduced bulk rock directly adjacent to the abovementioned macronodule, but without U-nodules and approx. 50 cm from the mineralised zone.

The results of the Cd analysis are shown in Table 6:2-IV (Appendix 6:2) and Figure 6-13. The figure shows the very good agreement of the two sample sets. Geochemically it is important to note that:

- bleached pitchblende nodules and enclosing typical oxidised rocks have identical Cd contents (pairs of analysis: 2-03 and 1-3);
- reduced non- or only weakly U-mineralised bulk rocks have low Cd contents, even if they are from the zone of maximum U-mineralisation and directly adjacent to pitchblende nodules;
- Cd is strongly and very selectively concentrated inside the pitchblende (macro-) nodules of RFI;

- directly adjacent to the redox front no specific Cd geochemical processes could be noted.

The enrichment/precipitation of Cd at the redox front is certainly related to the observed dissolution of sphalerite during the formation of the oxidised rocks. Its precipitation within the first generation pitchblende nodules, together with second generation pyrite and cryptocrystalline U-oxides, is very similar to the observations made in the case of the “fossil” massive pitchblende nodules. In the latter case, S-isotopes indicated a biochemical origin for the second generation pyrites (Waber *et al.*, this report; Appendix 1).

From the mineralogical-textural and geochemical evidence, it is believed that the related active redox front formation of (first generation) pitchblende nodules containing paragenetic second generation pyrite and Cd enrichments was facilitated by bio-geochemical processes, probably through the action of sulphate-reducing bacteria. Specific Cd minerals could not be identified. However, from analogy with the massive pitchblende nodules, it is believed that the Cd mineral in this case is also greenockite (CdS), present in such fine-grained and low total abundances that its detection using microscopic and XRD techniques is precluded.

According to the author, the observed precipitation of U-oxides, of Cd and related second generation pyrite exclusively within the microenvironments of the related redox front pitchblende nodules, and involving bacterial/bio-geochemical processes, is apparently an as yet unobserved geochemical association.

It is known from literature (Bambauer *et al.*, 1988, 1989) that Cd enters the oxidised Fe mineral jarosite under low-temperature weathering conditions. For the RFI sample (RFI-1C), which showed high U-contents and the possible presence of jarosite, unfortunately no Cd analyses exist. However, in the oxidised samples (RFI-1A, RFI-1B) the Cd-contents are higher than in the non-mineralised reduced rocks and it is positively correlated with the  $\text{Fe}_2\text{O}_{3\text{tot}}$  contents. In these cases this may indicate the coprecipitation of Cd with HFO minerals (mainly limonite).

## 7. Summary

Fundamental to all interpretations is the ability to distinguish the primary magmatic and later superimposed reducing hydrothermal processes from the final supergenic processes which resulted in bedrock oxidation and in the formation of the redox fronts.

The primary magmatic composition of the RFI rocks consisted of extremely fine-grained, almost aphanitic, weakly porphyritic (mainly orthoclase, nepheline and pseudoleucite phenocrysts) and (micro-)xenolithic (phonolite and nepheline syenite fragments) hololeucocratic volcanic phonolites. Geochemically they are silica-unsaturated peralkaline rocks, particularly rich in  $K_2O$  and Zr, La, Ce and Nd when compared to the regional magmatic rocks. Primary magmatic differences between the RFI phonolite samples could not be detected.

Post-magmatic, pneumatolytic and auto-hydrothermal processes (earlier than the potassic rock hydrothermal alteration) could not be identified. If present, such processes are normally quite weak in rapidly cooled volcanic rocks.

The potassic rock reducing hydrothermal alteration, associated with weak (hydrothermal) U- (Th) – Zr (Hf) – Y mineralisation, is responsible for the main present-day characteristics of the RFI rocks. Globally, one can consider the governing mineralogical processes as K-feldspathisation (through exchange reactions), sericitisation/illitisation associated with argillation (major kaolinisation and minor smectite formation) and pyritisation. Chemically, the main processes involved alkali exchange reactions resulting in K enrichment,  $SiO_2$ ,  $Al_2O_3$  and Rb enrichments and Sr losses. Physical parameters such as porosity increased, together with a lower global density and higher grain (solids) density. The penecontemporaneous but irregular mineralisation (of U, Th, Zr, Hf, Y and others) is considered to be the main factor explaining the localised heterogeneous geochemical (and mineralogical) trace element (and minor mineral) variations observed between the non- or weakly redox front-affected RFI rocks.

The redox front processes, in fact, appear to have had only a very restricted mineralogical and geochemical influence. In the reduced rocks these processes resulted in a zone of more important U-mineralisation with certain analogies to the 'roll-front type' that consists of nodular pitchblende. The U-nodules contain 2 pyrite generations, an unidentified Cd mineral (probably CdS-greenockite) and the rock-forming minerals. Most probably they formed in association with bio-geochemical activity involving sulphate-reducing bacteria. Such microbial activity is discussed in more detail in West *et al.* (this report series; Rep. 10). Geochemically the related redox front U-mineralisations are mainly characterised by the U-enrichment itself, minor Th and (?radiogenic) Pb enrichment, and very selective Cd enrichment (only in the U nodules).

The oxidic redox front-related processes are restricted to a very proximal zone; in the case of RFI within a zone of less than 5 cm directly adjacent to the redox front. Geochemical processes consist essentially of an (oxidic) enrichment of Fe, U and

(sulphate) S. Mineralogically, the formation of HFO minerals (mainly limonite) could be observed and the formation of Fe(III)-sulphates (possibly of the jarosite type) inferred. The oxidised Fe species are considered the most important phases for explaining the other systematic trace element variations observed in the direct vicinity of the redox front.

A few more centimetres distant, the influence of the redox front disappears and the 'normal' oxidised rocks show only minor mineralogical and geochemical alterations typical of incipient lateritic weathering, i.e. the formation of a second kaolinite generation correlated with Al and Ga enrichment and U-loss.

## 8. References

- Bambauer, H.U., Gebhard, G., Holzapfel, Th. and Krause, Chr., 1988. Schadstoff-Immobilisierung in Stabilisaten aus Braunkohlenaschen und REA-Produkten. *Fortschr. Miner.*, 66, 2, 281-290.
- Bambauer, H.U., Steffes-Tun, W. and Krause, Chr., 1989. Immobilization of thallium in a pyrite ash dump by jarosite formation. Inter. Conf. on Applied Mineralogy (GAC-MAC-ICAM-CAM), *GAC-MAC Ann. Meet.*, Program with Abstracts, Vol. 14, p. A 118, Montreal.
- Barrington, J. and Kerr, P.F., 1961. Uranium mineralisation at the Midnite Mine, Spokane, Washington. *Econ. Geol.*, 56, 241-258.
- Blanchard, R., 1968. Interpretation of leached outcrops. *Nevada Bureau of Mines, Bull.*, 66 (chapt. 7), Nevada Bureau of Mines & Geology, Univ. of Nevada, Reno, Nevada, 196 pp.
- Goldschmidt, V.M., 1954. Geochemistry. *Clarendon Press*, Oxford, 730 pp.
- Le Maître, R.W., 1984. A proposal by USGS-Subcommission on the systematics of igneous rocks for a chemical classification of volcanic rocks based on the total alkali silica (TAS) diagram. *Austral. J. Earth Sci.*, 31, 243-255.
- O'Neil, J.R. and Taylor, H.P. Jr., 1967. The oxygen isotope and cation exchange chemistry of feldspars. *Amer. Miner.*, 52, 1414-1437.
- Porto da Silveira, C.L., 1986. Geoquímica da mineralização metassomática urano-sódica de Espinharas (PB). *PhD-thesis* (unpubl.), Dept. of Chemistry, PUC-RJ (Pontifícia Universidade Católica do Rio de Janeiro), 287 pp.

- Porto da Silveira, C.L., Schorscher, H.D. and Miekeley, N., 1989. The geochemistry of albitization and related U-mineralization, Espinharas, Pb, Brazil. *13th Inter. Geochem. Explor. Symp.*, Abstracts, 101-102, co-publ. SBGq-CPRM/DNPM, Rio de Janeiro.
- Ramdohr, P., 1975. Die Erzminerale und ihre Verwachsungen. 4th ed., *Akademie-Verlag*, Berlin, 1277 pp.
- Rogers, J.J.W. and Adams, J.A.S., 1978. Thorium (part E). In: K.H. Wedepohl (Editor), *Handbook of Geochemistry*, Vol. II-5, *Springer*, Berlin, Heidelberg, New York.
- Swanson, H.E. and Fuyat, R.K., 1953. Standard X-ray diffraction powder patterns, VII: *NBS Circular 539*, p. 33 (cit. in: Barrington and Kerr, 1961).
- Ulbrich, M.N.C., 1983. Aspectos mineralógicos e petrológicos de nefelina sienitos do maciço alcalino de Poços de Caldas, MG-SP, *PhD-thesis* (unpubl.), University of São Paulo, 369 pp.
- Ulbrich, M.N.C., Gomes, C.B. de and Ulbrich, H.H.G.J., 1984. Nefelina sienitos do maciço alcalino de Poços de Caldas MG-SP: caracterização mineralógica e petrológica. *33° Cong. Bras. Geol.*, anais, 4.362–4.376 (Vol. IX), Rio de Janeiro.

**Appendix 6:1**  
**PLATES 6:1-1 – 6:1-9.**

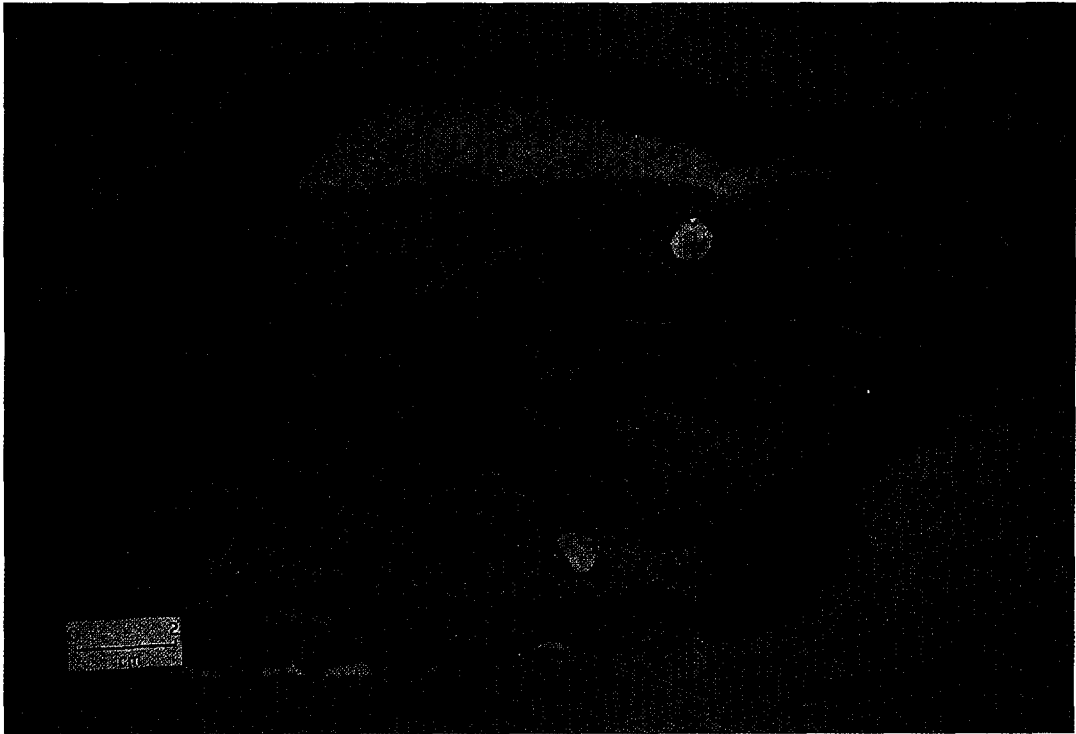


*PLATE 6:1-1. Composed sample RFI-2 of oxidised phonolite, yellow-brown in colour (lower major portion of the sample), separated from the reduced phonolite of white-grey colour (uppermost part of the sample) by the sharp redox front. The white nodules in the oxidised rock resulted from the dissolution of former pitchblende nodules by the progressive redox front. Note nodule alignment (in partial preservation) along the lowermost part of the sample delimiting a cleaved fracture face.*



*PLATE 6:1-2. Detail of the redox front and oxidised phonolite from sample RFI-2 (PLATE 6:1-1). Note "oscillatory zoning" of HFO (hydrous ferric oxides – mainly limonite) distributions, and that the oxidation may be incomplete even in residual zones of the oxidised phonolite clearly left behind by the passage of the redox front (e.g. in the right-hand lower portion of the sample that shows greyish colours unaffected by brown HFO staining). Note also that the dissolution of the pyrite-enriched pitchblende nodules occurred without the precipitation of "indigenous" HFO, thus resulting in white, particularly HFO-poor nodules/rock portions.*

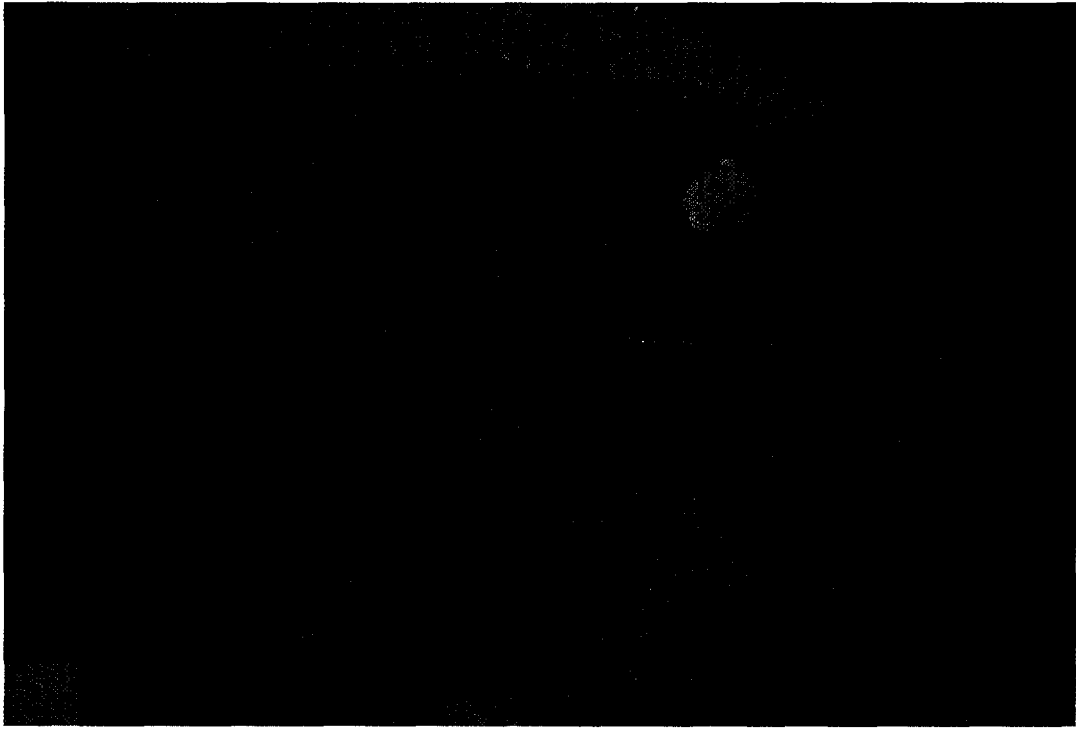


*PLATE 6:1-3. Composed sample RFI-3 comprising minor portions of oxidised phonolite and redox front (in the extreme lowermost left-hand part of the sample), reduced phonolite of whitish-grey colouration without pitchblende nodules, forming an approximately 10 cm wide zone directly preceding the redox front (major, central part of the sample) and reduced phonolite with pitchblende nodules (black) of zone of maximum (redox front-related) U-mineralisation (right-hand topmost part of the sample, delimited approximately by the dashed markings). Note the fine-grained (micro-)xenolithic nature of the phonolite and the fracture related/controlled formation of the pitchblende nodules. At the top edge of the sample a delimiting (horizontal) fracture controls both visible nodules. However, in addition, the right-hand nodule shows more clearly the influence of a second fracture system that intersects the horizontal fracture system obliquely at a steep angle (running parallel to the right-hand delimitation of the sample).*



*PLATE 6:1-4. Sample RFI-4 of reduced phonolite from the zone of maximum (redox front-related) U-mineralisation. The view is from a highly mineralised natural fracture plane containing five major pitchblende nodules that crosscut the mineralised zone in the reduced phonolite. Note the different densities of the pitchblende impregnation in the nodules (shown by the colour variations from totally black decreasing to medium grey), the forms of the circular, irregular and composed nodules, and the internal textures of homogeneous nodules (right-hand middle and top of sample) and inhomogeneous nodules. The latter show regular concentric zoning (left-hand middle and top of the sample) or irregular zoning (composed nodule touched by the upper left-hand corner of the scale). It should, however, be noted that the 3-dimensional forms of the nodules are normally flat-lenticular and only very rarely thick-lenticular to subspherical. Maximum cross sections always occur on the faces of the fracture planes.*

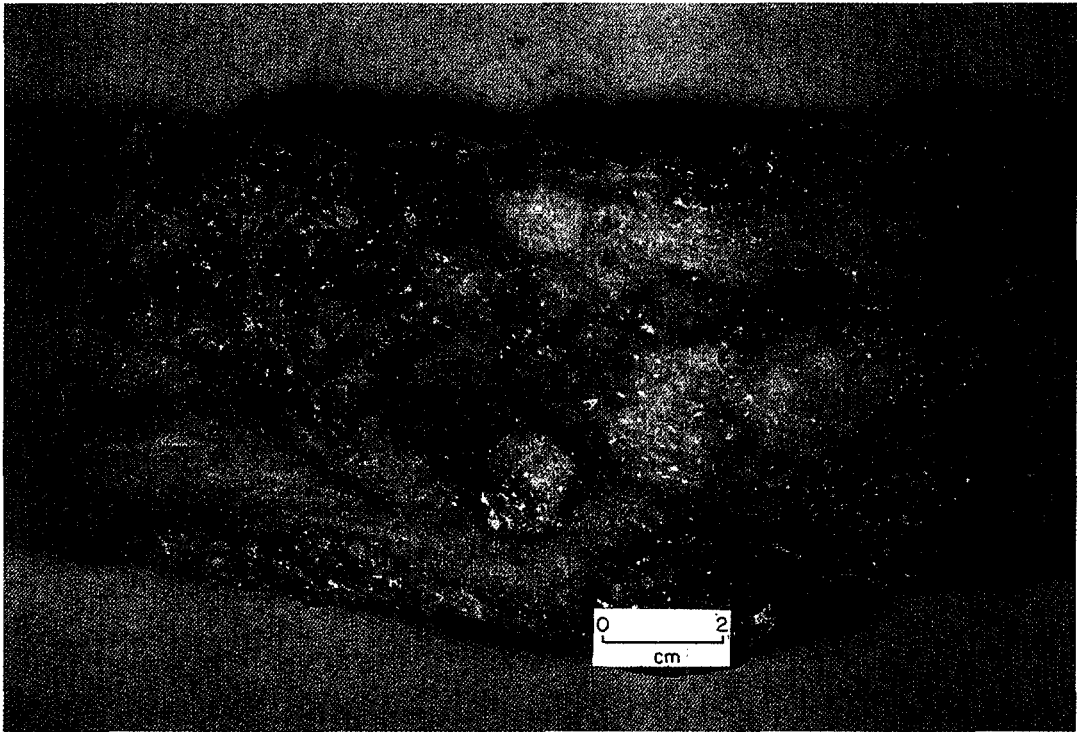


*PLATE 6:1-5. Reduced phonolite (sample RFI-5) about 35 cm away from the zone of maximum U-mineralisation (cf. Fig. 6-1). Note the very fine-grained rock groundmass, the content of microxenoliths, and the microporosities.*

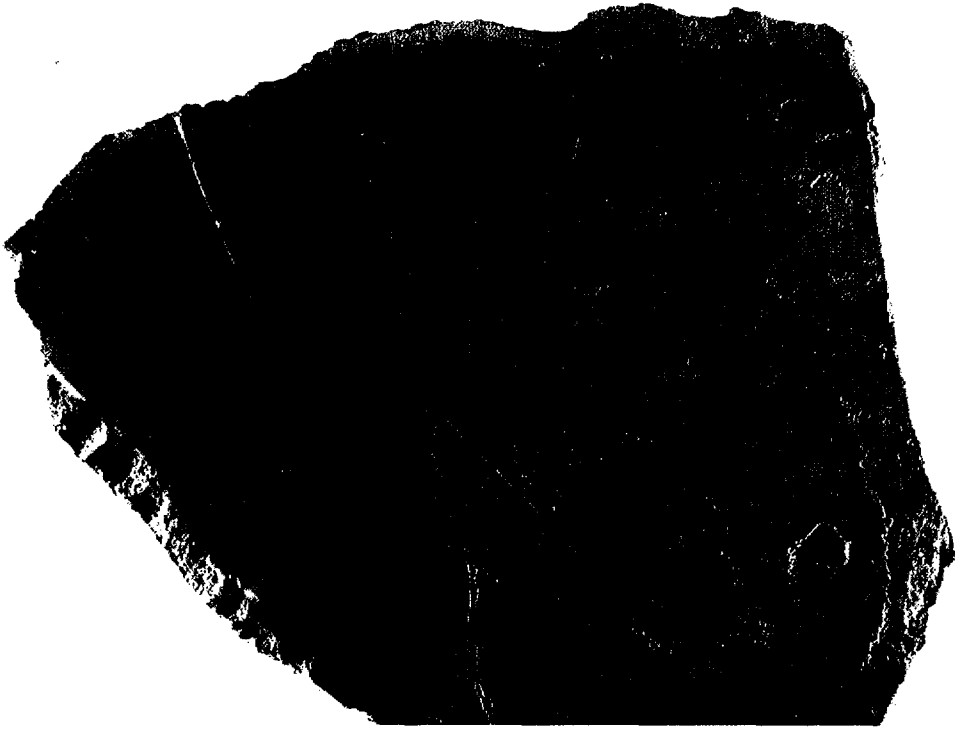


*PLATE 6:1-6. Reduced composite rock sample (RFI-6) collected about 1 m away from sample RFI-5 (cf. Fig. 6-1). The sample comprises a larger sized reduced nepheline syenite xenolith (right-hand side) of medium to coarse grain-size and lighter colours, enclosed by a very fine-grained reduced phonolite (left-hand side). The phonolite shows medium grey colours with dark grey veining (due to absorbed moisture during preparation) and a microporosity and flow orientation subparallel to the contact with the nepheline syenite xenolith. The phonolite and nepheline syenite portions were separately prepared and studied (about 4/5 of nat. size; see rectangular thin section mark across phonolite/nepheline syenite contact).*

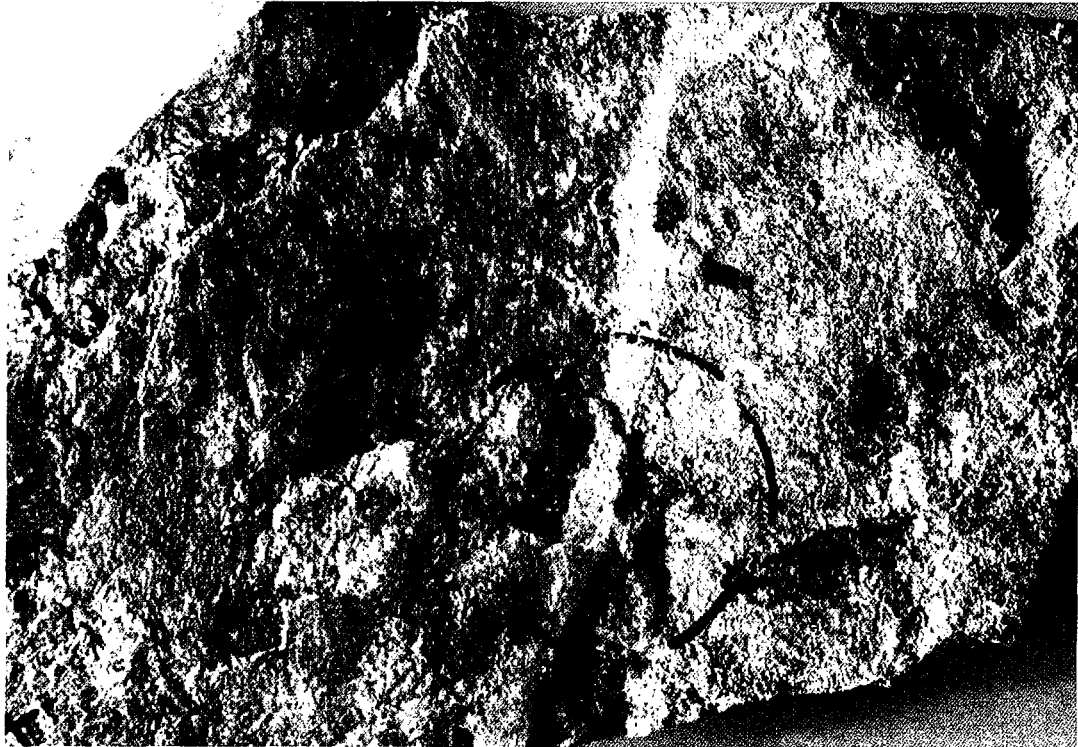


*PLATE 6:1-7. Redox front in a fine-grained phonolite (sample U – 7G; near open pit coordinates: 8.1 KK; about 1.6 x nat. size), showing the development of a narrow zone (of millimetric width) free from U-mineralisation, but pyrite-bearing (white coloured), crossing the centre of the hand specimen. The zone separates the reduced and U-mineralised portion of the sample (medium grey colouration and containing dark grey rounded irregular shaped, not very well defined pitchblende nodules of low U-oxide grade; right-hand side of the photograph) from the oxidised part (yellow-brown colouration after hydrolysis and HFO mineral (mainly limonite)-precipitation; left-hand side). The white zone is not a kaolinite/clay mineral layer, but simply a reduced and bleached rock zone identical in composition with the adjacent areas which are characterised by total U-oxide dissolution associated, probably, with incipient sulphide mineral (including pyrite)-dissolution. Note the sharp dissolution boundary of dark grey pitchblende nodules towards the white zone.*

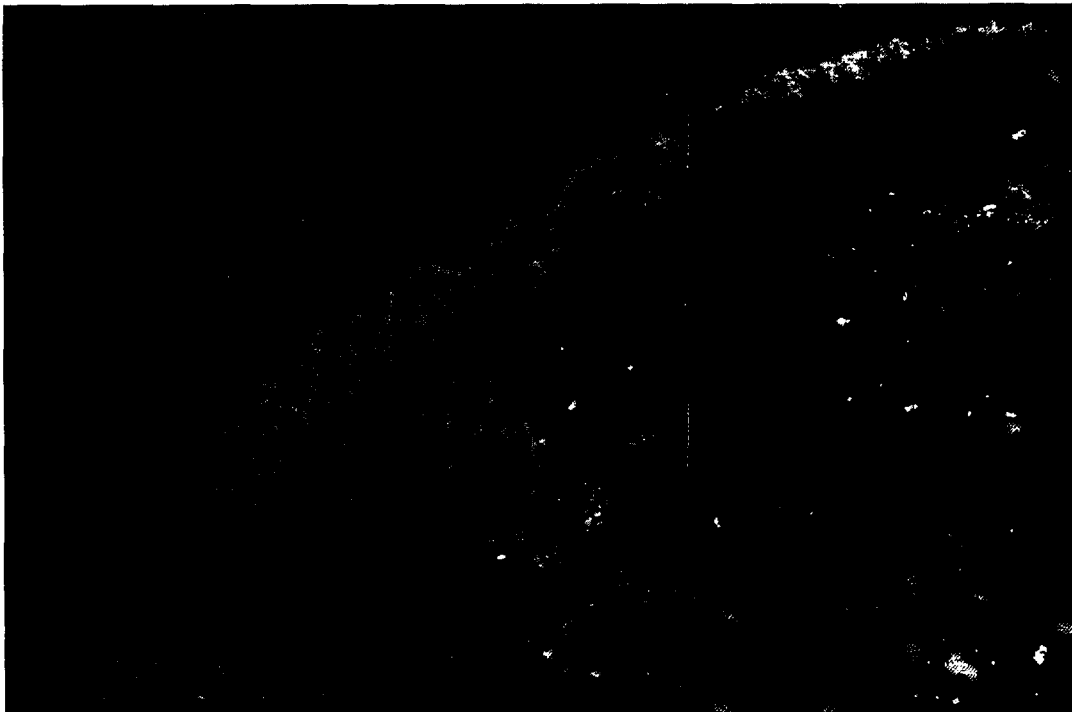


*PLATE 6:1-8. Cathodoluminescence image of (two quarters of) a pitchblende nodule of total maximum diameter about 10 mm from a redox front in fine-grained phonolite. Note the non-emission of pitchblende impregnated (dark to black) portions of the nodule and the light yellowish-reddish emission of the illite – K-feldspar – kaolinite silicate mineral matrix of the nodule after pitchblende dissolution along the borders and in the left-hand part of the nodule (seen only in the upper photograph). Open pores in the nodule show light-blue or dark-(ink) blue emission (depending on the presence of preparation adhesives covering the glass support of the polished rock thin section) and dark- (ink) blue emission, if within the surrounding silicate matrix of the nodule (which was better impregnated by the preparation adhesives). The emission colours of the surrounding rock matrix are medium yellowish-grey and the finely disseminated black minerals are non-emitting (mostly submillimetric) pyrites. Compare with same nodule in plain light view (PLATE 6:1-9).*

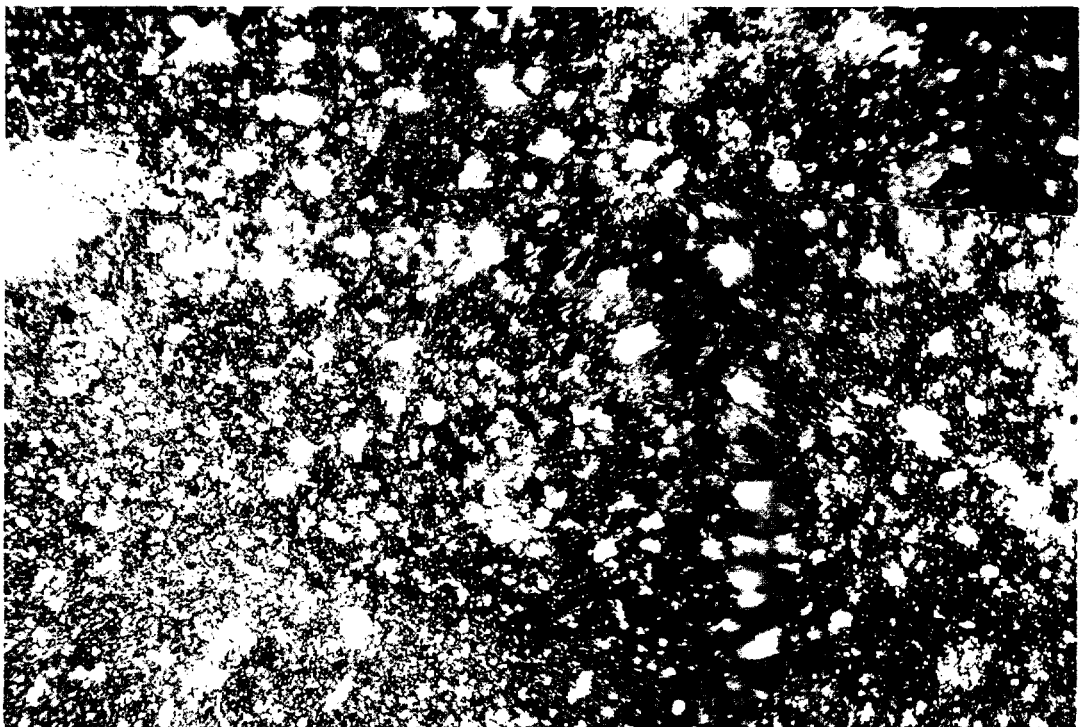
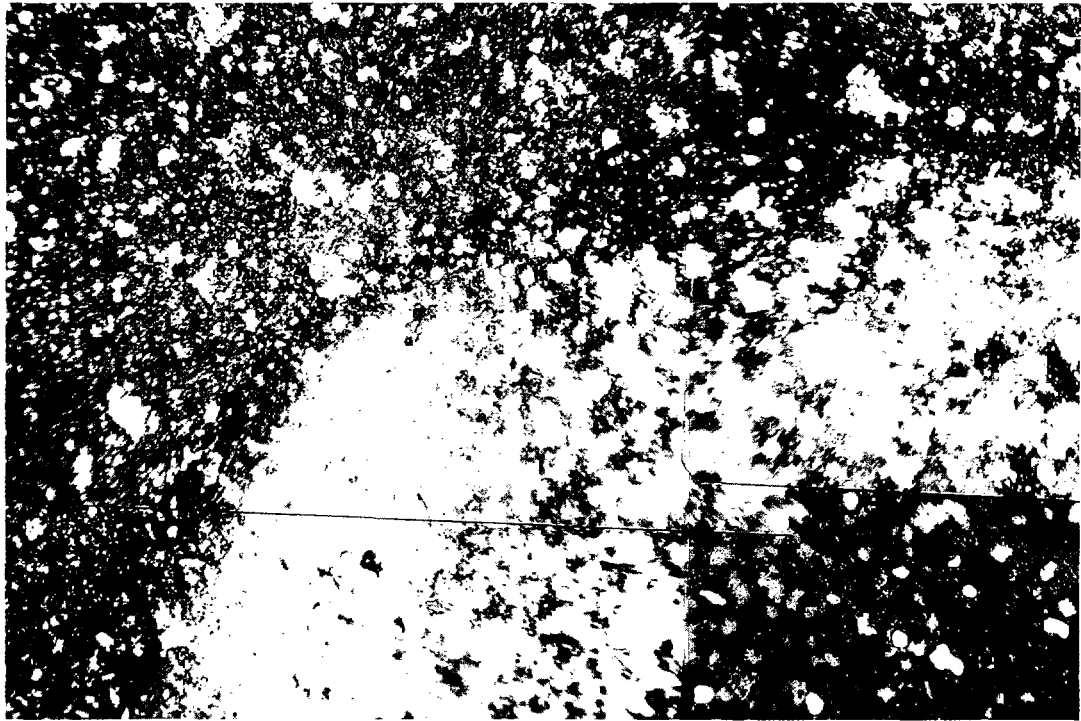


*PLATE 6:1-9. Plain light, equal magnification view of the same pitchblende nodule shown in PLATE 6:1-8. Note the variable density distribution and the type of pitchblende impregnation within the nodule (black-opaque with maximum density and very dark brown-semitranslucent with less dense cryptocrystalline pigmentations). The leached uranium barren parts of the nodule are the bright, light yellow translucent portions. The surrounding rock mass is fine-grained and contains abundant opaque (black coloured) pyrite microcrystals.*

**Appendix 6:2**  
**Rock chemical data for RFI.**

## Appendix 6:2

### Rock chemical data for RFI.

TABLE 6:2-I  
Chemical data for sample set I (Table 6-II) comprising large-sized samples.

Sample no. (Anal. no.)	Analytical methods and elements						Petrography
	Classic (wt.%)				AAS (ppm)		
	S <sup>1)</sup>	Fe <sub>2</sub> O <sub>3</sub> tot <sup>1)</sup>	FeO <sup>1)</sup>	LOI <sup>1)</sup>	Mo <sup>1)</sup>	Cd <sup>2)</sup>	
RFI-1A (03)	0.13	1.63	<0.2	2.87	85	4.0	Oxidised rock 25-15 cm from redox front
RFI-2B (04)	0.09	1.10	<0.2	1.88	55	0.658	Oxidised rock 10-0 cm from redox front
RFI-3B (05)	0.55	0.48	<0.2	2.29	115	1.1	Reduced rock 0-10 cm from redox front; pyrite-bearing
RFI-4B (06)	0.55	0.46	<0.2	2.01	145	0.788	Reduced rock of max. U-mineralisation; pyrite-bearing
RFI-5B (07)	1.09	1.05	<0.2	3.38	143	2.2	Reduced rock ~ 70-90 cm from redox front; pyrite-bearing

Analysis carried out by:

- 1) Paulo Abib Engenharia S.A., São Paulo;  
2) University of Bern.

LOI was determined at 900°C.

FeO analysis was not successful (as shown by the results indicating below detection limit values obtained for the reduced pyrite-bearing rocks, probably due to the presence of greater amounts of oxidised uranium).

Cd values represent the results from triplicate analysis.

TABLE 6:2-II  
XRF analysis of sample set II (Table 6-II) selected from detailed sampling of RFI.

Elements (wt.%)	RFI-1A ox. Ph.	RFI-1B ox. Ph.	RFI-1C ox. Ph.	RFI-3 red. Ph.	RFI-4A-1 red. Ph.	RFI-4A-2 red. Ph.	RFI-4B red. Ph.	RFI-5A red. Ph.	RFI-5B red. Ph.	RFI-6B red. NeS-x
SiO <sub>2</sub>	59.9	59.42	58.45	60.06	60.9	60.83	60	60.42	59.31	58.45
TiO <sub>2</sub>	0.46	0.53	0.46	0.49	0.45	0.41	0.43	0.41	0.42	0.57
Al <sub>2</sub> O <sub>3</sub>	22.41	22.05	22.07	22.11	20.93	20.04	21.42	20.48	21.05	23.39
Fe <sub>2</sub> O <sub>3</sub>	1.37	2.06	2.52	0.97	1	0.93	0.9	1.35	1.74	1.24
MnO	0.01	0.01	0.01	0.01	0.01	0.01	0.01	0.01	0.01	0.01
MgO	0.14	0.1	0.1	0.1	0.1	0.1	0.1	0.1	0.1	0.1
CaO	0.03	0.01	0.01	0.01	0.01	0.01	0.01	0.01	0.01	0.01
Na <sub>2</sub> O	0.01	0.01	0.01	0.01	0.01	0.01	0.01	0.01	0.01	0.01
K <sub>2</sub> O	14.23	14.18	14.04	14.36	14.48	14.51	14.06	14.11	13.87	13.26
P <sub>2</sub> O <sub>3</sub>	0.1	0.09	0.09	0.09	0.08	0.14	0.09	0.14	0.13	0.07
H <sub>2</sub> O	2.29	2.35	2.8	2.32	2.35	2.82	2.65	3.35	3.68	3.5
Total wt.%	100.95	100.81	100.56	100.53	100.32	99.81	99.68	100.39	100.33	100.61
Ba (ppm)	327	285	235	225	198	483	114	292	293	523
Rb	284	283	287	282	273	253	320	258	254	273
Sr	554	436	448	454	445	869	488	834	743	345
Pb	16	22	30	91	78	37	195	32	31	27
Th	45	34	42	15	26	71	144	65	62	57
U	106	130	861	175	448	121	4876	204	660	84
Nb	262	299	266	290	282	251	361	270	241	295
La	47	44	60	40	31	55	72	76	100	7
Ce	71	63	91	57	44	72	90	90	125	38
Nd	6	4	15	1	1	8	16	10	18	0
Y	40	37	34	56	55	132	59	159	105	89
Zr	82	97	86	99	114	459	153	678	326	545
V	357	342	307	293	170	91	175	115	197	322
Cr	5	8	8	3	2	3	4	5	5	10
Ni	6	6	9	6	6	17	9	20	17	16
Co	0	1	3	0	0	5	1	6	12	3
Cu	0	0	0	0	0	0	0	0	0	0
Zn	46	56	93	139	177	353	158	354	392	38
Ga	57	55	54	50	32	17	34	23	33	59
Hf	2	2	3	1	2	11	4	15	7	15
S	1039	1534	27354	4536	9196	12956	10359	13162	15532	58618

Analysis carried out by the University of Bern.

red. Ph. - reduced phonolite  
 ox. Ph. - oxidised phonolite  
 red. NeS-x - reduced nepheline syenite xenolith

TABLE 6:2-III

Mean compositions from oxidised and reduced, non-mineralised and mineralised RFI and F1 rocks, and from the regional magmatic nepheline syenites and phonolites.

Oxides (wt.%)	Redox front-1 rocks				Borehole F1 rocks		Regional rocks (10) U<5 ppm
	Oxidised (3)		Reduced (7)		Oxidised (16)	Reduced (29)	
	U<210 ppm(2)	U = 861 ppm(1)	U<210 ppm(4)	U>210 ppm(3)	U<310 ppm	U<210 ppm	
SiO <sub>2</sub>	59.66	58.45	59.94	60.07	56.00	56.17	52.86
TiO <sub>2</sub>	0.50	0.46	0.47	0.43	0.47	0.45	0.64
Al <sub>2</sub> O <sub>3</sub>	22.23	22.07	21.51	21.13	23.37	21.77	19.53
Fe <sub>2</sub> O <sub>3</sub> tot	1.72	2.52	1.12	1.21	2.92	3.05	3.96
MnO	0.01	0.01	0.01	0.01	<0.01	0.08	0.24
MgO	0.12	0.10	0.10	0.10	0.05	0.07	0.28
CaO	0.02	0.01	0.01	0.01	0.01	0.14	1.70
Na <sub>2</sub> O	0.01	0.01	0.01	0.01	0.68	0.38	7.49
K <sub>2</sub> O	14.21	14.04	14.06	14.14	13.02	13.40	8.16
P <sub>2</sub> O <sub>5</sub>	0.10	0.09	0.11	0.10	0.05	0.05	0.08
LOI	2.32	2.80	3.00	2.89	3.11	3.54	1.75
Total wt. %	100.88	100.56	100.34	100.11	99.68	99.10	96.68
Ba (ppm)	306	236	381 <sup>1)</sup> 334 <sup>2)</sup>	202	972	614	252 <sup>1)</sup> 50 <sup>2)</sup>
Rb	284	287	267	282	338	298	154
Sr	495	448	626	559	168	181	1.913
Pb	19	30	47	101	25	<6	6
Th	40	42	52	77	60	25	9
U	118	861	146	1.995	89	32	<5
Nb	281	266	277	295	152	226	249
La	46	60	45	68	227	305	263
Ce	67	91	64	86	301	314	350
Nd	5	15	5	12	60	69	92
Y	39	34	109	73	66	50	41
Zr	90	86	445	198	922	929	965
V	350	307	205	181	205	196	67
Cr	7	8	<6	<6	<6	<6	<6
Ni	6	9	15	11	5	5	<3
Co	<8	<8	<8	<8	<8	<8	9
Cu	<3	<3	<3	<3	4	<3	<3
Zn	51	93	121	242	19	225	168
Ga	56	54	37	33	39	22	n.a.
Hf	2	3	11	4	n.a.	n.a.	12
Sc	n.a.	n.a.	n.a.	n.a.	4	2	<1
F	n.a.	n.a.	n.a.	n.a.	1.158	1.638	1.757
S	1.287	27.354	22.318	11.696	<50	8.790	928

TABLE 6:2-III (contd.).

**Borehole F1 oxidised means include samples:**

1-1B; 10-1A; 14-1A; 16-1A; 20-1B; 26-1A; 31-1A; 33-1A; 34-1B; 43-1A; 1-1C; 20-1A; 23-1A; 47-1A; 55-1A; 59-1B.

Excluding sample 1-1C the following trace element means were determined:

Zr = 7.847 ppm; V = 1.352 ppm; Y = 206 ppm;

20-1A: Ce = 1.606 ppm;

23-1A: La = 1.498 ppm; Ce = 1.276 ppm; Nd = 288 ppm;

47-1A: Ce = 2.331 ppm.

**Borehole F1 reduced means include samples:**

39-1A; 74-1A; 75-1B; 77-1A; 81-1A; 85-1A; 90-1B; 101-1A; 106-1A; 111-1A; 112-1A; 119-1A; 121-1A; 126-1A; 68-1A top;  
68-1A mid; 68-1A bot; 69-1B; 71-1A; 75-1B; 77-1B; 78-1A; 109-1B; 112-1AD; 113-1B; 117-1A; 126-1A; 126-1B.

Excluding 74-1A the following trace element means were determined:

La = 6.843 ppm; Ce = 6.272 ppm; Nd = 1.854 ppm; Y = 461 ppm.

- 1) = means of all the rocks;
- 2) = number of analysed phonolites;
- n.a. = not analysed;
- (n) = number of analysed rocks.

TABLE 6:2-IV  
Cadmium AAS analysis from RFI samples.

Sample no.	Analysis no.	Cd	Petrography of analysed sample fraction
RFI-1A	03	4.0 ppm	Oxidised bulk phonolite; ~25–15 cm from the redox front
RFI-2B	04	658 ppb	Oxidised bulk phonolite; ~10 cm adjacent to the redox front
RFI-3B	05	1.1 ppm	Reduced bulk phonolite, non-mineralised zone ~10 cm wide, adjacent to the redox front
RFI-4B	06	788 ppb	Reduced bulk phonolite (without pitchblende nodules) from zone of max. U-mineralisation
RFI-5B	07	2.2 ppm	Reduced bulk phonolite weakly U-mineralised (with pitchblende micronodules)
RFI-1B/2A	1	4.1 ppm	Bleached nodules from samples RFI-1/2 (mixed sample)
RFI-1A	2	2.6 ppm	Bleached nodule from sample RFI-1A
RFI-1B/2A	3	3.0 ppm	Oxidised bulk phonolite (mixed material adjacent to bleached nodules; sample RFI-1/2)
RFI-2C	4	844 ppb	Reduced bulk phonolite; ~0.5 cm from the redox front
RFI-3B	5	1.0 ppm	Reduced bulk phonolite; ~5 cm from the redox front (middle of non-mineralised zone)
RFI-4B	6	19.5 ppm	Pitchblende nodule from sample RFI-4B
RFI-4B	7	307 ppb	Reduced bulk phonolite directly adjacent to pitchblende nodule RFI-4B
KU-6	KU-6	≥1.000 ppm	Massive pitchblende nodule (“fossil” nodule) containing microscopic CdS greenockite; from the Urânio do Brasil collection (semiquantitative analysis)

## **Appendix 7**

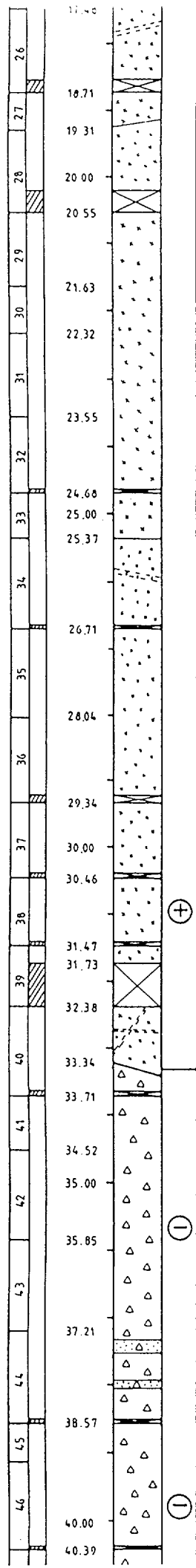
**Detailed geological logs of boreholes F1, F3 and F4.**

# BOREHOLE F1(9-1WC11) - OSAMU UTSUMI MINE

Drilling owner : Poços de Caldas Project  
 Drilling company : Geoserv  
 Drilling time : 24.9. - 2.10.1986

Geological log 1:50  
 Geological logging : N. Waber  
 H.A. Scalvi

CORE NUMBER	CORE LOSS	DEPTH	LITHOLOGY	CHEMICAL ENVIRONMENT	DESCRIPTION	TECTONIZATION	FISSURE MINERALS	THICKNESS OF FISSURES	OPEN FISSURES / m	NOTES
1		0.22			PHONOLITE; oxidised, orange-brown porphyritic, strongly altered to clay minerals. K-feldspar phenocrysts up to 1 cm, partly or totally altered to clay minerals.		CM FeOx	5mm	4	Microbiology
		0.65			FRACTURE ZONE in phonolite; oxidised, strongly altered, porous. Matrix: grey clay minerals, orange-brown spots and cavities with clay minerals, oxidised PY and Fe-Oxides.		CM Fe O <sub>x</sub> oxPY	1cm	2	Microbiology
2		1.00								
		1.06								
		1.32								
3		1.76			PHONOLITE, oxidised, porphyritic, strongly altered, porous, orange-brown, strongly fractured. K-feldspar altered to white + grey clay minerals.		CM ZEO? FeOx	5mm	3	
4		2.00								
		2.11								
		2.30								
		2.61								
		2.83								
		3.11								
		3.53								
		4.02								
		4.17								
		4.38								
		4.97			FRACTURE ZONE in phonolite; oxidised, very porous, matrix grey clay minerals, cavities filled with ox.PY + Fe-Ox.		CM oxPY FeOx		2	Microbiology
		5.13								
		5.46								
		5.81								
		6.17								
		6.39								
		6.59								
		6.71								
		7.07			PHONOLITE; oxidised, orange-brown, coarse-grained, strongly altered.					
		7.45								
		7.69								
		7.89			FRACTURE ZONE in oxidised phonolite; white clay minerals around fractures, very porous.					
		8.32								
		8.50								
		8.74								
		9.43								
		9.76			PHONOLITE; oxidised, alternating orange-brown and grey, fine-grained with K-feldspar phenocrysts, very porous.					Microbiology
		10.00								
		10.44								
		10.87								
		11.24			FRACTURE ZONE filled with grey clay minerals.		CM FeOx oxPY	3mm	2	
		11.89								
		12.18								
		13.17			FRACTURE ZONE filled with grey CM.					
		13.30			PHONOLITE; oxidised, grey-brown, porphyritic with a fine-grained matrix, strongly altered. K-feldspar phenocrysts, porous.					
		14.20								
		15.00								
		15.28			PHONOLITE; oxidised, with large altered greenish spots (1-2 cm).					γ-spec., U-series, Ra-isotopes, microbiology
		16.22								
		17.48								



PHONOLITE; oxidised, porphyritic alternating porous and compact zones. Porous parts grey-brown, compact-parts orange-brown in colour.

PHONOLITE; oxidised, grey-brown, fine-grained with K-feldspar phenocrysts (-1.5 cm), pseudoleucite phenocrysts (-2 cm). Porous with steeply dipping fractures exhibiting leaching zones.

PHONOLITE; oxidised, strongly fractured.

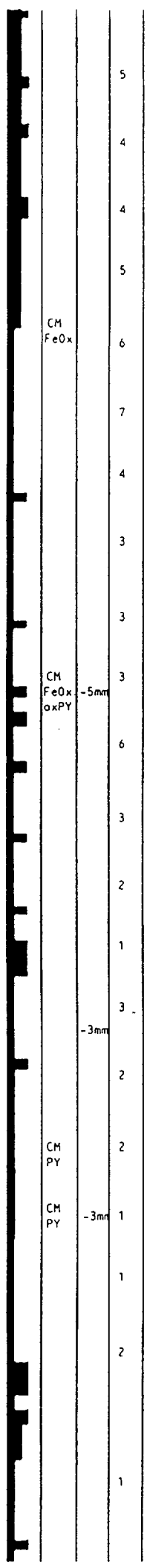
PHONOLITE; reduced, bright grey, fine-grained with K-feldspar, phenocrysts. Very porous with a sharp contact with the oxidised phonolite.

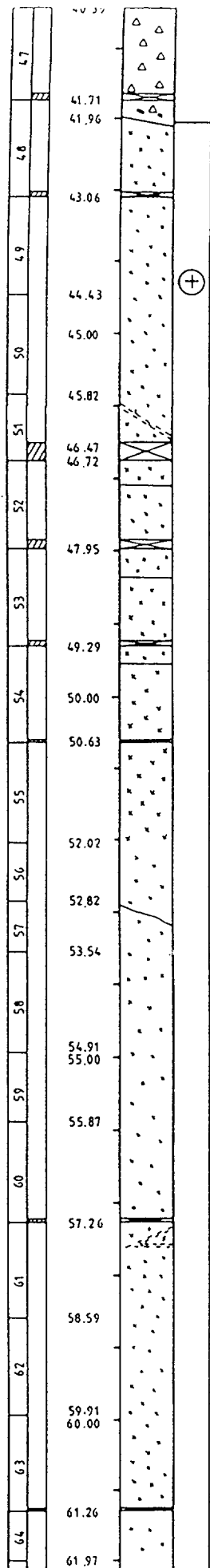
PHONOLITE; reduced, cataclastic zone with much PY enrichment along fractures.

PHONOLITE reduced, fine-grained, strongly fractured, bright grey, porous, strongly altered.

ARGILLIC ZONE in reduced phonolite, greyish white.

ARGILLIC ZONE in reduced phonolite, greyish white.





PHONOLITE; reduced, grey, fine-grained with K-feldspar, phenocrysts and pseudoleucite phenocrysts. Two open fractures with PY + U-phase plus two U-mineralised spots; border to oxidised phonolite characterised by a 5 mm thick white clay layer.  
 PHONOLITE; oxidised, fine-grained with K-feldspar phenocrysts, pseudoleucite phenocrysts, strongly altered. First 5 cm is bright orange-brown, changing into dark orange-brown.

PHONOLITE; oxidised, porphyritic medium-grained, K-feldspar phenocrysts totally altered. Leaching zones along fractures; pores filled with Fe-Ox, ox PY and clay minerals.

PHONOLITE; oxidised, porous, orange-brown.

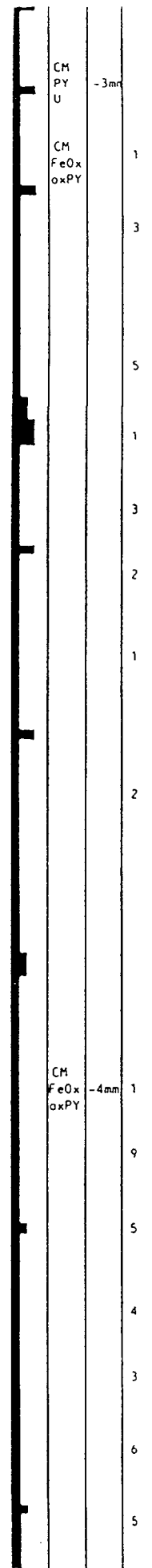
PHONOLITE; oxidised, compact, orange-brown.

PHONOLITE; oxidised, porous, orange-brown.

PHONOLITE; oxidised, medium-grained and compact with K-feldspar phenocrysts (-1.5 cm). Fe-Ox along grain boundaries.

PHONOLITE; oxidised with K-feldspar and pseudoleucite phenocrysts, orange-brown.

Leached, bright zone along steeply dipping fractures.

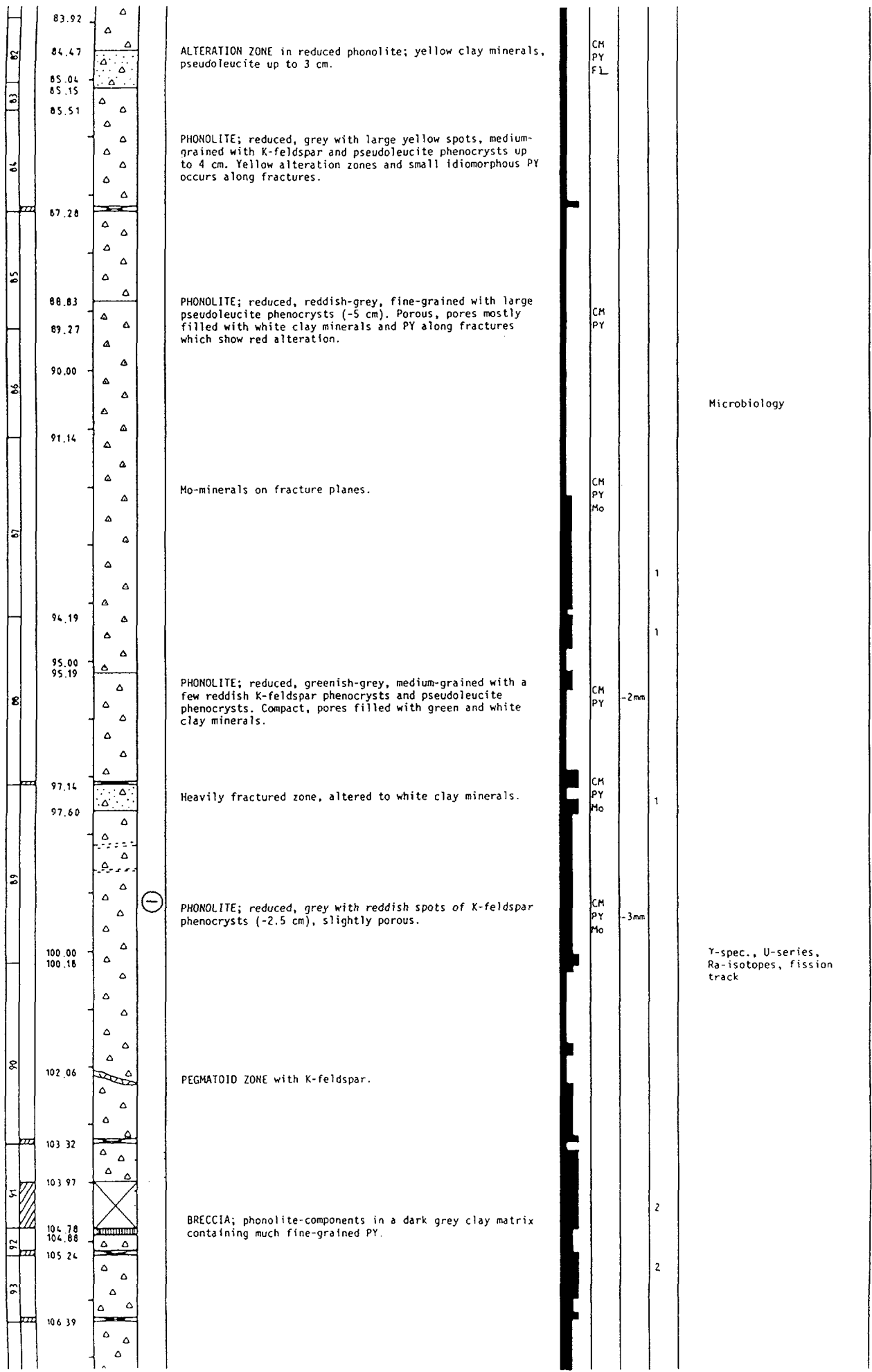


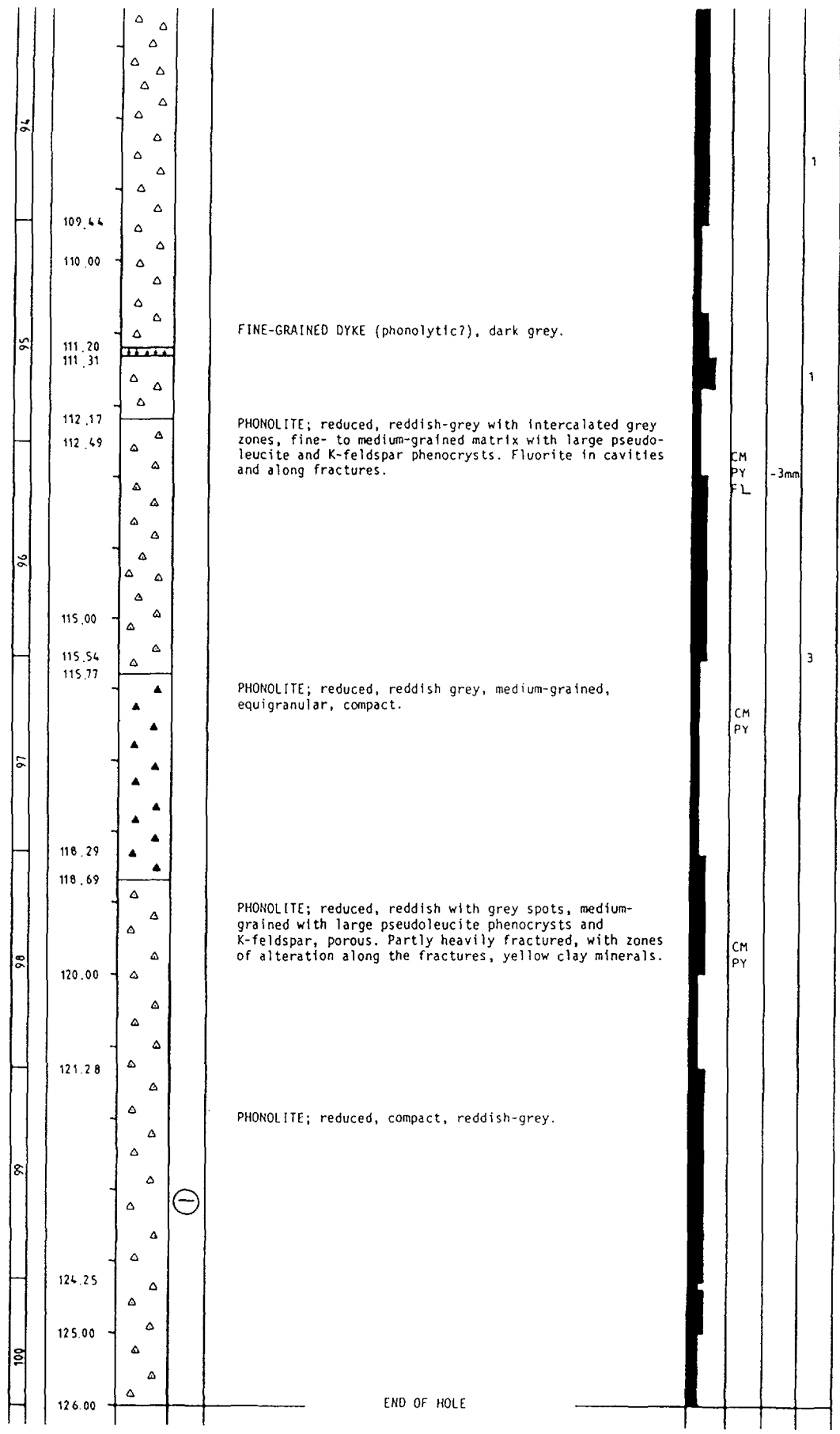
γ-spec., U-series, Ra-isotopes, microbiology, fission track, permeability, porosity, diffusivity  
 Permeability, porosity, diffusivity

Microbiology

Permeability, porosity, diffusivity, microbiology







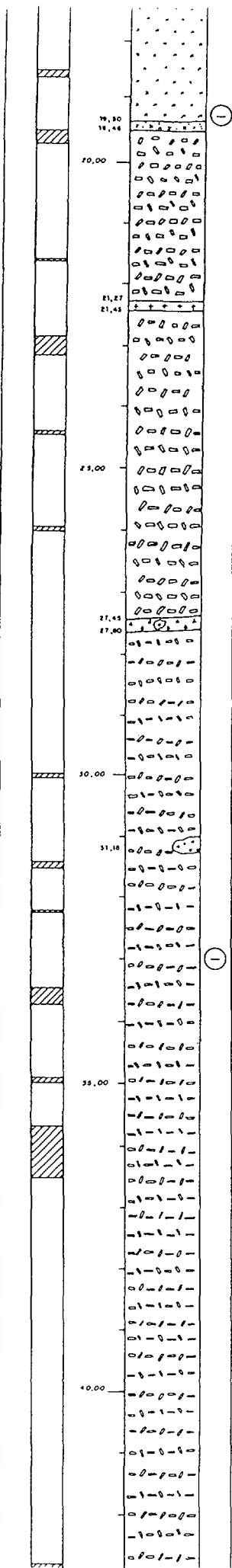
- |                    |                 |                   |
|--------------------|-----------------|-------------------|
| Fe - iron          | KF - K-feldspar | CM - clay mineral |
| Mn - manganese     | BA - barite     | SM - smectite     |
| Mo - molybdenum    | SID - siderite  | ILL - illite      |
| Ti - titanium      | ZR - zirconium  | KAOL - kaolinite  |
| U - uranium        | FL - fluorite   |                   |
|                    | ANH - anhydrite |                   |
| PY - pyrite        | Ox - oxide      |                   |
| CCP - chalcopyrite |                 |                   |
| GAL - galena       |                 |                   |
| PBL - pitchblende  |                 |                   |

# BOREHOLE F3 (9-1NH47) - OSAMU UTSUMI MINE

DRILLING OWNER : POÇOS DE CALDAS - PROJECT  
 DRILLING COMPANY : GEOSERV - NUCLEBRÁS  
 DRILLING TIME : 21/09 - 25/09 1987

GEOLOGICAL LOG : 1:50  
 GEOLOGICAL LOGGING : N. WABER

CORE LOSS	DEPTH	LITHOLOGY	CHEMICAL ENVIRONMENT	DESCRIPTION	TECTONISATION	FRACTURE MINERALS	THICKNESS OF FRACTURES	OPEN FRACTURES
[Hatched]	1,10	[Dotted]		PHONOLITE; reduced, bright grey, fine-grained to equigranular with a strong PY-impregnation and strong argillic alteration.	[Hatched]	CM, PY	2mm	
[Hatched]	1,34	[Dotted]		ARGILLIC ZONE; associated with pyrite and shows higher radioactivity than the surrounding phonolite.	[Hatched]			
[Hatched]	1,93	[Dotted]	①	PHONOLITE; reduced, bright grey, fine-grained to equigranular with a very strong argillic alteration; PY-impregnation.	[Hatched]			
[Hatched]	4,88	[Dotted]		U-MINERALISATION; reduced phonolite; aggregates of pitchblende and pyrite (0.5 - 1 cm in diameter) occur disseminated in the phonolite and along small fissures; the grain-size of the aggregates decreases towards the redox-front.	[Hatched]	CM, PY PBL	2mm	
[Hatched]	8,88	[Dotted]	+	PHONOLITE; oxidised, orange-brown with PY mostly replaced by Fe-oxides and Fe-hydroxides.	[Hatched]	CM FeOx	2mm	+
[Hatched]	10,00	[Dotted]		PHONOLITE; reduced, bright grey, fine-grained to equigranular with argillic alteration and PY-impregnation; in several small zones the phonolite displays a tectonic breccia with a clay-pyrite matrix.	[Hatched]	CM, PY GAL?	3mm	
[Hatched]	15,00	[Dotted]			[Hatched]	CM, PY GAL? Mo ?	3mm	
[Hatched]	19,00	[Dotted]			[Hatched]	CM, PY KF, BA GAL? Mo	4mm	+



ARGILLIC ZONE; phonolite is totally altered to clay; zone shows a higher radioactivity without any visible U-mineralisation.

PHONOLITE; reduced, grey, porphyritic with a fine-grained matrix of clay minerals, K-feldspar and pyrite; phenocrysts of K-feldspar (fresh, 0.5 - 1 cm), pseudomorphic replaced nepheline (0.4 cm) and pseudoleucite (0.5 - 2 cm); moderate to strong argillic alteration and PY-impregnation.

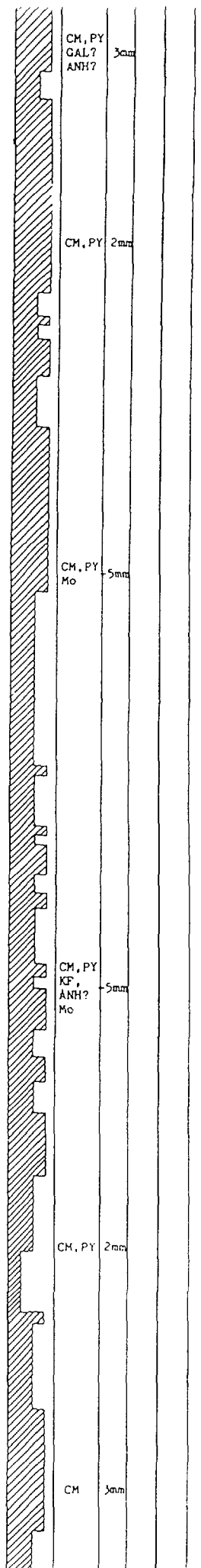
DYKE? or XENOLITH?; fine- to medium-grained and dark grey with K-feldspar and nepheline-pseudomorphs somewhat longer than the totally altered matrix; fluorite occurs in the nepheline-pseudomorphs.

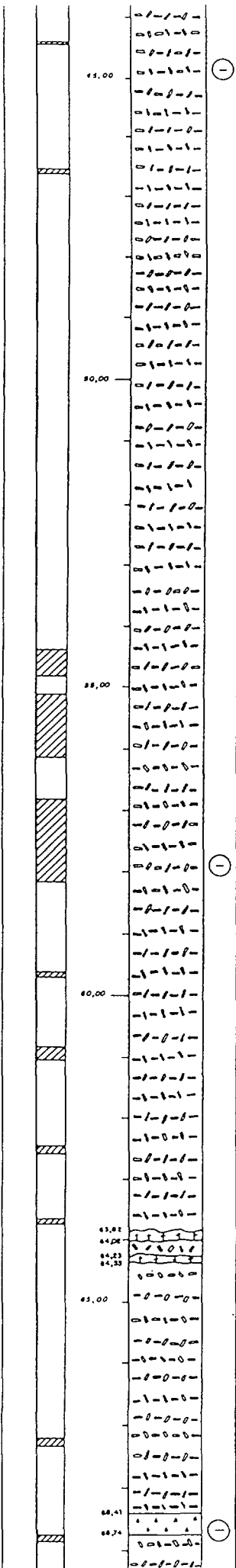
VOLCANIC BRECCIA; foyaitic and phonolitic components in a matrix of clay minerals, K-feldspar and pyrite.

FOYAITIC XENOLITH; in the phonolite.

Several zones with very strong argillic alteration and pyritisation.

PHONOLITE; reduced, grey, fine-grained to porphyritic with phenocrysts of mainly K-feldspar and nepheline-pseudomorphs.



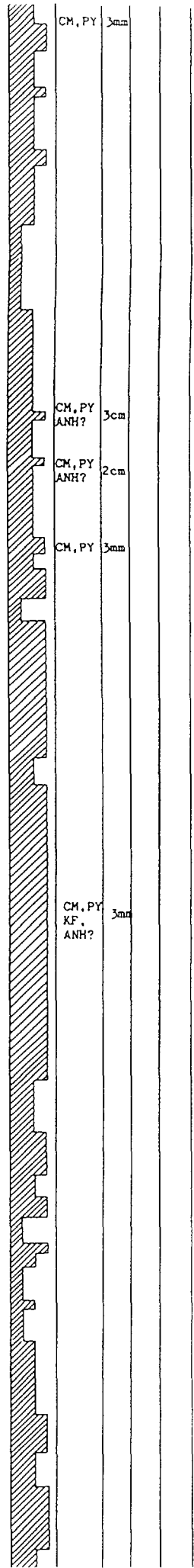


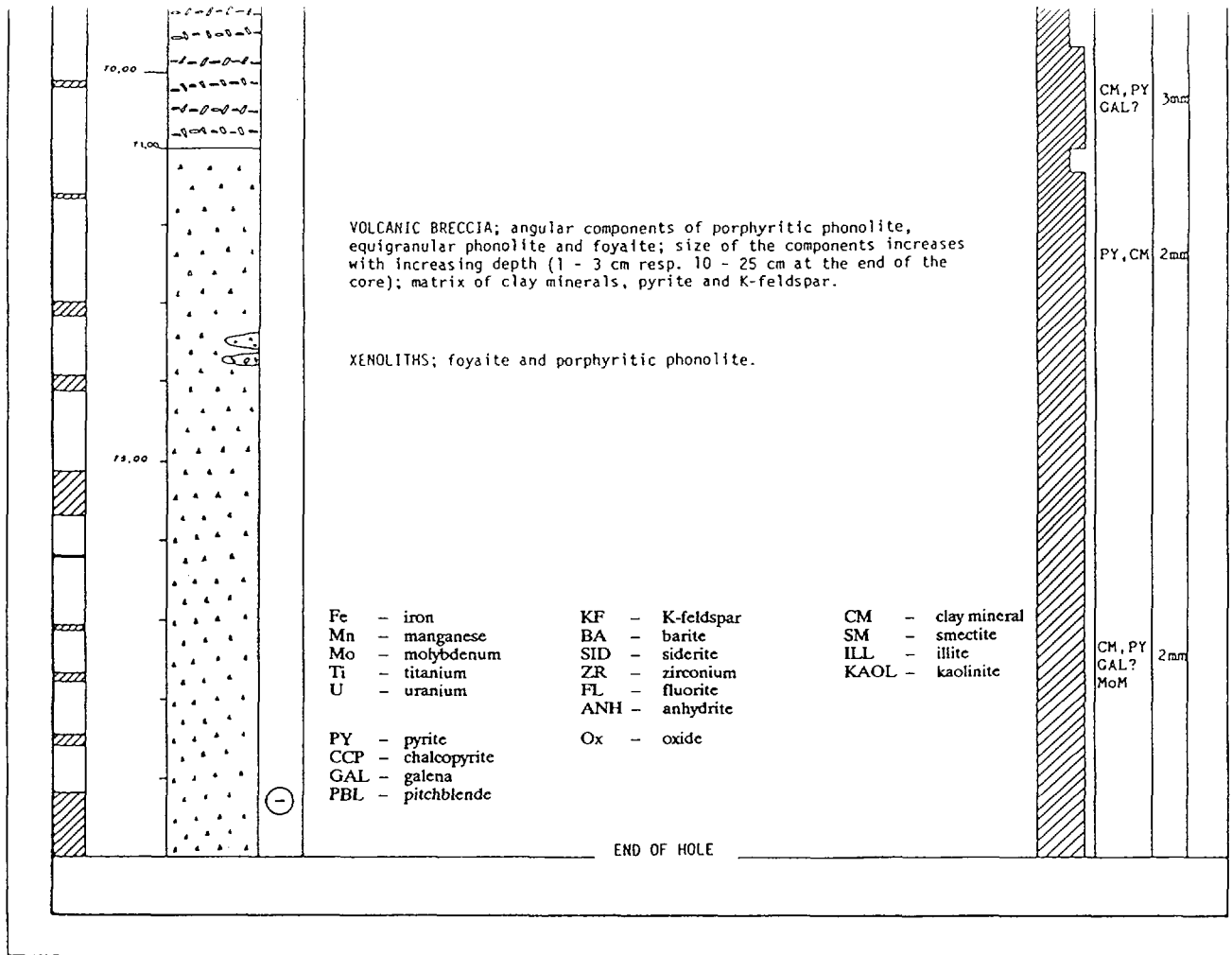
Zones rich in nepheline-pseudomorphs alternate with zones nearly free of them.

DYKES ?; medium-grained with much K-feldspar but mostly devoid of nepheline-pseudomorphs; strong argillic alteration but still with distinct contacts to the surrounding phonolite.

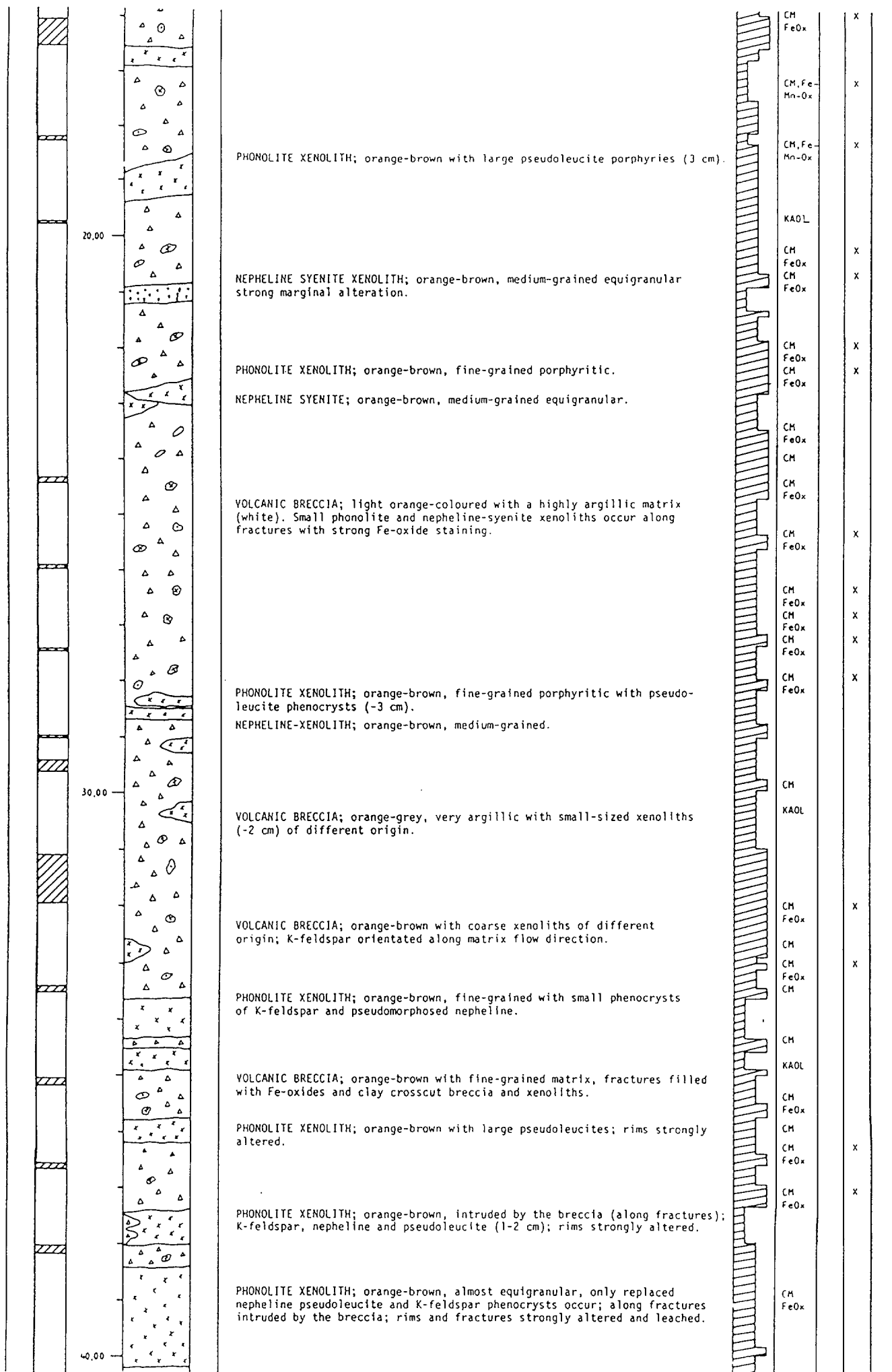
High porosity and leaching textures.

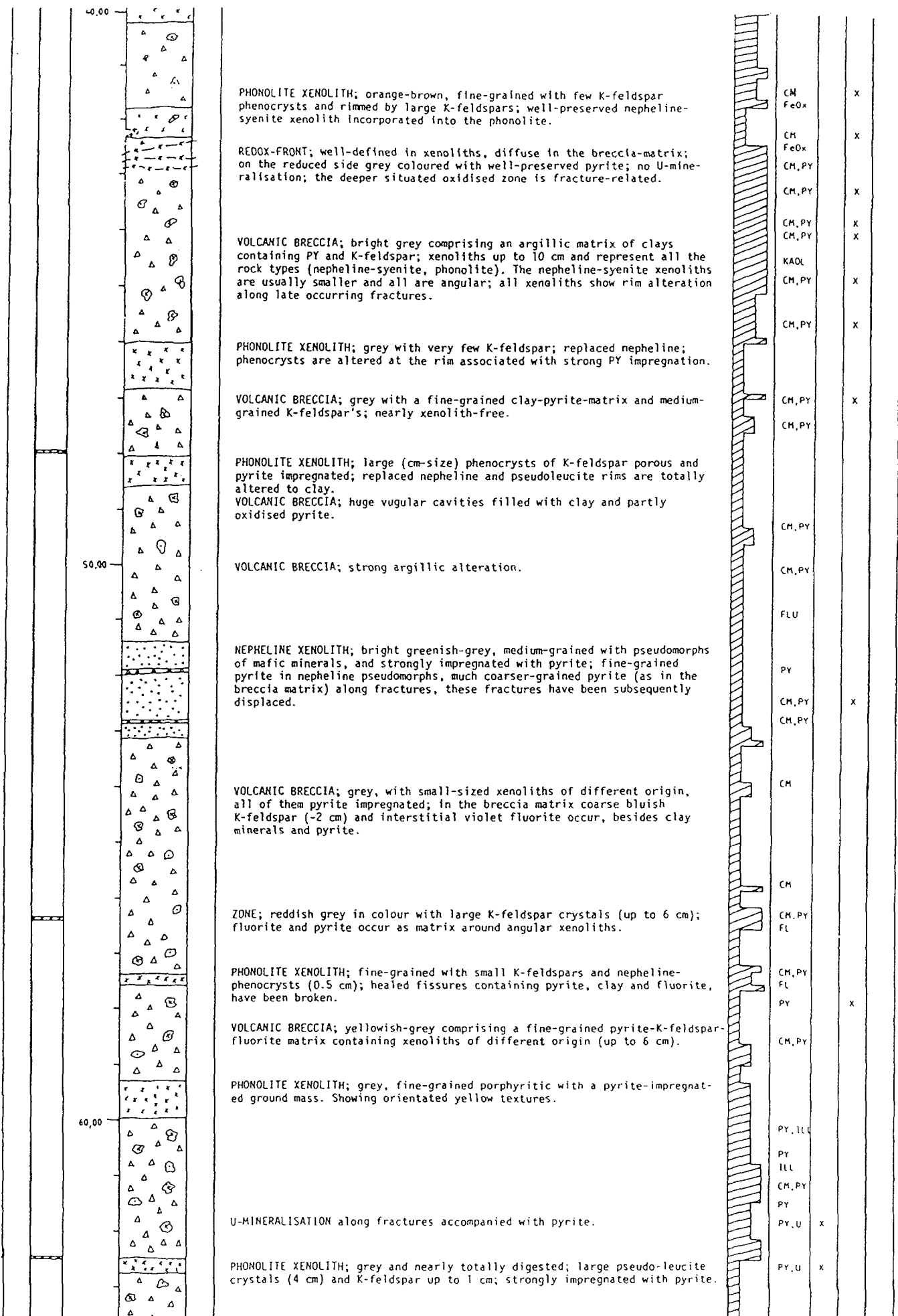
VOLCANIC BRECCIA; totally altered foyaitic and phonolitic components, matrix mainly clay minerals and pyrite; around the breccia the K-feldspar of the phonolite is altered to clay.

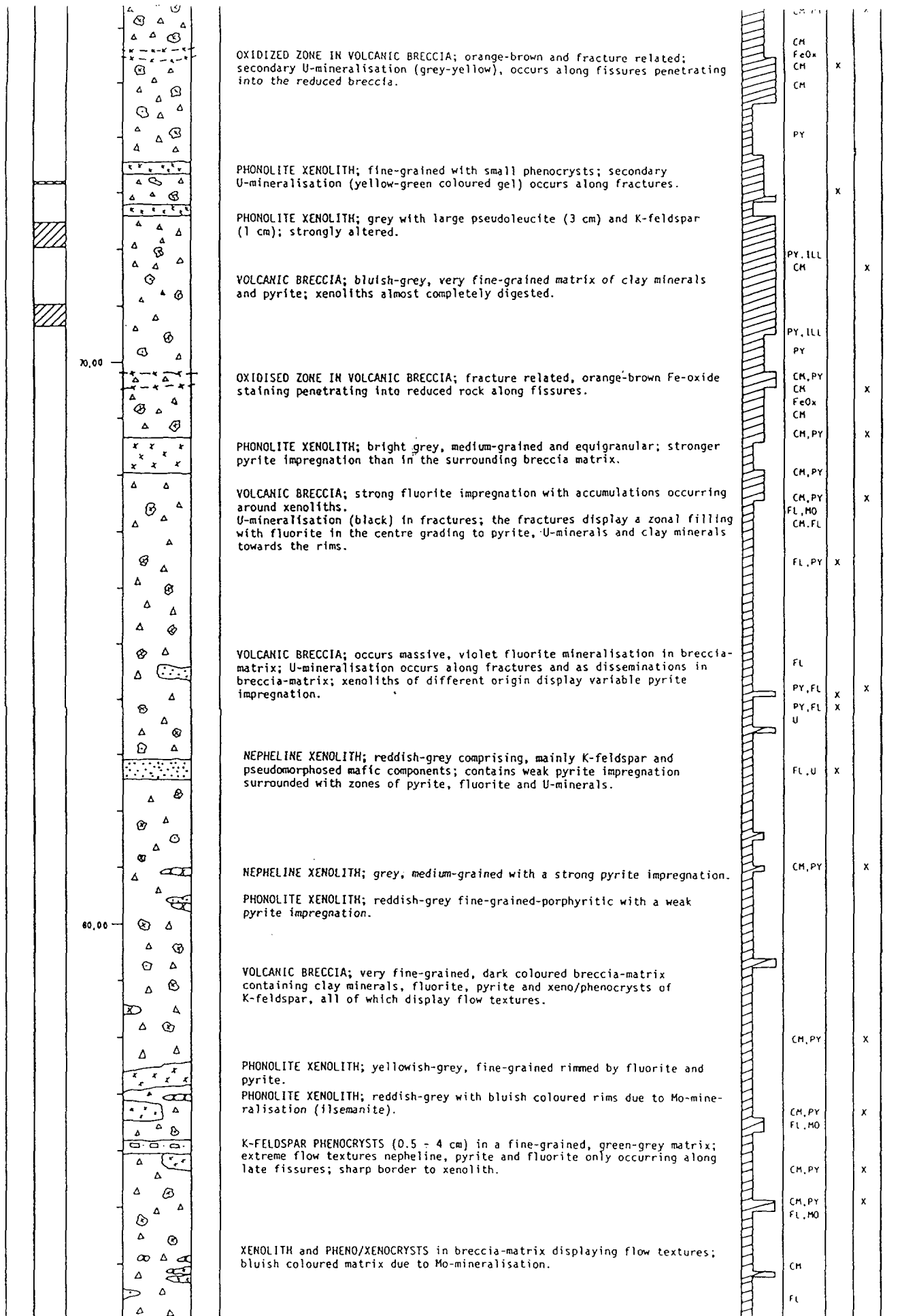








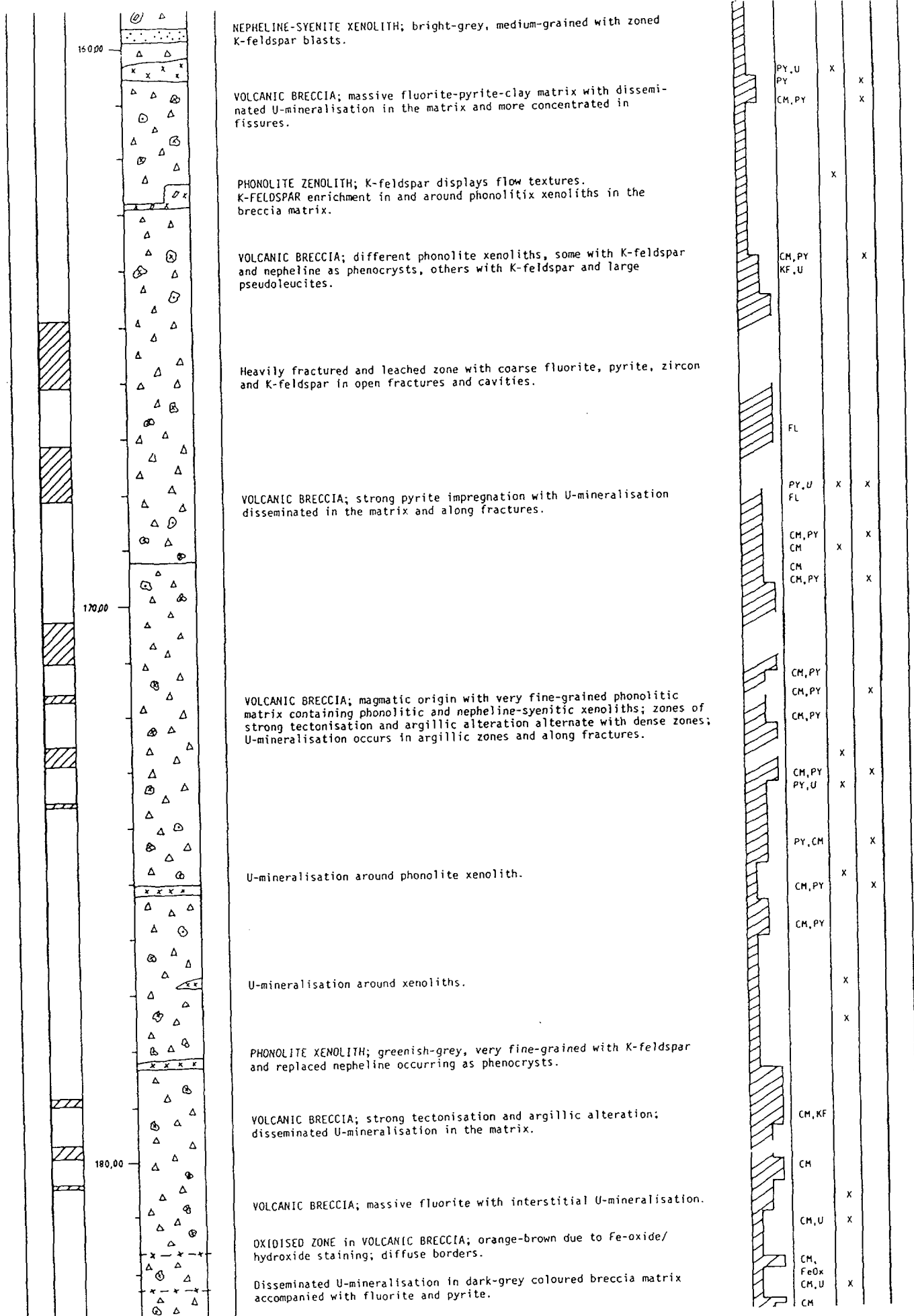




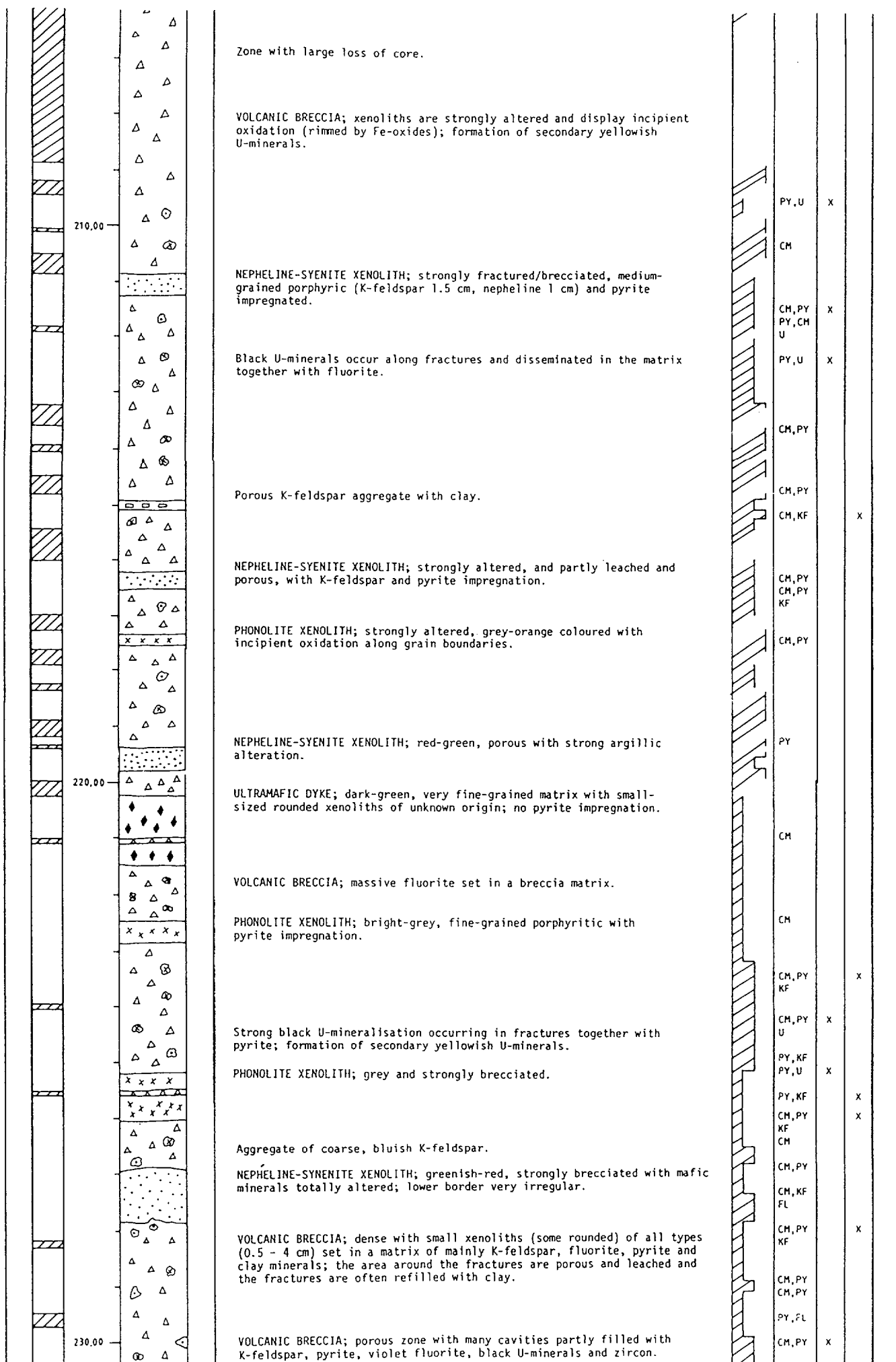


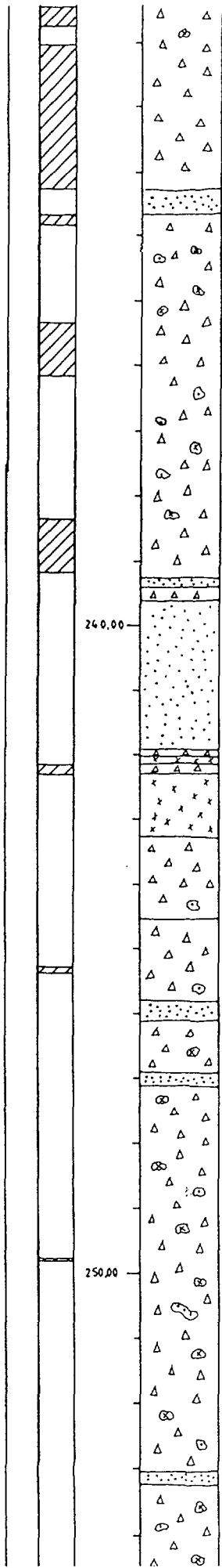












Extensive core loss.

NEPHELINE-SYENITE XENOLITH; grey, medium-grained and equigranular with some coarser-grained K-feldspar; many replaced mafic minerals.

U-mineralisation occurs along fractures and as matrix disseminations together with pyrite.

U-mineralisation around xenoliths.

Disseminated U- and Mo-mineralisation in breccia-matrix and concentrated at xenolith margins.

NEPHELINE-SYENITE XENOLITH; medium-grained with many mafics; intruded several times by cm-thick breccia-zones; around these and at both rims, strong leaching and a change of colour from grey-red to red occurs (mafic leached, K-feldspar stable).

PHONOLITE XENOLITH; fine-grained porphyritic with pseudoleucite as phenocrysts.

U-mineralisation occurs in fractures together with an unidentified red mineral; incipient oxidation is present along grain-boundaries with the formation of secondary yellow U-minerals.

NEPHELINE-SYENITE XENOLITH; reddish-grey, with strong pyrite impregnation.

VOLCANIC BRECCIA; fine- to medium-grained with a matrix consisting mainly K-feldspar, pyrite and clay; all types of xenolith occur (1-15 cm), mostly angular but some small ones slightly rounded; several K-feldspar enrichments along fractures; phonolite and xenoliths occur with and without large pseudoleucites; Ti-minerals present.

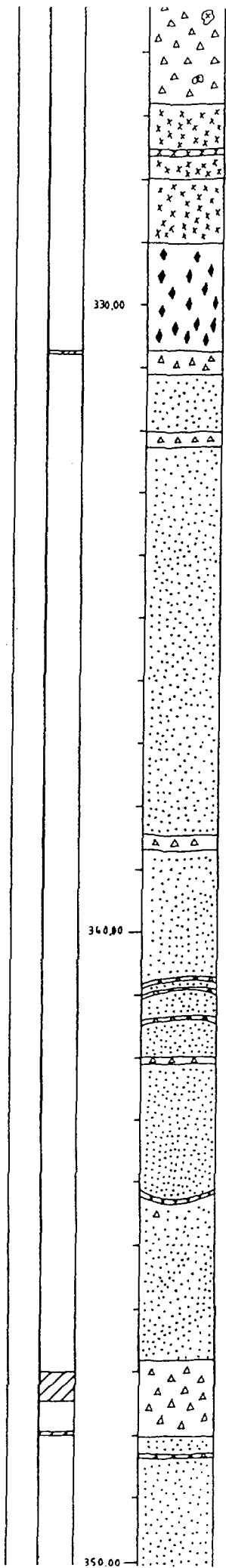
NEPHELINE-SYENITE XENOLITH; leucocratic, red-grey and medium-grained.

CM, PY			
U			
CM			
CM, PY	X	X	
KF, FL, U			
CM			
CM, PY		X	
FL, U			
PY			X
		X	
CM, KF			
CM, Mo	X		
CM, PY			
CM			
CM, PY			
CM			
CM, PY			
KF, FL			
CM, PY			
CM, PY			
CM			
PY, U		X	
PY, U		X	
CM			
CM			
PY, KF			
CM			
PY, KF			X
CM, PY			
FL, KF			X
CM, PY			
FL			
CM, PY			
FL			
PY, KF			X
CM, PY			X
FL			
CM			
CM, PY			X
FL, TI			
KF			
CM, PY			X
KF, FL			
CM, PY			
CM, PY			
TI			
CM, PY			
CM			
CM			
CM			









PHONOLITE XENOLITH; grey, fine-grained and non-porphyritic with pyrite impregnation; exists has a xenolith of porphyritic phonolite with a distinct contact; not brecciated.

PHONOLITE XENOLITH; bright grey and fine- to medium-grained porphyritic; K-feldspar and nepheline phenocrysts (0.5 cm) both altered to clay; sharp contact with the dyke; not brecciated.

ULTRAMAFIC DYKE; yellow-green at the rims and dark black-green in the relatively well-preserved central part; in the fine-grained matrix biotite, K-feldspar and pyroxene are present as crystals up to 3 mm; in the middle of the dyke are well-preserved nepheline-syenite xenoliths up to 1.5 cm.

NEPHELINE-SYENITE XENOLITH; grey-rose-yellow, medium-grained and equigranular; K-feldspar (pink) is partly altered; nepheline is altered to clay (white, yellow, grey); often the preserved core mafics are all altered to green-yellow clay and pyrite impregnated; between 332.80 - 333.56 the nepheline is darker; more black fine-grained minerals and large patches of dark black pseudomorphoses after pyroxene also occur.

Around the fractures is evidence of leaching and K-feldspar enrichment.

VOLCANIC BRECCIA; breccia vein with fine-grained phonolitic matrix.

Two leucosomes (5 cm, 2 cm thick); mainly K-feldspar with xenoliths (1.5 cm).

Leucosomes as above.

PHONOLITIC DYKE; with sharp contacts and chilled margins; no xenoliths.

VOLCANIC BRECCIA; displaying incipient oxidation along grain boundaries and around xenoliths.

